Comprehensive Summaries of Uppsala Dissertations
From the Faculty of Science and Technology 715

VUV emission and energy transfer phenomena in rare gas mixture discharges.

by

ANDREI MOROZOV

ACTA UNIVERSITATIS UPSALIENSIS
UPPSALA 2002

Dissertation for the Degree of Doctor of Philosophy in Physics presented at Uppsala University in 2002.

ABSTRACT

Morozov, A., 2002. VUV emission and energy transfer phenomena in rare gas mixture discharges. Acta Universitatis Upsaliensis. *Comprehensive Summaries of Uppsala Dissertations from the Faculty of Science and Technology* 715. 57 pp. Uppsala ISBN-91-554-5318-X

VUV emission spectra of Xe-X (X = He, Ne, Ar and Kr) and of Kr-Y (Y = He, Ne and Ar) mixtures with low concentrations of the heavier gases (0.1 - 1 %) and moderate total pressures (50 - 200 hPa) are recorded near each of the two resonance lines of Xe and Kr in DC glow capillary discharges. A tentative identification of the emission structures is given.

Numerical simulations of absorption spectra from Kr-Xe mixtures close to the Xe resonance line at 146.96 nm are performed. It is shown that the absorption structures can result from bound-bound and bound-free transitions in XeKr molecules between the ground state and the weakly-bound $1(^3P_1)$ excited state. The depth of the excited state is estimated.

Simultaneous observations of the VUV and visible - near IR emission from DC and RF discharges in gaseous Kr with small Xe admixture concentrations are conducted. A scheme of energy transfer processes in Kr-Xe mixtures is proposed. The emission spectra are used for investigation of energy transfer from the lowest excited states of both atomic krypton and krypton molecules to the ground state xenon atoms. Values of energy transfer rates from the 1_u state of Kr_2* molecules and from the system of the four lowest Kr excited states to Xe ground state atoms are obtained.

Energy transfer processes in gaseous Ar with a small admixture of N_2 excited in a transverse pulse discharge are investigated and an energy transfer scheme is proposed. The results confirm that all emitting species have Ar metastable state $^3P_2$ as their common source of excitation energy. Evidences of strong energy transfer from $Ar_2^*(1_u)$ molecules and the reabsorbed Ar state $^3P_1$ to atomic nitrogen are also obtained.

Key words: VUV spectra, excimers, energy transfer, rare gas discharges

Andrei Morozov, Department of Physics, Uppsala University, Box 530, SE-751 21, Uppsala, Sweden.

ISSN 1104-232X
ISBN 91-554-5318-X

Printed in Sweden by RK-tryck 2002

To Anita
and my parents

“Physics is full of surprises”
usually said by Reinhold Hallin

List of Papers

This thesis consists of the summary and the following papers. In the summary, the papers are referred by their roman numerals (I - V).

I **VUV emission spectra from binary inert gas mixtures near the resonance lines of Xe I and Kr I**
A. Morozov, B. Krylov, G. Gerasimov, A. Arnesen, R. Hallin
(Submited to J.Phys.B)

II. **Identification of structures in absorption spectrum of Kr – Xe gas mixtures close to the Xe resonance line at 146.96 nm**
A. Morozov, B. Krylov, G. Gerasimov, R. Hallin, A. Arnesen
Eur.Phys.J. D **11**, 379 (2000)

III. **Energy transfer studies in krypton-xenon mixtures excited in a cooled DC discharge**
B. Krylov, G. Gerasimov, A. Morozov, A. Arnesen, R. Hallin and F.Heijkenskjold.
Eur.Phys.J. D **8**, 227 (2000)

IV. **Study of atomic and molecular energy transfer channels in Kr - Xe gas mixtures excited with RF discharges**
A. Morozov, B. Krylov, G. Gerasimov, A. Arnesen and R. Hallin.
(accepted for publication in J.Phys.B)

V. **Energy transfer in argon-nitrogen mixtures excited in a pulsed discharge**
B. Krylov, A. Morozov, G. Gerasimov, A. Arnesen, R. Hallin and F.Heijkenskjold.
(in manuscript)

I have also made a minor contribution to the following paper which is excluded from the thesis:
Influence of VUV radiation from DC discharges in rare gas mixtures on MgF_2 window transmission.
G. Gerasimov, R. Hallin, E. Zhukova, B. Krylov, A. Morozov, F. Heijkenskjold, A. Arnesen, O. Kononova.
Optical Journal, **69,** 29 (2002) (in Russian)

Contents

1. Introduction.

The vacuum ultraviolet (VUV) wavelength region is the spectral range between the ultraviolet (UV) and the soft X-ray regions. The long wavelength limit of the VUV range (200 nm) is where the continuous absorption by oxygen begins and expands towards longer wavelengths. For this reason all observations of emission and absorption in this range are carried out in vacuum and the region is therefore called the "vacuum" UV.

Recently an increasing attention has been paid to VUV emission from various types of discharges in rare gases and their mixtures. The main reason for the interest is connected with a great scientific and technological demand for VUV radiation sources, including VUV lasers. Nowadays a specially great technological need exists for short wavelength radiation sources suitable for microlithography.

Discharges in rare gases have served for long time as simple and versatile broad VUV radiation sources in VUV spectroscopy. The principal properties of the emission from rare gas discharges originate from the structure of rare gas diatomic molecules, which belong to the *excimer* class of molecules. The word 'excimer' was created by combining the two words *excited* and *dimer* (diatomic molecule). The term is used for a broad class of diatomic molecules, homo- and heteronuclear, which have stable excited states while the ground state is repulsive or has just a very shallow potential well (van der Waals minimum).

However, the VUV emission from pure rare gas discharges usually cannot be used in applications that require narrow-band and intense radiation. This is why the emission from rare gas mixtures became the subject of a considerable number of experimental and theoretical studies: it was shown that at certain conditions these mixtures produce intense VUV radiation in a narrow band around the atomic resonance lines of the heavier gas admixture [1-3].

A second stimulating factor for these studies was that at even very small heavier gas admixtures did not only these intense bands appear, but it was observed that the VUV emission from the main gas could undergo a drastic reduction [1-3]. This suggests the existence of very efficient energy transfer processes from the main gas to the admixture.

Nevertheless, while the understanding of the internuclear potentials of the ground and excited states of homonuclear dimers is well established and emission spectral structures from pure rare gas discharges are reliably identified, the situation for heteronuclear dimers is much less satisfactory. Detailed data exist only for the ground states and were obtained by fitting theoretical potentials to a compilation of experimental results [4]. Data on the lowest excited states is much more scarce. Some information has been obtained from absorption spectroscopy [5,6] and from surface VUV emission results [7]. A few theoretical studies in the form of semiempiric calculations on the lowest excited states have been performed. These supply the principal information on the internuclear potential curves for some of the lowest excited states [8,9].

Therefore considerable work is still to be done to obtain reliable parameters of the excited heteronuclear dimer potentials and to identify the emission structures from discharges in rare gas mixtures. In this thesis an attempt is made to interpret these emission spectra based on spectroscopic data, both from emission (**Paper I)** and absorption (**Paper II)**, using data supplied by semiempiric calculations [9]. The results of these studies were in turn used in energy transfer studies in an attempt to build a reliable scheme of the energy transfer processes in Kr – Xe mixtures (**Paper III)** and to obtain the values of the energy transfer rates (**Paper IV)**.

Energy transfer processes in Ar – N_2 mixture discharges, which are known to produce intense N I lines in the VUV, were also studied and a scheme of energy transfer from Ar to atomic nitrogen was proposed (**Paper V**).

2. VUV emission from pure rare gas discharges.

2.1 General VUV emission features and molecular properties.

The first feature which attracted the attention of spectroscopists to the rare gas excimers was the observation of a broad VUV emission from discharges in rare gases and its identification as the emission from homonuclear rare gas dimers [10] (see Fig. 1).

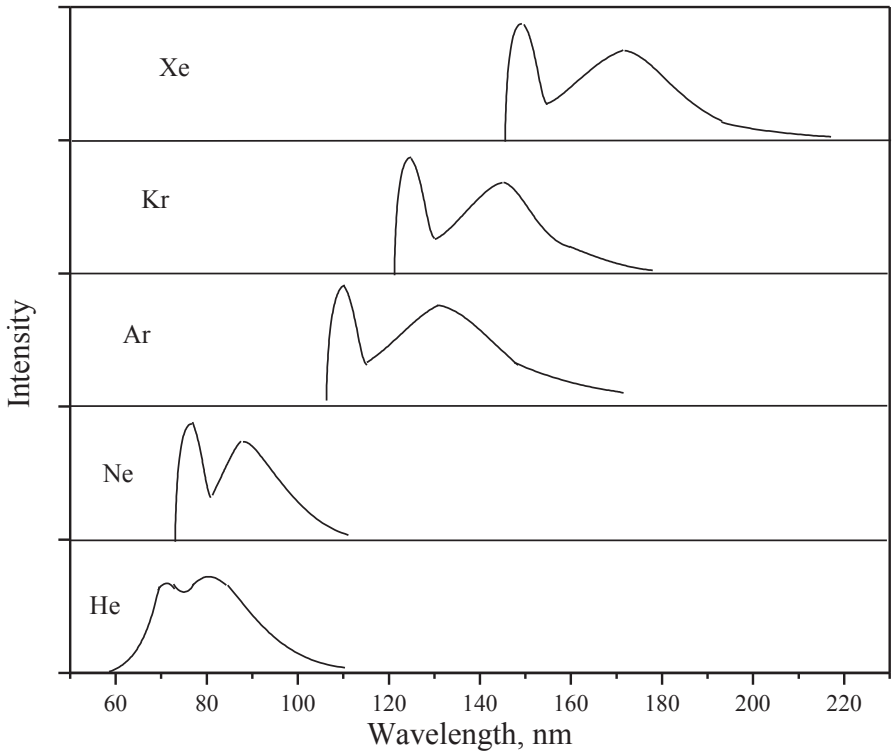

Fig. 1 Schematic diagram of the emission continua from pure rare gases.

The general emission features can be shown taking krypton as an example since the rest of the rare gases have similar molecular structure and, as the result, exhibit similar spectroscopic properties. Fig. 2 shows a typical emission spectrum from a direct current (DC) capillary discharge in 200 hPa of Kr.

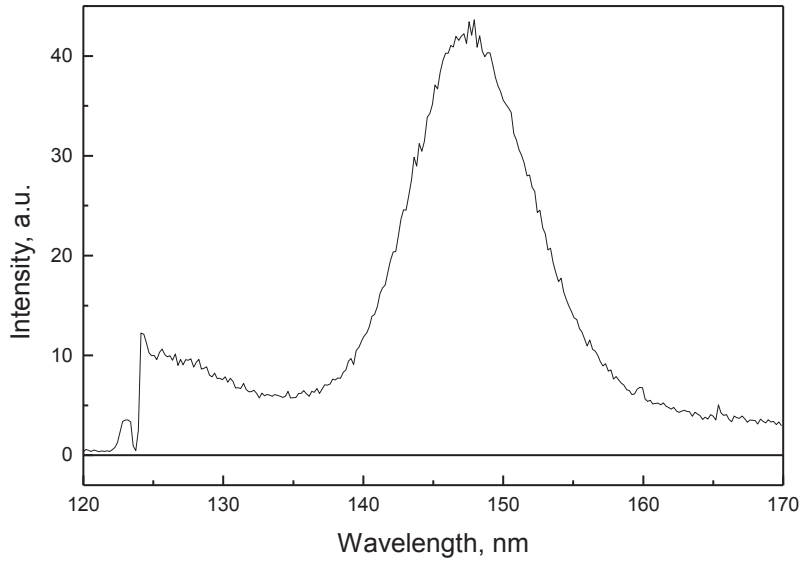

Fig.2 Emission spectrum from a DC capillary discharge in 200 hPa of Kr.

One can see that the emission, which starts from the first resonance line of Kr I at 123.58 nm, is a broad continuum with two maxima. The first maximum is situated close to the strongly self-absorbed resonance line and the second is located near 150 nm. The part of the continuum emission from the resonance line to the minimum at about 135 nm is usually called 'the first continuum', while the part from this minimum and towards longer wavelengths is called 'the second continuum'.

To explain the origins of these structures we regard the potential curves of Kr_2 molecular states. Fig. 3 contains schematic potential curves of Kr_2 molecules for the ground state and the two lowest excited 0^+_u and 1_u states. These are the states that are involved in the molecular bound-free transitions which form the continuous emission: transitions from vibrational levels of the excited states down to the repulsive part of the ground state result in a broad continuous emission.

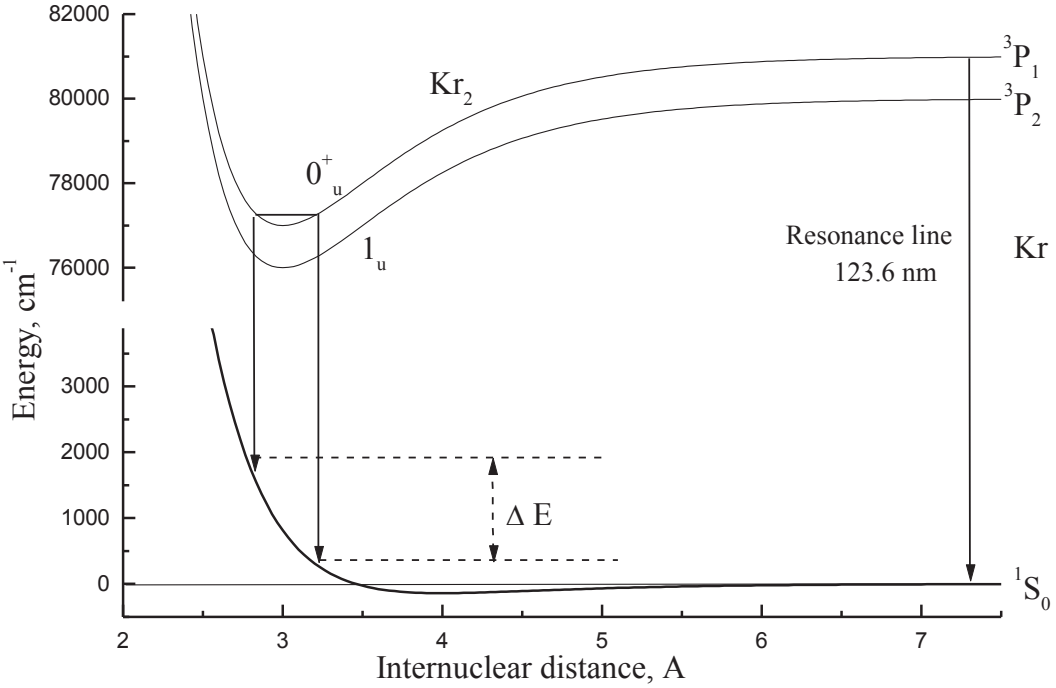

Fig.3 Schematic potential curves of the ground state and the two lowest excited states 0^+_u and 1_u of the Kr_2 molecule. ΔE indicates how broad in an energy scale the contribution from a single vibrational level of the excited 0^+_u state could be in bound-free transitions.

The potential well depth of the excited states is about 4000 cm^{-1} while the ground state well is only about 200 cm^{-1} deep, which is of the same order as ***kT*** for room temperature. Note that the internuclear equilibrium distance (the internuclear distance where the potential energy is lowest) for the excited states is considerably (about 1 Å) smaller than the equilibrium distance for the ground state. Therefore even the transitions from the lowest vibrational levels of the excited states produce broad spectral profiles. Note that the highest vibrational levels contribute mainly to the first continuum (short wavelengths) while the lowest vibrational levels are mainly responsible for the second continuum emission (long wavelengths).

The shape of the emission profiles from excimer molecules depends critically on the gas pressure and temperature, but also, on the method of gas excitation.

2.2 DC glow discharges in rare gases

The main gas excitation technique used in our studies was the DC (direct current) glow discharge. This discharge appears in a gas between two electrodes when a sufficient voltage is applied. The current in this type of discharge is of the order of milli-amperes, which is in contrast to the two other types of discharge that could be formed between two electrodes: at low pressures a Townsend discharge with typical currents of micro-amperes could occur as well as an arc discharge in the form of short-living sparks with currents reaching the level of amperes [11] (see Fig. 4).

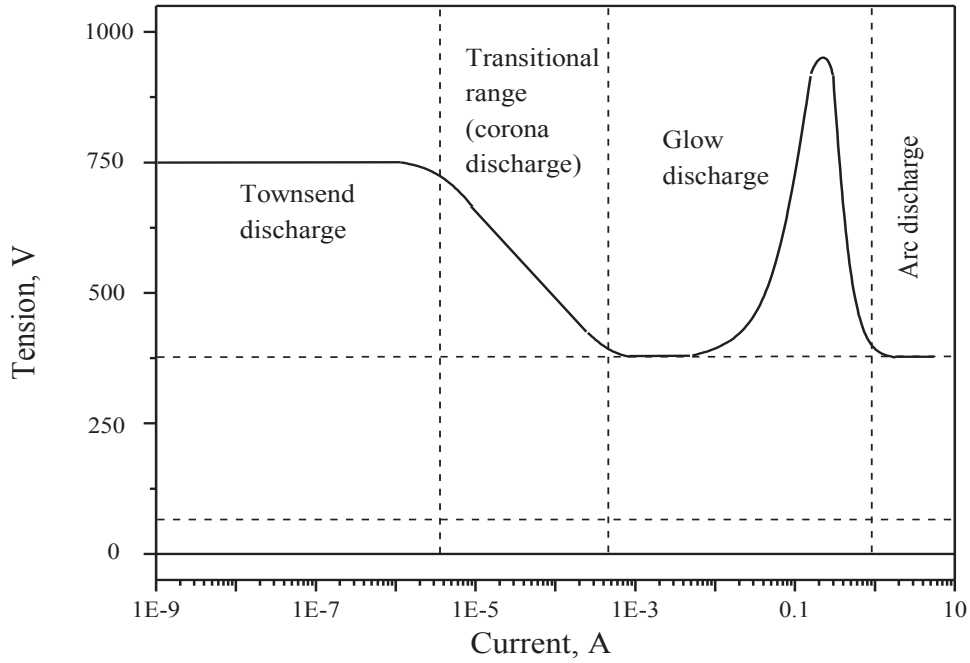

Fig. 4 Volt-current characteristics of a DC discharge.

A glow discharge has several regions with quite different properties, as can be seen from luminous phenomena. Fig. 5 presents these phenomena for a particular case.

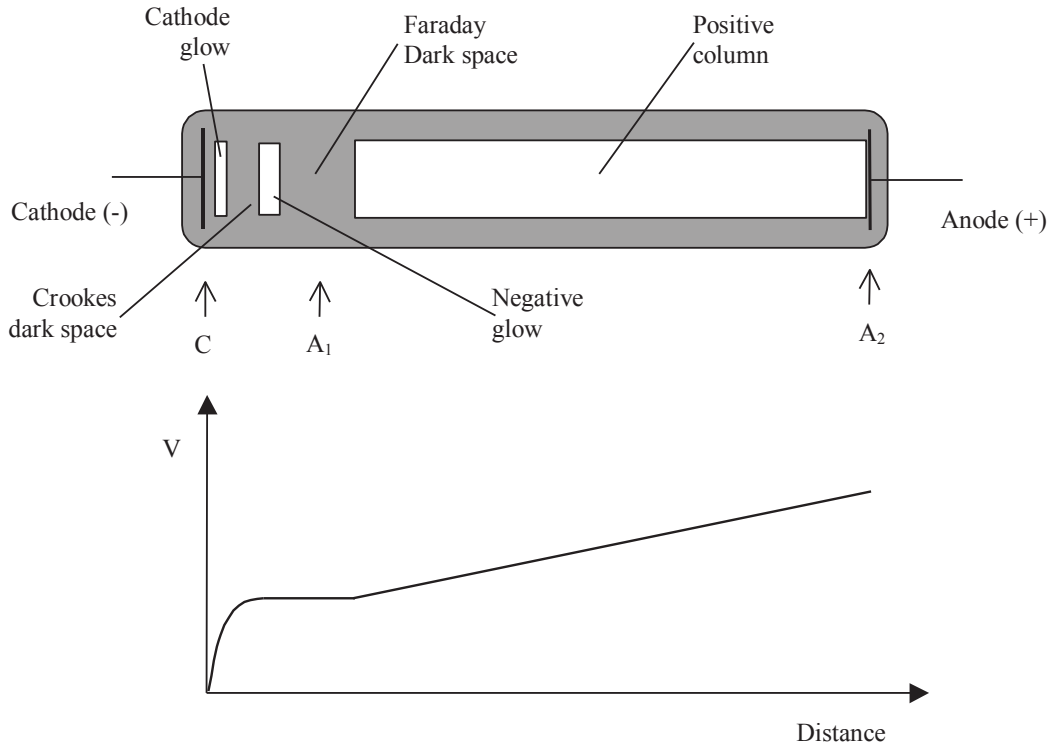

Fig. 5 A simplified diagram of a glow discharge between cathode C and anode A_2. The upper part shows the optical phenomena, while a typical potential distribution between the electrodes is presented below.

Note that a positive column is formed only if the cathode-anode separation is long enough: if we take A_1 to be the original position of the anode and increase the cathode-anode separation to CA_2 we will see how the positive column appears gradually, while the phenomena at the cathode end remain practically unchanged. A further increase of the distance between the electrodes merely lengthens the positive column.

It is the positive column that was used for gas excitation in our studies. More precisely, we used a homogeneous positive column, i.e. a column with the same structure throughout the length of the discharge tube. The most remarkable fact about the homogeneous column is that the strength of the electric field in the column is constant [11]. From this we may immediately conclude that the gas in the column contains an equal number of positive ions and electrons per cm^3. Here, then, we have a perfect example of a plasma.

The type of gas excitation determined the design of our discharge tubes. The principal details of the setup will now be discussed. The DC discharge tube (see Fig. 6) which was used in our studies of VUV emission from rare gases was made of fused silica with windows of magnesium fluoride to allow detection of the VUV

spectrum down to 115 nm. Two cold tungsten electrodes were melted into side branches to reduce the deposition of sputtered metal on the windows. The DC glow discharge with currents of 10 - 40 mA and a voltage across the tube of about 1 kV took place in a cylindrical capillary of 100 - 800 mm length and 1.4 mm inner diameter which was connected to a vacuum system so that it could be evacuated and filled with gas.

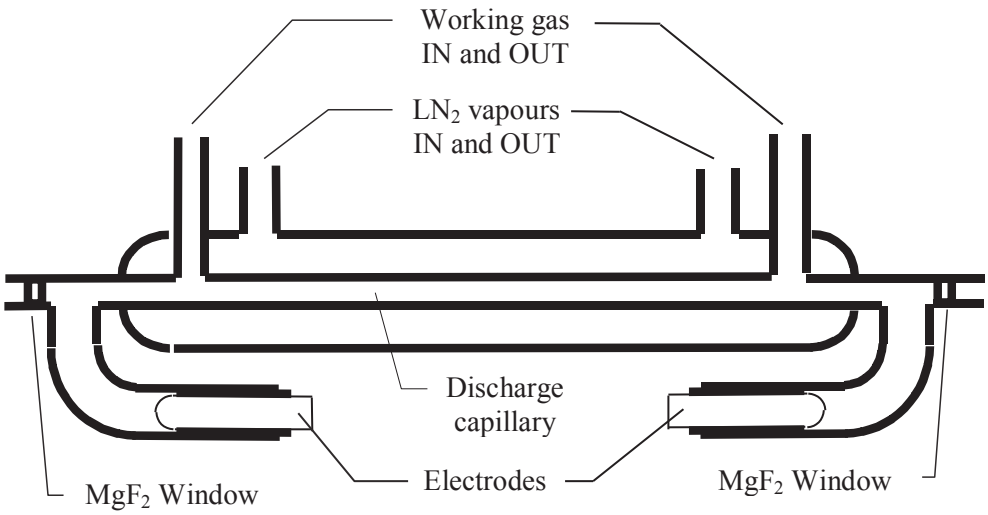

Fig. 6. Scheme of a DC discharge tube.

The capillary was surrounded by a concentric tube also made of fused silica. The volume inside this tube could be either flushed with cold nitrogen vapours or filled with liquid nitrogen in order to cool the capillary wall.

2.3 Creation of excimer molecules in rare gas discharge media.

The main process of excimer formation in rare gas discharge media has two phases. The first stage is the creation of excited atoms in the lowest excited and relatively long-living states $^3P_2$ and $^3P_1$. The state $^3P_2$ is metastable and the state $^3P_1$ is resonant, but due to strong radiative trapping the $^3P_1$ state usually has an effective lifetime of the same order as the metastable state.

The second stage is the formation of dimers in three-body collisions between an excited atom in one of these two states and two atoms in the ground state (see e.g. [12]):

$X^* + X + X \rightarrow X_2^* + X$,

where X could be any rare gas: Ne, Ar, Kr or Xe. Note that for the dimer creation, the probability of the three-body reaction is much higher than the probability of the two-body reaction, when only one ground state atom is participating, as follows from the law of energy and momentum conservation (we do not treat the cases of extremely low pressures). Note that since the dimers are created in three-body collisions, the formation rate is proportional to the square of the rare gas pressure.

As for the first stage, the excited atoms in the lowest states are created in two different ways. Firstly, by direct electron excitation:

$$X + e^- \rightarrow X^* (^3P_1, ^3P_2) + e^-,$$

and secondly, from rare gas ions, after recombination and radiative cascades:

$$X^+ + X + X \rightarrow X^+_2 + X \qquad \text{(creation of molecular ions)},$$

$$X^+_2 + e^- \rightarrow X^{**} + X + X \qquad \text{(recombination)},$$

$$X^{**} \xrightarrow{h\nu} \ldots \xrightarrow{h\nu} X^* (^3P_1, ^3P_2) \qquad \text{(radiative cascades)},$$

where X** are highly excited states of the rare gas atoms, which have very short lifetime. Note that the atomic ion recombination is not included, since its rate is much smaller than the rates for the molecular ion creation and molecular recombination if the total pressure is not extremely low.

There is also another possible way of excimer formation by direct electron excitation of ground state dimers:

$$X_2 + e^- \rightarrow X_2^* + e^-,$$

However, the rate of this reaction [12] is quite low in comparison with the rate of the process discussed above for the pressure range and excitation technique used in our present studies.

2.4 Pressure, current and temperature dependencies of emission profiles.

Our experiments with Ar, Kr and Xe showed a quite weak dependence of the continuum intensity on the discharge current in the range 10 – 40 mA. This might seem strange, since an increase of the current from 10 to 40 mA should increase the power input in the gas at least four times. There is, however, an optical process that hinders the light propagation along the axis inside the capillary. This process is the so cold “thermal lens” – a defocusing effect due to the

temperature gradient (and consequently, density gradient) from the capillary axis, where the temperature is highest, towards the capillary wall. Thus an increase of the current also increases the strength of the thermal lens which reduces the observed intensity. The very strong influence of the current on the thermal lens effect was confirmed by passing visible laser light through the discharge capillary and observing the laser beam spot size for different currents. The increase of the temperature also reduces the gas density in the discharge volume, decreasing the emission intensity.

DC discharges in rare gases exhibit strong dependence on the gas pressure. As an example, the emission from 300, 130 and 80 hPa of xenon is shown in Fig. 7.

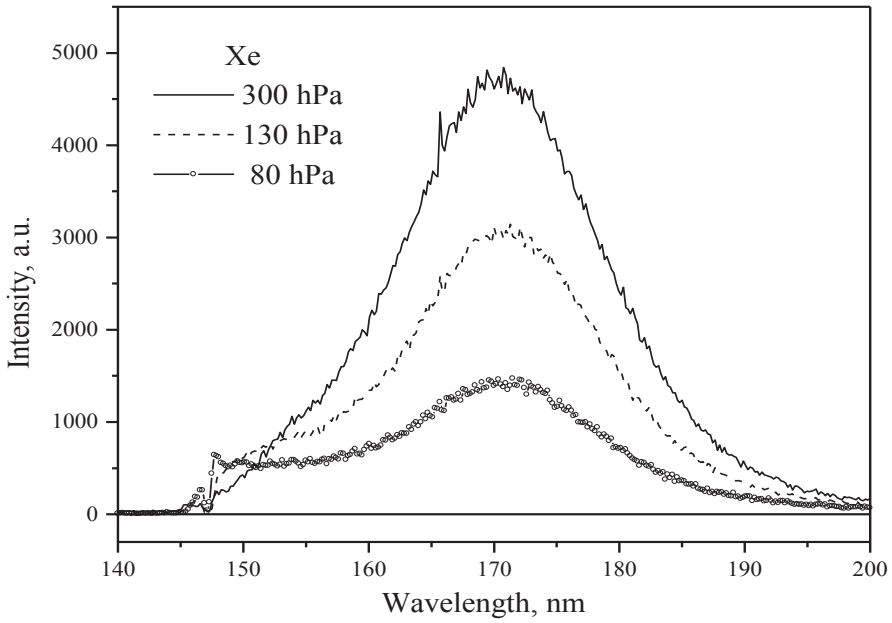

Fig. 7 Xe_2^* emission from DC discharge in 300, 130 and 80 hPa of xenon.

The first resonance line of Xe at 146.9 nm is completely self-absorbed in all spectra. The second continuum intensity grows with the gas pressure. The reason is that the formation rate of excimers in three body collisions, as was discussed earlier, is proportional to the square of the gas pressure. The growth rate is stronger for lower pressures, most probably due to the strong reduction of the continuum intensity by the thermal lens effect at high pressures, since the higher is the gas pressure the stronger is also the gas heating. The intensity of the first continuum, on the contrary, decreases with increasing gas pressure. This is because of the strong

absorption close to the resonance line by Xe_2 ground state molecules but also because of an increased rate of collisional relaxation, which depopulates upper vibrational levels in favour of the lower vibrational levels.

The effect of the gas temperature on emission intensity is shown in Fig. 8.

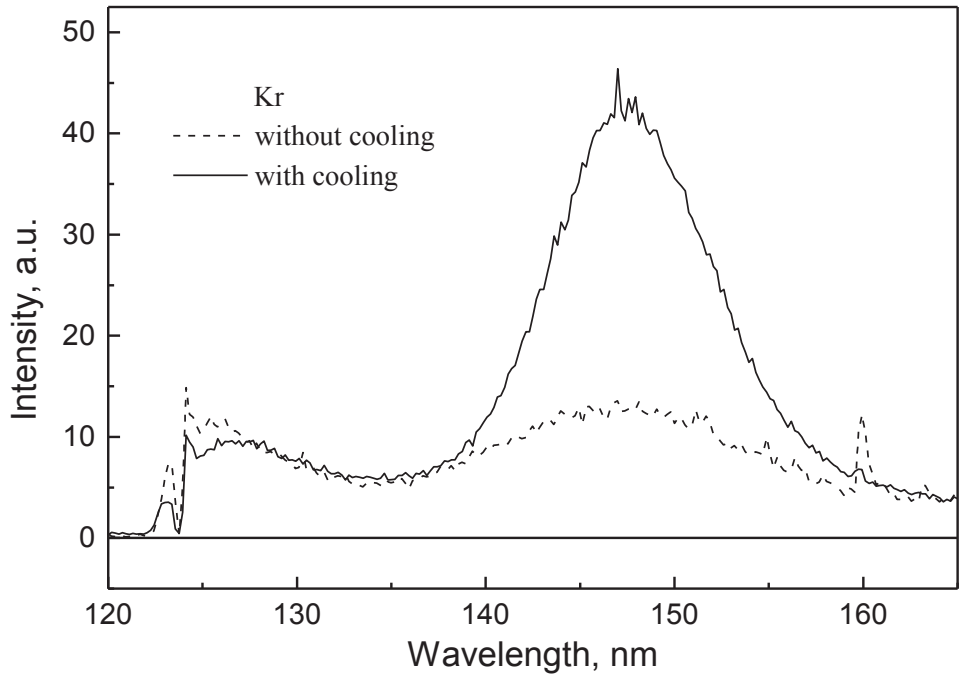

Fig. 8 Emission spectra from a DC discharge in 200 hPa of Kr without cooling and with liquid nitrogen vapour cooling.

One can see that the intensity of the second continuum greatly increases with gas cooling, while the intensity of the first continuum remains practically unchanged. This increase of intensity could in part be explained by the increased Kr density and by the freezing of impurities, since a considerable reduction in CO bands (emission and absorption) was observed. However, improved relaxation down the vibrational levels of the Kr_2* molecules at low gas temperatures can also be a highly contributing factor. Indeed, an increase in population of the lowest vibrational levels will cause a growth of the second continuum, while a decrease of the highly situated level populations would cause a decrease in the relative intensity of the first continuum.

3. VUV emission from DC discharges in rare gas mixtures.

The VUV emission of homonuclear rare gas excimers, which was described in the previous chapter, has found a broad range of scientific application, especially where a continuum VUV source is required (e.g. in absorption spectroscopy [6]). The complete population inversion of the bound-free transitions, which give rise to the second continuum, has attracted the attention to the rare gases as an active medium for VUV lasers. As a result, Ar_2, Kr_2 and Xe_2 laser action with electron beam pumping was obtained (e.g. [13,14]). However, the gain of these media is quite weak, and the power output of such lasers is very low. Nevertheless a strong technological demand for bright and practical VUV light sources stimulated research in a related area, namely the VUV emission from discharges in binary rare gas mixtures. In this chapter we discuss firstly the general properties of emission from such mixtures, then give a detailed description of the intense and narrow VUV emission that appears close to the resonance lines of the heavier gas admixture and finally discuss the origin of the spectral structures.

3.1 General VUV emission properties.

The first observations of VUV emission from discharges in rare gas mixtures were performed in the beginning of the 1970's [1,2] and showed a remarkable feature: if a small amount of a rare gas admixture is added to a lighter main rare gas, an intense and narrow emission appears close to the atomic resonance lines of the admixture gas. This effect is accompanied by an intensity decrease of the continuum emission from the main gas homonuclear excimer, and the higher is the concentration of the admixture, the stronger is this decrease. As an example, Fig. 9 shows the VUV emission from DC discharge in 400 hPa of pure Kr and from a mixture of 400 hPa of Kr with 0.1% of Xe.

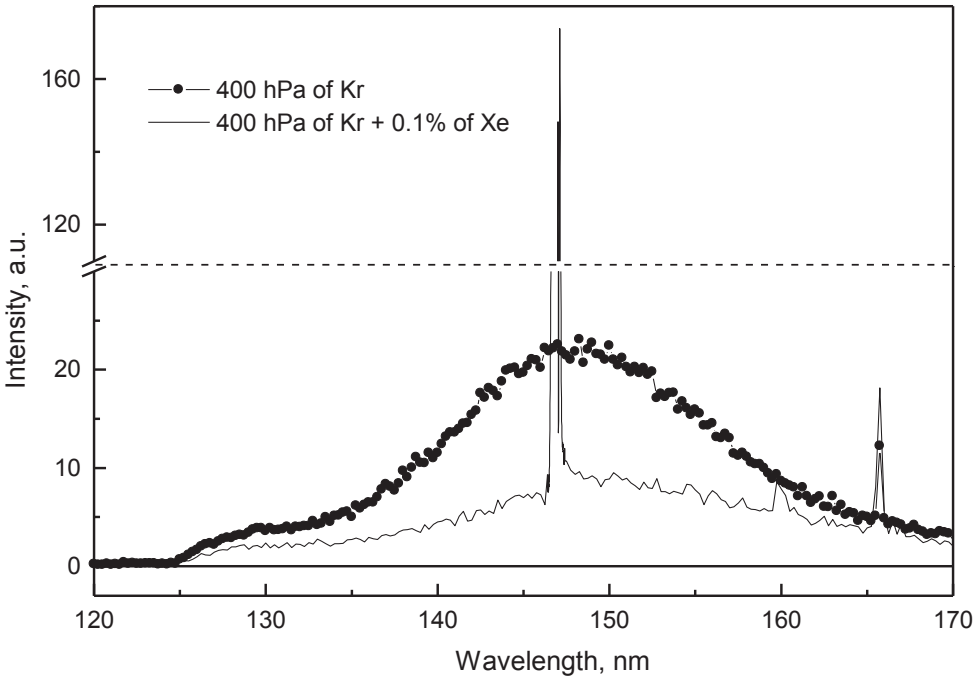

Fig. 9 Emission spectra from a DC discharge in pure Kr and in a Kr-Xe mixture.

When one gradually increases the admixture concentration, new broad spectral structures appear towards longer wavelengths from the resonance lines. A spectral structure which is easily identified as the second continuum of the admixing gas (e.g. [15]) appears already at about 0.5 % of admixture concentrations if the total gas pressure is high enough (starting from ~ 300 hPa). Fig. 10 gives an example of this phenomenon with emission spectra from a DC discharge in a Kr-Xe gas mixture.

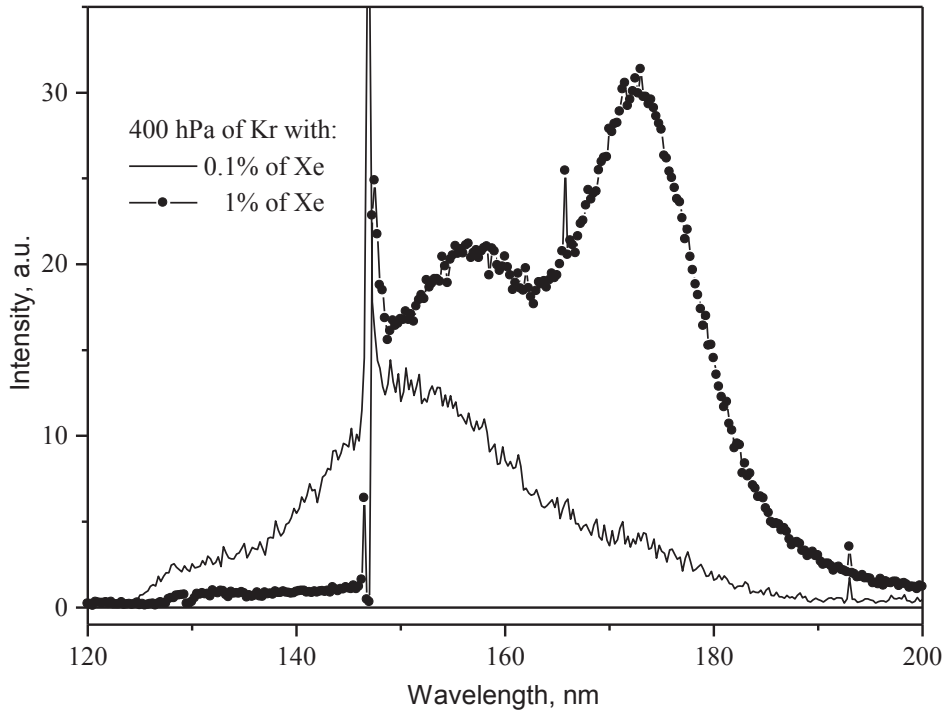

Fig. 10 Emission spectra from a DC capillary discharge in 400 hPa of Kr with 0.1% and 1% of Xe. The temperature of the capillary wall is kept very low, but higher than the gas condensation temperature.

The broad structure at ~ 157 nm in Kr-Xe mixtures (see Fig. 10), as well as the corresponding structure in Ar-Xe and Ar-Kr mixtures close to the first resonance lines of the heavier gas admixtures, were identified as the emission from heteronuclear excimer molecules (e.g. see [3,7]). The origin of the structure was found to be in bound-free transitions from the relatively strongly bound lowest excited states of the binary heteronuclear molecules down to the repulsive part of the ground state, that is the spectral structures are similar in origin to the first and second continua from the discharges in pure rare gases.

Already the earliest studies [1] showed that such a reduction of the host gas emission intensity and the appearance of the strong admixture-related emission could not be the result of direct electron excitation of the admixture atoms. The only possible explanation is then the existence of an efficient energy transfer process from the main gas to the admixture. Chapter 4 is devoted to the discussion of this phenomenon.

While the origins of the broad structures were established, the nature of the narrow emission around the resonance lines is still to be

established. The next two chapters describe our contribution to the study of the spectral profiles of these narrow structures and present a discussion of their possible identifications.

3.2 VUV emission spectra from binary rare gas mixtures close to the resonance lines of Kr I and Xe I.

The authors of the first experimental studies of VUV emission from rare gas mixtures [1,2] interpreted the intense and narrow bands close to the resonance line of the admixture solely as self-absorbed resonance lines. However, emission spectra recorded at higher resolution showed that the emission profiles are quite complex and show a number of structures. As an example, a spectrum from an Ar-Xe mixture is shown in Fig. 11:

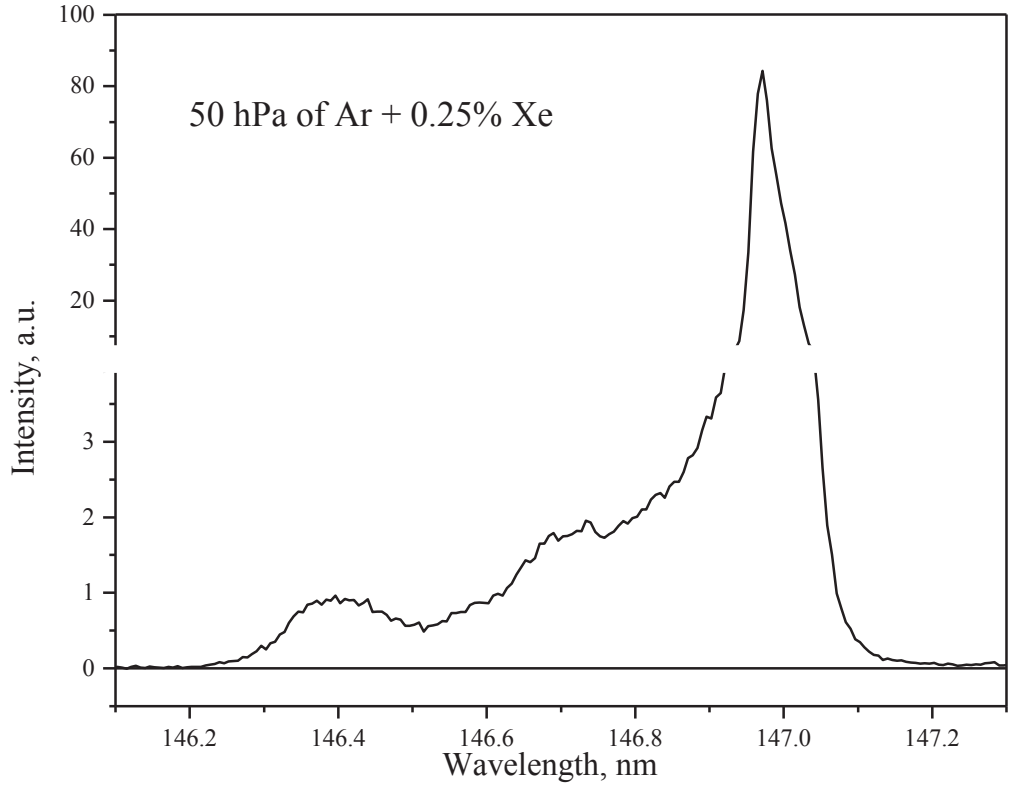

Fig. 11 Emission spectrum from a DC capillary discharge in an Ar-Xe mixture close to the first resonance line of Xe.

Paper I presents a study of emission spectra of Xe-X (X = He, Ne, Ar and Kr) and of Kr-Y (Y = He, Ne and Ar) rare gas mixtures with low concentrations of the heavier gases (0.1 - 1 %) and moderate total pressures (50 - 200 hPa), which have been recorded

near each of the two resonance lines of Xe and Kr in DC glow capillary discharges. In this review only a short discussion of the principle results is given.

Fig. 12 shows the pressure dependence of spectral profiles from Xe-X (X = He, Ne, Ar, Kr) mixtures close to the first resonance line of Xe at 146.96 nm. Note that the intensity is given in a logarithmic scale and the wavelength range is different for all four charts, while the wavelength scale increment is the same.

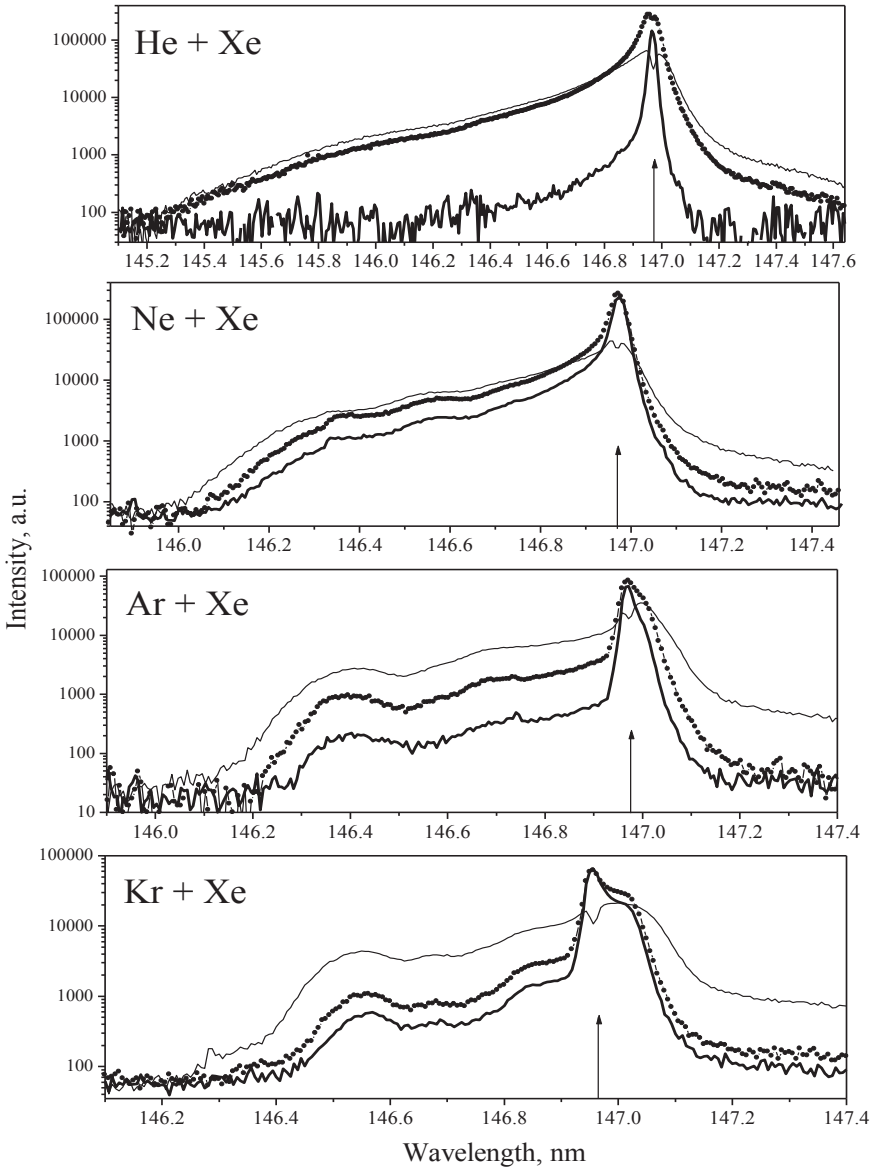

Fig. 12 Emission spectra from binary mixtures containing small amounts of Xe with He (top), Ne, Ar and Kr (bottom) near the first resonance line of Xe I. The conditions are: 100 hPa main gas pressure + 1 % Xe (thin line), 50 hPa main gas pressure + 0.25 % Kr (dotted line) and 50 hPa main gas pressure + 0.1 % Kr (thick line). The arrow marks the position of the atomic resonance line.

The analysis of the emission profiles around the four resonance lines (two of Kr I and two of Xe I) gave the following facts for the mixtures with heavier gas concentrations ≤ 1 %:

* The spectra have the highest intensity in the vicinity of the resonance line (± 0.05 nm)

* The self absorption, which appears around the resonance lines, depends heavily on the geometry of the discharge and on the pressures of both the admixture and the main gas.

* All the spectra have 'blue' and 'red' wings on the short and long wavelength sides of the resonance lines.

* Starting from a certain admixture concentration and for higher concentrations, the blue wings have a fairly well defined cut-off wavelength, i.e. where the intensity reaches the background level. The cut-off wavelength decreases very slowly with an increase of the main or admixture gas pressure.

* For a certain admixture gas, the lighter the main gas, the longer is the blue wing for the same pressures and the fewer are the structures that appear in the wing.

* The red wings from the heavy mixtures (mixtures with Ar and Kr as the main gas) contain a narrow and intense shoulder in the vicinity of the resonance lines. The spectral profiles from light mixtures (mixtures with He and Ne as the main gas) do not have this structure.

* The red wings for the heavy mixtures expand significantly towards longer wavelengths with increasing admixture concentration.

In the mixtures with Kr, the effect of gas cooling was also studied. To decrease the temperature of the gas mixture in the discharge volume, the wall of the capillary was cooled with liquid nitrogen (details of the experimental setup are the same as discussed in section 2.2). The spectral profiles close to both resonance lines of Kr behave in a similar way: the intensity of the blue wing decreases while the intensity of the red wing increases with cooling. Fig. 13 gives an example of this effect in Ne-Kr and Ar-Kr mixtures.

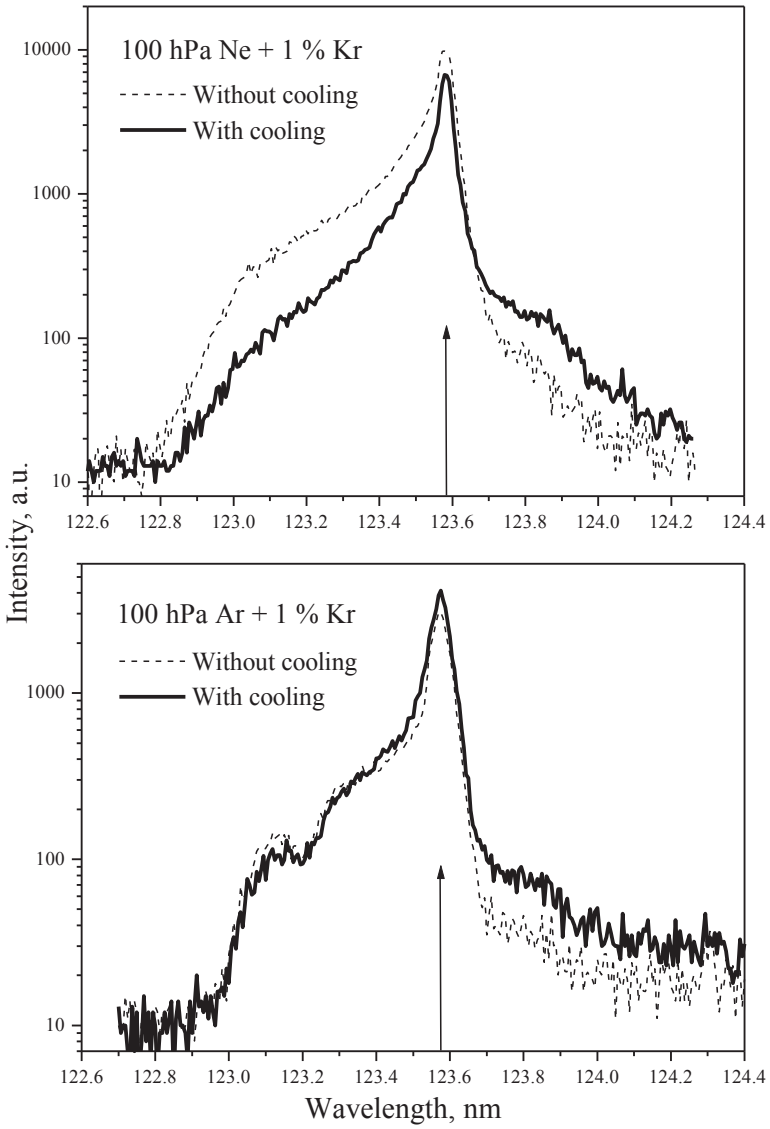

Fig. 13 The effect of cooling on emission profiles near the first resonance line of krypton is demonstrated for Kr mixtures with Ne (top) and Ar (bottom). Dashed lines represent the case when no cooling is applied while solid lines show the spectral profiles from discharges when the outer wall of the capillary was cooled with liquid nitrogen.

The information obtained from the emission profiles near the resonance lines, which was described above, together with data supplied by the corresponding high resolution absorption spectra, which are available in the literature, will serve as a basis for the identification of these spectral structures, presented in the next section.

3.3 Identification of the emission structures from binary rare gas mixture discharges close to the resonance lines of admixture atoms.

When one compares emission spectra from rare gas mixtures close to the atomic resonance lines of the heavier gas admixture with the corresponding high resolution absorption spectra, there is a striking similarity between the absorption and emission spectral profiles for all mixtures. This is demonstrated in Fig. 14, where two pairs of emission and the corresponding absorption spectra are given for Kr – Xe mixtures near the first resonance line of Xe and for Ar – Xe mixtures near the second resonance line of Xe.

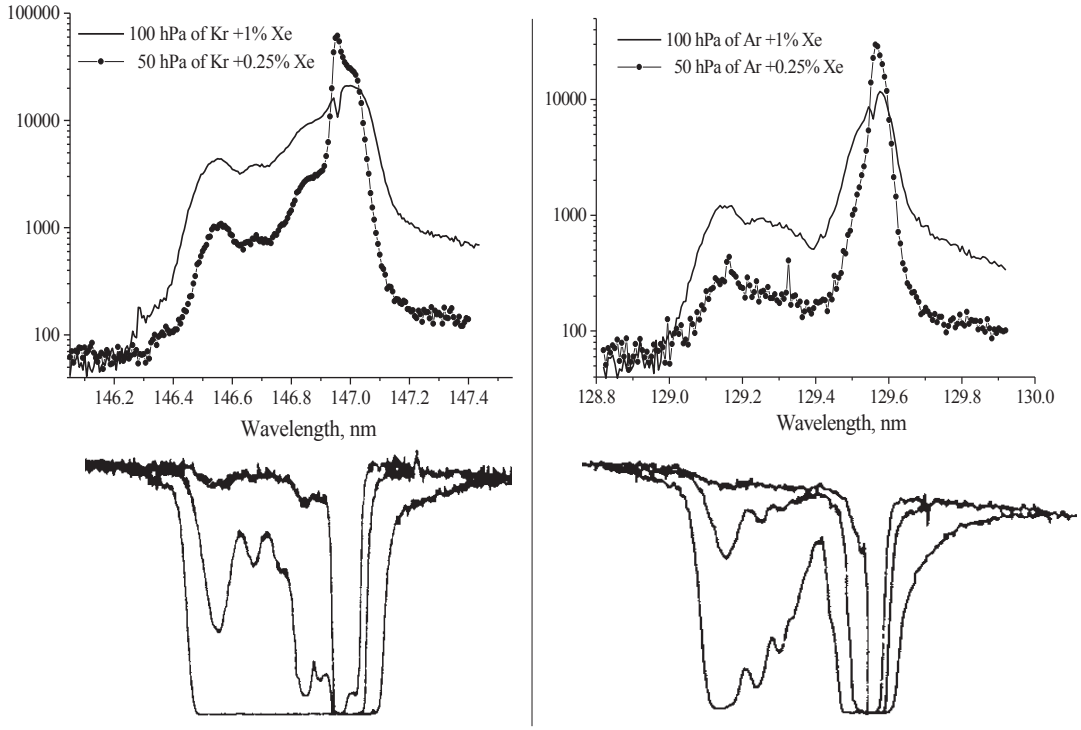

Fig. 14 A comparison of emission and absorption [6] spectral profiles is given for mixtures of small amount of Xe with Kr (left) and Ar (right). The top charts show the emission spectra, while the bottom charts present the corresponding absorption spectra (densitometer traces). Two emission profiles are given: 100 hPa main gas pressure + 1 hPa of Xe (solid line) and 50 hPa main gas pressure + 0.13 hPa of Xe (dotted line). The absorption spectra from [6] were recorded with a Xe pressure of 0.13 hPa and main gas pressures of 8, 215 and 650 hPa.

This similarity suggests that the same transitions give rise to the main spectral features in both absorption and emission. This can help to identify the origins of the emission structures, using the data on the transitions obtained from absorption studies. There are two factors that make it considerably easier to interpret absorption spectra. First

of all, in absorption studies practically all atoms and molecules are in their ground states, while in emission studies several molecular and quasimolecular excited states could be populated and give their spectral contribution at the same wavelengths, and therefore their relative populations, which depend on the type of excitation and the gas conditions, should be taken into account. The second important factor is that absorption studies can be performed at very low temperatures (e.g. the temperature of liquid nitrogen), assuring that the rotational blurring will be quite weak. In emission studies with DC discharge excitation, the gas heating may cause closely situated discrete structures to overlap.

3.3.1 Absorption structures and their identification.

The absorption spectra from binary rare gas mixtures were studied experimentally at very high resolution (~ 0.002 nm) by Castex [5] and by Freeman et al [6].The studies showed that the absorption spectra close to the resonance lines of the heavier gas admixture contain a number of bands in both the red and blue wings, and the heavier the gases, the larger is the number of bands. As an example, an outline of Kr – Xe mixture absorption data around the first resonance line of Xe is given in Fig. 15.

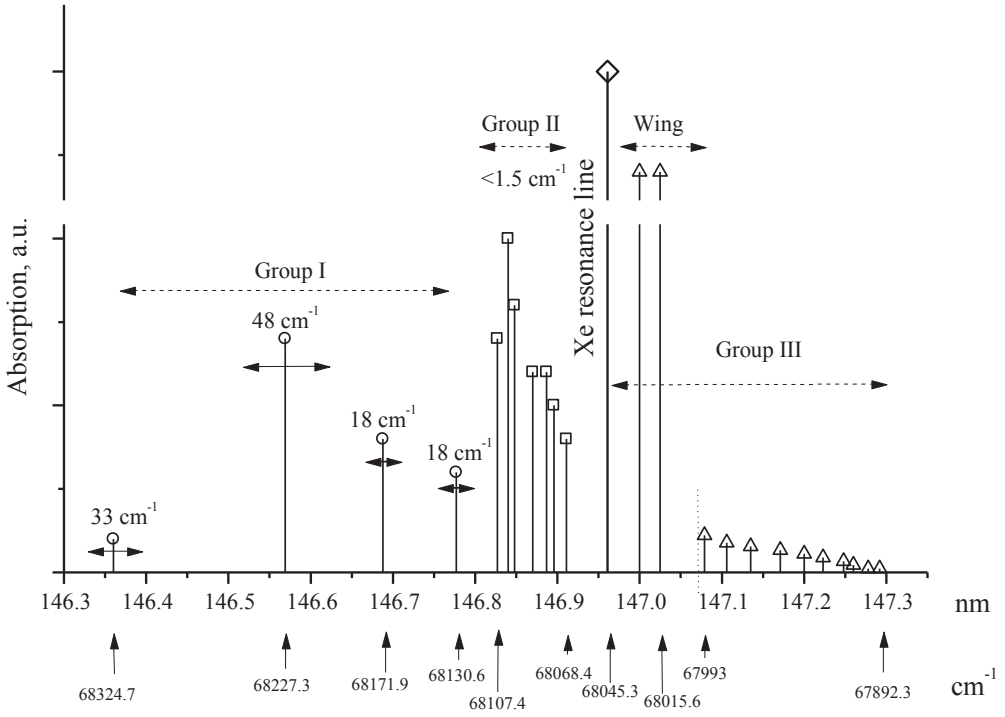

Fig. 15 An outline of experimental results obtained by Freeman *et al* [6]. Vertical lines represent the positions (in nm and cm^{-1}) of spectral bands. The height of the lines gives only the relative absorption of the band within the Band Group it belongs to. Where available, the width of a band is shown on top of the line. The Xe resonance line is marked with a diamond. Band Group III (triangles) contains also the diffuse wing, adjoined to the resonance line: two of the most intense bands represent the maxima of the wing. Band Group I (hollow dots) consists of four very broad and diffuse bands. Band Group II (rectangles) is composed of seven very narrow bands with widths less than 1.5 cm^{-1}.

A tentative identification of the bands, involving heteronuclear molecular states, was also suggested. The authors of [6] believed that the blue wing is due to bound-free transitions between the vibrational levels of the ground state and the repulsive part of the excited state (see Fig. 16) and that the red wing originates from bound-bound transitions between the vibrational levels of the ground and excited states. Castex gave a different identification: the blue wing is the result of all bound-free and bound-bound transitions, while the red wing arises from free-free transitions (i.e. transitions in free atomic pairs). In the latter type of transition, the absorbing atom is perturbed by a nearby atom of the main gas, but the atoms do not actually form a stable molecule with discrete vibrational levels. The wavelength of the transition is in this case given by the energy

difference between the potential curves of the heteronuclear molecule at the actual internuclear distance.

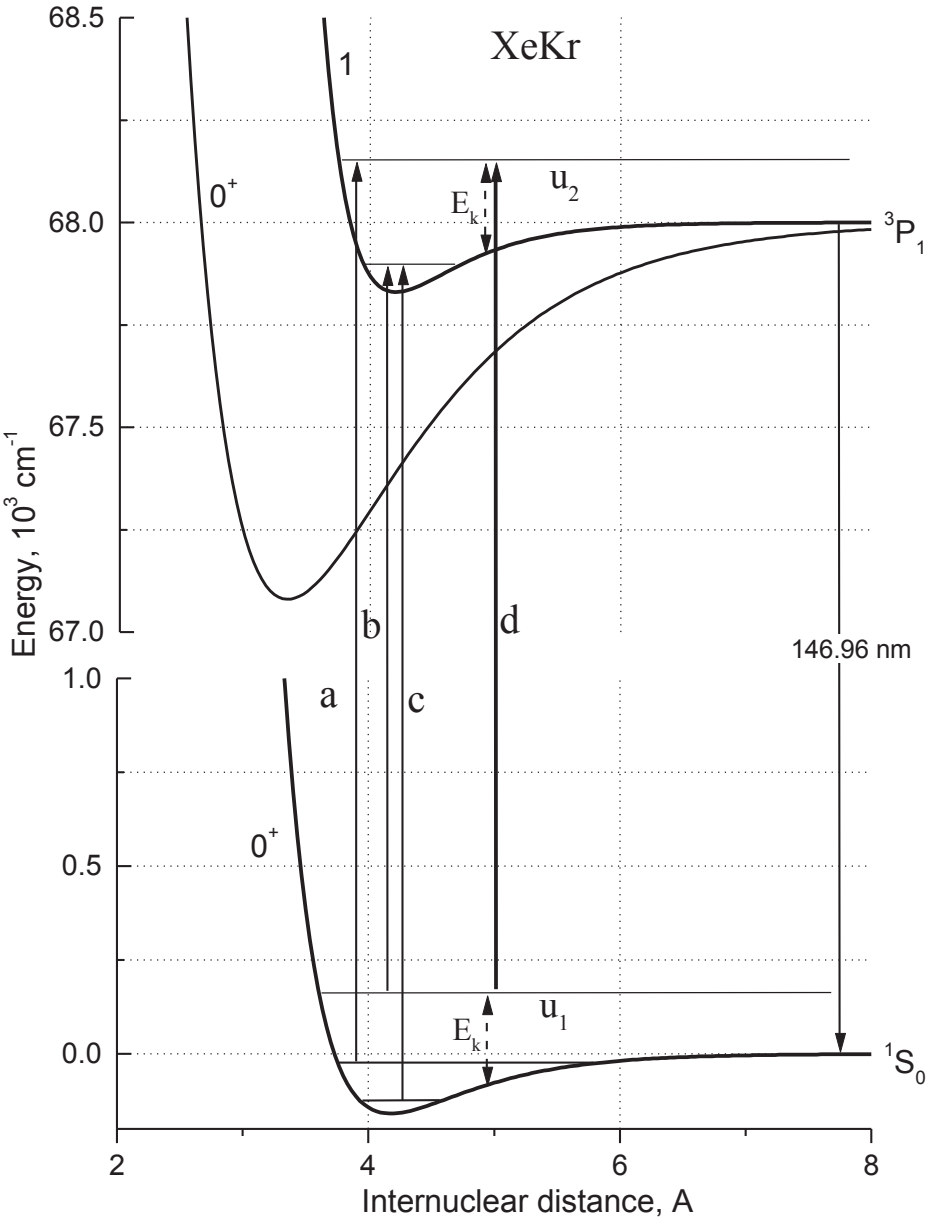

Fig. 16 A scheme of potential curves for the two lowest excited states and the ground state of the XeKr molecule. Examples of bound-free, free-bound, bound-bound and free-free transitions are marked with **a**, **b**, **c** and **d** respectively. The atomic resonance transition and its wavelength (146.96 nm) are also shown. For the free-free transition between the levels with total energy u_1 and u_2, $\mathbf{E_k}$ marks the kinetic energy of the Kr atom in the rest-frame of the Xe* atom. Since it is conserved in the emission/absorption, the wavelength of the transition corresponds to the energy difference between the excited and ground state potentials at the actual internuclear distance.

The idea that heteronuclear atomic pairs (bound or unbound) are responsible for the blue wing absorption was supported by the pressure dependence of the absorption intensity: the integrated intensity of every band in the blue wing increased linearly with the product of the main gas and admixture partial pressures [5]. Castex also reported that the dependence of the absorption intensity of the red wing on gas temperature supports her identification of the red wing.

One of the main obstacles to perform a reliable identification of the absorption structures was the lack of information on the potential curves of the excited states of heteronuclear molecules. Later semiempiric calculations were performed [8,9], and the existence of the weakly-bound molecular states $1(^3P_1, {}^1P_1)$ and relatively strongly bound states $0^+(^3P_1, {}^1P_1)$ was predicted for some configurations of Xe*Kr, Xe*Ar and Kr*Ar molecules. The parameters of these states (the equilibrium distances and well depths) were also estimated. The potential curves presented in Fig. 16 were prepared in the Morse form on the basis of these calculations.

The information supplied by the semiempiric calculations allowed us to support Freeman's identification for the Kr-Xe mixtures in a numerical spectral shape simulation (**Paper II**). The calculations were performed for bound-bound and bound-free transitions from the ground state of the XeKr molecule to the bound or repulsive part of the $1(^3P_1)$ state of the Xe*Kr molecule in order to simulate absorption structures close to the first Xe atomic resonance line. The simulations involved numerical calculations of the vibrational level energies and the corresponding radial nuclear wave functions for the ground and excited states from the radial Schroedinger equation. This information was then used to calculate the absorption profiles of bound-bound transitions in the adiabatic approximation from the overlap of the wave functions. As an example, the result of such a calculation is shown in Fig. 17.

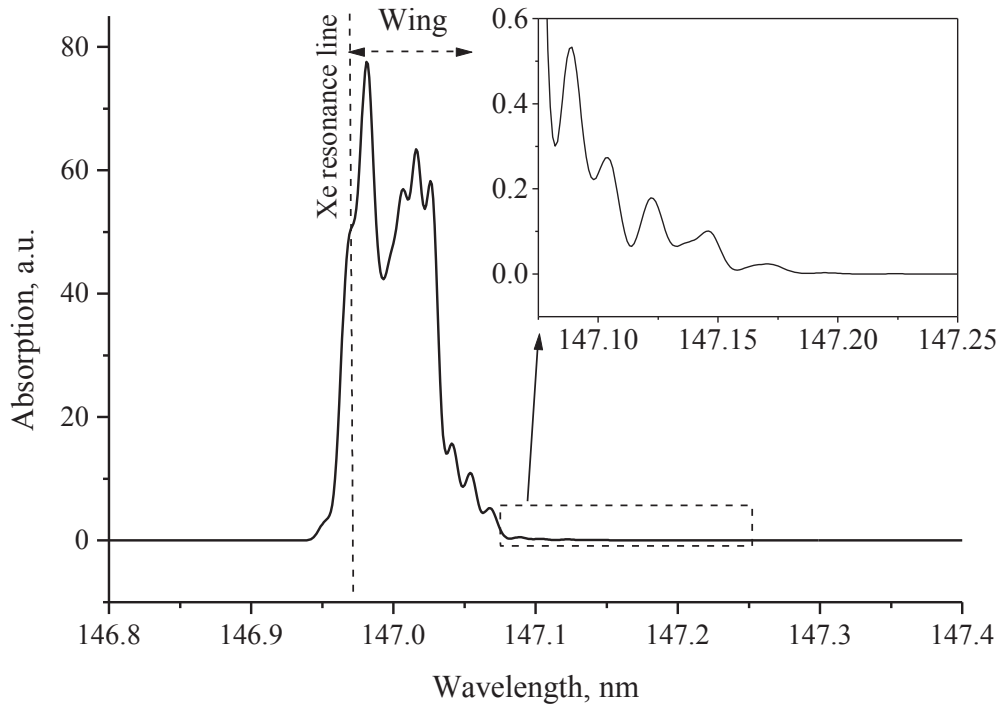

Fig. 17 A numerically calculated absorption spectrum which consist of all possible transitions between bound vibrational levels of the ground state and the excited state $1(^3P_1)$ of the XeKr molecule. Potentials in the Morse form were used for both states. The inset shows the long wavelength spectral structure.

The simulations showed that the red wing could indeed originate from bound-bound transitions between the ground state and the weakly-bound excited state with parameter values close to the values supplied by Zagrebin's calculations [9] (compare Fig. 17 with Fig. 15). The redshift of the center of this bound-bound structure was found to be directly proportional to the difference between the well depths of the excited and the slightly shallower ground states, since the most probable transitions are between levels with a difference of 0 and ±1 in vibrational quantum number.

Calculations on bound-free transitions showed that these transitions could produce absorption profiles similar to the absorption structures in the blue wing. However, the width and the shape of the absorption was found to be very sensitive to the shape of the repulsive part of the excited state, which was not supplied by the semiempiric calculations.

Nevertheless, Castex's concept [5] that the red wing is due to free-free transitions could also be supported. For a total pressure of 100 hPa, the average density of atoms is $3 \cdot 10^{18}$ cm^{-3} which means

that an excited atom will have within a sphere of radius 7 Å in average $4 \cdot 10^{-3}$ atoms. That is, 0.4 % of the excited admixture atoms will have an atom of the main gas in their vicinity so the resonant atomic transition will be noticeably perturbed. The radius of 7 Å was chosen since for longer internuclear distances the difference between the potential curves of the weakly bound ground and the excited states give practically the unperturbed atomic resonance transition. Note that if one considers, as predicted by Zagrebin's calculations [9], that the excited and the ground states have approximately the same equilibrium distance and the excited state is somewhat deeper than the ground state, the main contribution from free-free transitions would indeed be in the red wing. This is based on the fact that, as was mentioned before, the wavelength of a free-free transition is given by the energy difference between the potential curves of the excited and the ground states at the actual internuclear distance of the two atoms.

All aforesaid indicates that all these types of transitions (bound-bound, bound-free and free-free) contribute to some extent to the absorption spectra.

3.3.2 Identification of the emission structures.

By virtue of the similarity between emission and absorption structures, we will now discuss how the identification of absorption spectra can be applied to determinate the origins of the emission structures (see **Paper I** for details).

If one assumes that the blue wing in absorption is mainly due to transitions between vibrational levels of the ground state and the repulsive part of the states $1(^3P_1, {}^1P_1)$, then the same transitions should give the main contribution to the emission blue wing. This is supported by our results on the spectral temperature dependence in emission (Fig. 13) – the short wavelength part of the blue wing reduces its relative intensity with cooling, the reason being that the shorter the wavelength becomes, the higher kinetic energy is required for an atomic pair to produce emission in the blue wing. Another experimental fact, namely that the number of emission structures in the blue wing is smaller for a lighter main gas than for a heavier main gas with the same admixture, is most probably connected with the reduction of the number of vibrational levels in the ground state.

Concerning the emission in the red wing (see fig. 12), it is convenient to start the discussion with the well developed and extended long wavelength part of the red wing in the emission spectra from the heavy mixtures (mixtures where Ar and Kr is the main gas). Because of its width it is reasonable to attribute it to transitions between vibrational levels of the strongly bound $0^+(^3P_1, ^1P_1)$ states and the repulsive part of the ground state in Kr*X and Xe*Y heteronuclear molecules (see Fig. 16). We consider the contribution from excited Kr_2 and Xe_2 molecules to be small since the maximum concentration of the admixture in this study was 1 % and therefore the number of homonuclear molecules, created in three-body collisions, should be considerably smaller than the number of the heteronuclear molecules.

There are two other contributions to the red wing. The intense shoulder in the emission profile of the heavy mixtures close to the resonance lines is partially due to bound-bound transitions between vibrational levels of the 1 ($^3P_1$ or $^1P_1$) state and vibrational levels of the ground state of the heteronuclear molecule.

Another contribution to the red wings, and possibly to some extent also to the blue wing, arises from transitions in free atomic pairs (free-free transitions). The free-free transitions are probably the only origin of the red wing for the mixtures with He since the potential well depths of the lowest excited states of heteronuclear rare gas dimers with He are too shallow [8] to contain more than one vibrational level or may even contain none. Molecules with Ne also contain just a few vibrational levels. This may be the reason why the intense red shoulders are absent in the spectra from the light molecules (mixtures where He and Ne are the main gases).

We believe that the main contribution to the emission spectrum in the immediate vicinity of the resonance lines (± 0.01 nm), where the emission intensity is strongest, is from free-free transitions (including the unperturbed atomic resonance transitions), but all mechanisms mentioned above and especially the bound-bound transitions for the heavy mixtures give their contribution at these wavelengths.

4. Energy transfer processes in rare gas mixtures.

In this chapter a review of the energy transfer processes in rare gas mixtures is given, bases on the discussions and results of **Paper III** and **Paper IV**. The two papers treat Kr-Xe mixtures only, but similar energy transfer processes take place also in Ar-Kr and Ar-Xe mixtures.

4.1 Energy transfer or direct electron excitation?

As was discussed in section 3.1, discharges in Ar and Kr show a remarkable feature. If even a very small amount of a heavier rare gas is added, the intensity of the host gas continuous emission may undergo a considerable reduction while narrow and intense bands appear close to the atomic resonance lines of the admixture. Fig. 18 shows that an addition of only ~ 0.5 % of such an admixture seems to wipe out completely the emission from the host gas.

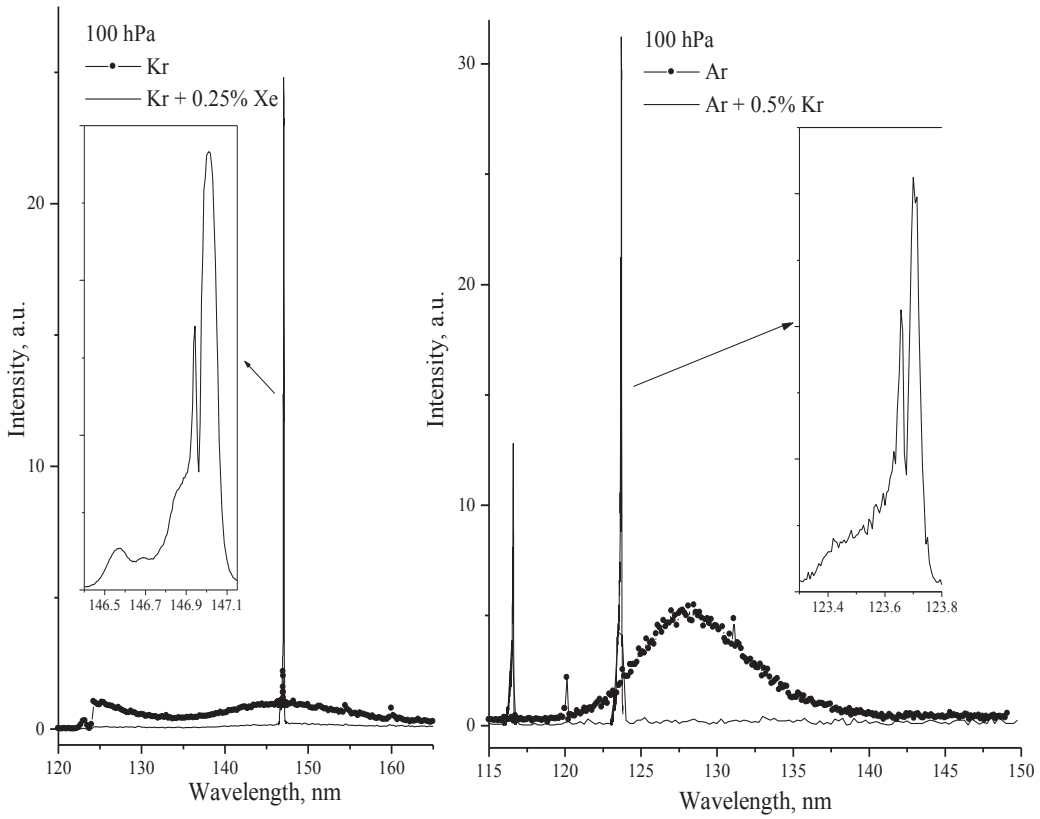

Fig. 18 VUV emissions from DC capillary discharges in Kr and Kr + 0.25 % Xe (left) and in Ar and Ar + 0.5 % Kr (right) at the total pressure of 100 hPa. The inserts show the narrow bands that appear close to the self-absorbed atomic resonance lines of the admixture.

There are two possible mechanisms that could explain these phenomena. The first is direct electron excitation of the admixture atoms. In order to explain the reduction of the continuum emission from the main gas in the mixtures by this process one has to conclude that a considerable part of the excitation energy flow, which in a pure gas is taken by the atoms from electrons, is diverted to the admixture atoms.

The second possible mechanism involves the existence of strong energy transfer processes which depopulate atomic and/or molecular states of the main gas and pump the electron excitation energy to the admixture atoms. Note that it is the main gas in the mixture that still acquires practically all excitation energy from the discharge, however a considerable fraction of the energy is transferred afterwards to the admixture atoms.

Both mechanism could actually contribute to the effect demonstrated in Fig. 18. Near infrared (IR) spectroscopic studies of rare gas mixtures excited in DC and radio frequency (RF) discharges (see [1] and **Paper IV)** have shown that only at concentrations of approximately 0.1 % and lower does direct electron excitation have a negligible effect. These experiments involved the observation of radiative cascades in the main gas (see section 4.3.3), which are in the IR spectral range, in the pure gases and in the mixtures. The results indicate that at concentrations below 0.1 % the emission lines of the cascades have the same intensities in the pure gas as in the mixtures at the same total pressures. The intensities should be very different if direct electron excitation of the admixture atoms is comparable with the direct excitation of the main gas.

In the next two sections, a discussion of the Kr-Xe energy transfer processes is presented in some detail.

4.2 Energy transfer processes in Kr-Xe mixtures excited in DC discharges.

As was discussed in section 2.3, the population of excited atoms of the main gas in the four lowest excited states (two metastable and two radiatively-trapped resonant states) is created in two ways: by direct electron excitation of the ground state atoms and by radiative cascades from ions after recombination. These four long-lived states, together with the two lowest excited homonuclear

molecular states, are the only candidates to be energy donors to the admixture atoms. All other atomic states cannot be effective energy donors since their radiative lifetimes are too short.

On the other hand, to be an efficient acceptor of the electron excitation energy in an atom-to-atom energy transfer channel, an atomic level of the admixture must have an energy close (difference less than ***kT***) to the energy of the donor atomic level. For a molecule-to-atom energy transfer channel, an admixture atom energy level should be within the range of photon energies of the molecular continuum to be able to accept the excitation energy.

For the heavy rare gas mixtures, when the admixture is a heavier gas, both conditions are satisfied for the atomic as well as for the molecular channels. As an example, Fig. 19 shows an energy-level diagram for the lowest excited states of krypton and xenon.

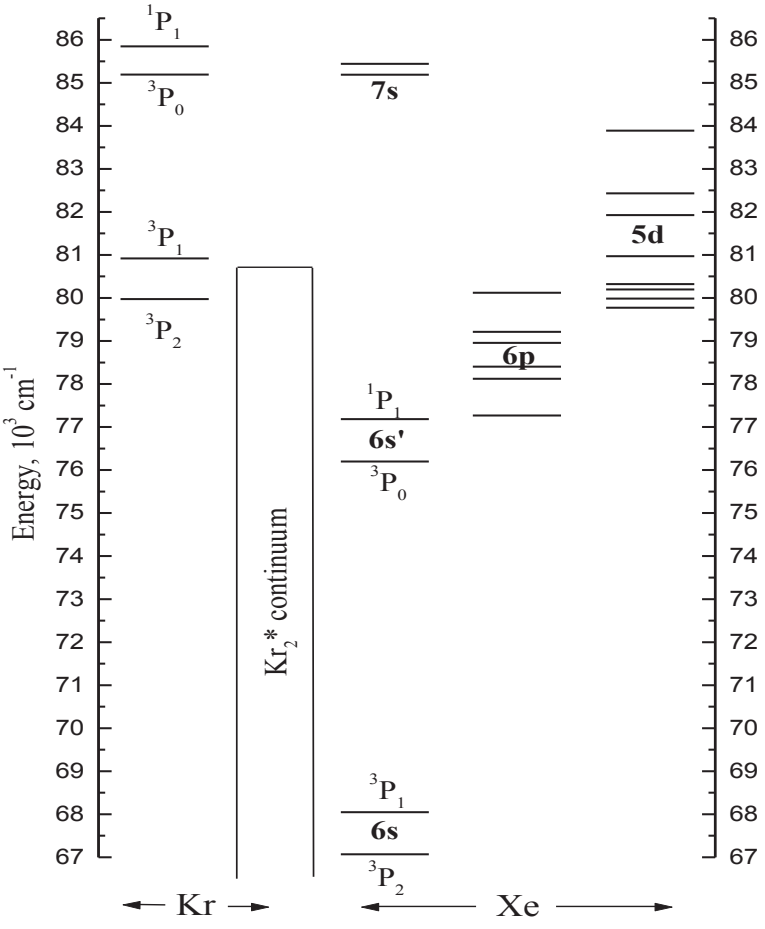

Fig. 19 Energy-level diagram for the lowest excited states of atomic Kr and Xe. The photon energies from the Kr_2* continuum are also indicated. The value of ***kT*** is about 200 cm^{-1} for room temperature.

The diagram shows that some of the atomic Xe 6p, 5d and 7s states have energies very close to the energy of some of the four lowest excited states of Kr. Besides, some of the excited Xe states, including the four lowest, are in the photon energy range of the Kr_2 continuum. These facts show that an efficient energy transfer, both atom-to-atom and molecule-to atom, can indeed exist in the excited Kr-Xe mixtures.

A number of experimental studies of energy transfer phenomena were performed for different excitations and gas conditions. A review of them is given in **Paper III**, and a summary of the results is presented in Fig. 20, where a simplified energy transfer diagram for Kr-Xe mixtures and energy transfer rates are shown.

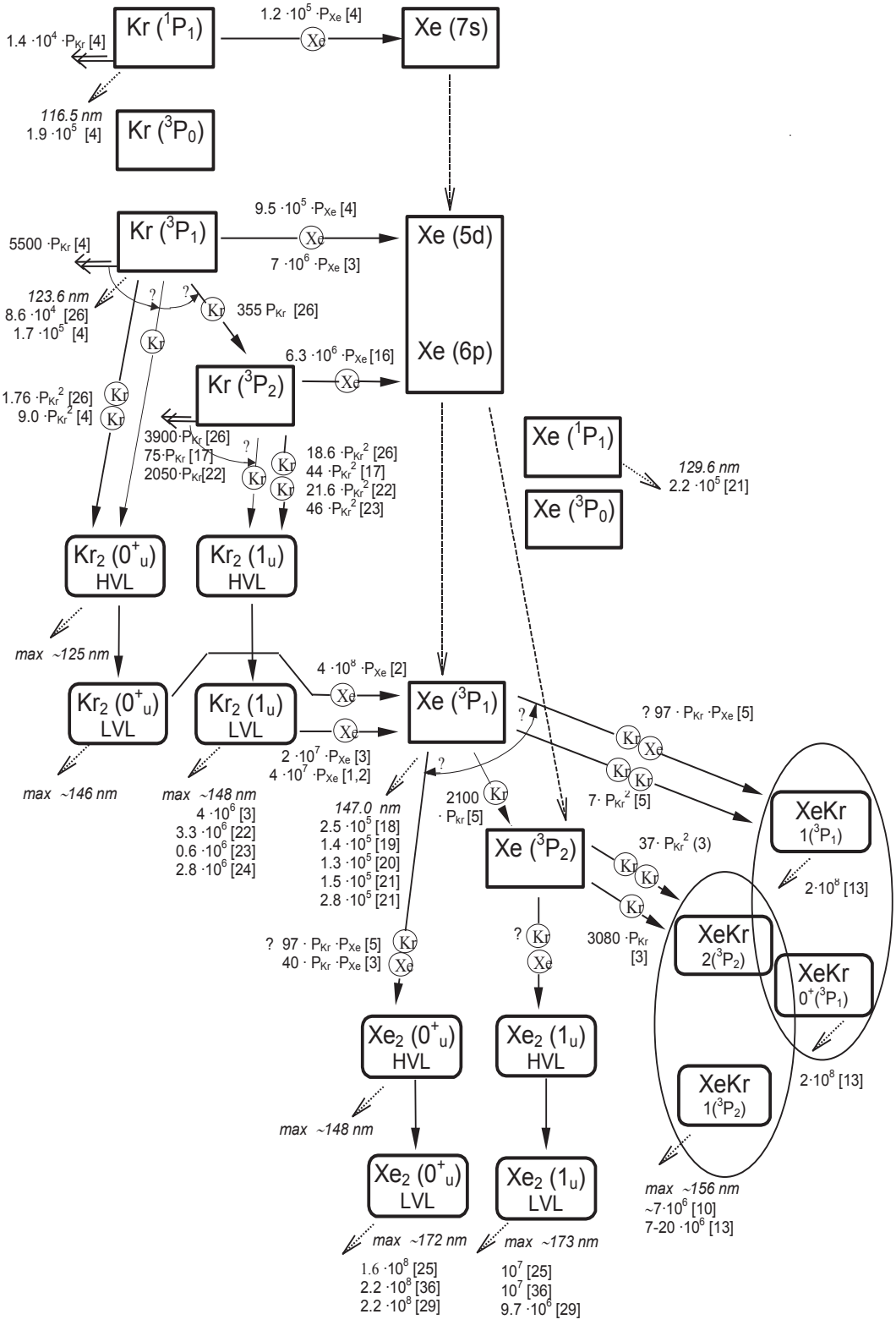

Fig. 20 Diagram of energy transfer processes in a Kr- Xe mixture, according to literature data. Reactions with a participation of electrons were not included. Rates are given in s^{-1}, $Torr^{-1}s^{-1}$ and $Torr^{-2}s^{-1}$. HVL (LVL) means high (low) vibrational levels. References are to the publications listed in Paper III.

Let us now follow the scheme and discuss the channels of energy transfer in Kr-Xe mixtures and how they affect the emission spectra. The four lowest excited Kr states work as an intermediate reservoir of excitation energy: as was mentioned above, no energy transfer takes place from higher Kr states. If there is no Xe admixture, the excitation energy can be dissipated radiatively from the resonant states or the excited atoms could form excited diatomic molecules in three-body collisions which emit the broad molecular continua.

If a small admixture of Xe is added, two channels of energy transfer start to work. The Xe 6p, 5d and 7s states acquire energy from the four lowest Kr excited states and then transfer the excitation energy radiatively down to the two lowest excited states of Xe: the resonant $^3P_1$ and metastable $^3P_2$. These two Xe states also acquire energy from Kr_2 molecules in the resonant 0^+_u and metastable 1_u states. Experimental data on VUV emission suggests that the Xe resonant state $^1P_1$ and metastable state $^3P_0$, which are situated higher in energy, obtain nearly a negligible part of the excitation energy in comparison with the two lowest excited Xe states.

While the Xe concentration is low, the main channel of energy dissipation from the lowest Xe exited states is VUV emission: both through an unperturbed resonant atomic transition and by way of transitions in free Xe* - Kr pairs (especially if the krypton pressure is high). The other channels involve the creation of molecules: first of all, as it seems from VUV observations, Xe*Kr molecules are created in the state $1(^3P_1)$ which gives rise to a narrow band emission close to the first Xe resonance line. With increasing Xe partial pressure the spectral contribution from the Xe*Kr $0^+(^3P_1)$ state, as a broad continuum, becomes more and more significant. We believe that this is connected with the increase of the effective lifetime of the atomic $^3P_1$ and molecular $1(^3P_1)$ states due to enhanced radiation trapping. If the Xe partial pressure is increased further, even Xe_2* molecules could be formed in their lowest excited states 0^+_u and 1_u by three body collisions.

The observed dependence of the Kr-Xe spectral profiles on the discharge gas temperature, i.e. that the contributions from the $0^+(^3P_1)$ Xe*Kr state (center at ~156 nm) and the Xe_2* second continuum (center at ~173 nm) increase with cooling, could be explained in part by the increase of the Xe density. There is however a second phenomenon that also contributes to this spectral profile

redistribution. This is the improved stability of the XeKr ground state molecules at lower temperatures which leads to increased self-absorption in the narrow band close to the resonance line and thus in turn reduces the effectiveness of the radiative energy dissipation channel from the Xe*Kr state $1(^3P_1)$ and from Xe*-Kr free pairs. This reduction weakens the competition for the two other channels: creation of $0^+(^3P_1)$ Xe*Kr and Xe_2* molecules.

4.3 Determination of energy transfer rates in Kr-Xe mixtures excited with RF discharges.

This section contains a review of experimental details and results of the determination of atom-to-atom and molecule-to-atom energy transfer rates based on VUV emission spectra from Kr-Xe mixtures excited with radio frequency discharges. First the experimental setup is described. Then the kinetic model of energy transfer and the rate calculation procedures are presented. Finally the results of IR emission studies from the same type of discharge are analyzed.

4.3.1 Experiment setup.

The gases were excited by radio frequency (RF) discharges. RF excitation took place in a very short cylindrical volume that was 3 mm along the observation axis and 8 mm in diameter (See Fig. 21).

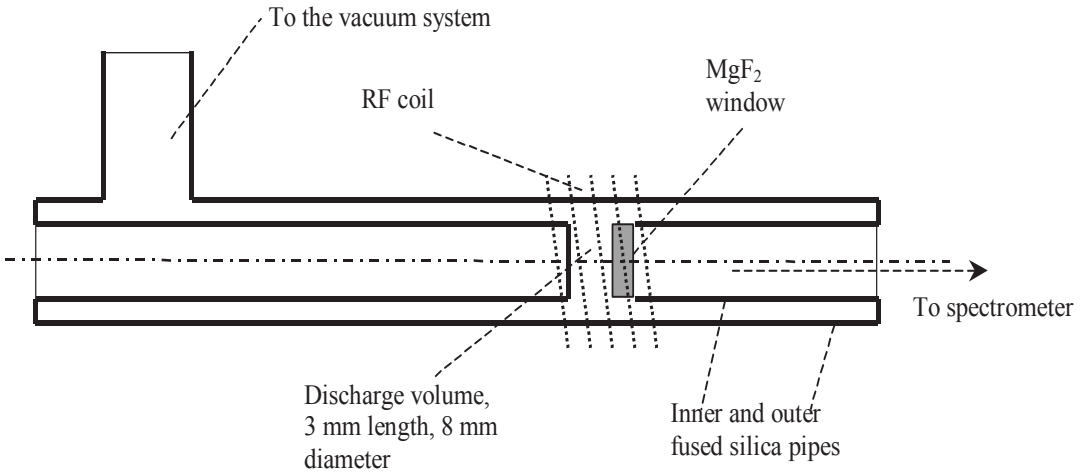

Fig. 21 Discharge tube for RF excitation.

This geometry greatly reduces the influence of self-absorption on the narrow band emitted from Kr – Xe mixtures close to the Xe resonance line at 147 nm in comparison with capillary DC discharges. The importance of this will be explained in section 4.3.2. RF excitation at 13.56 MHz was produced by a 15-turn 10 mm diameter helical coil of 1 mm copper wire, which surrounded the gas volume. The power inserted into the plasmas was estimated to be about 25 W for all gas conditions. Upon ignition, the entire discharge volume inside the RF coil was homogeneously filled with plasma.

4.3.2 Kinetic model and rate calculations.

The determination of the atom-to-atom and molecule-to-atom energy transfer rate values is based on the same kinetic scheme as was discussed in section 4.2:

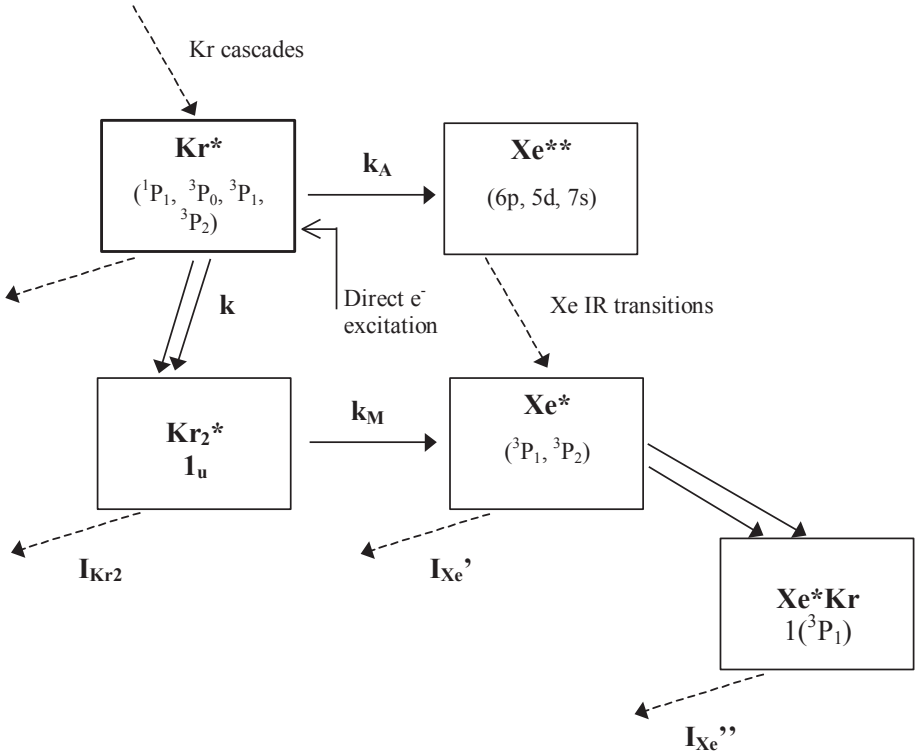

Fig. 22 Simplified diagram of energy transfer processes in Kr – Xe gas mixture discharges. I_{Kr2} represents the broad continuum emission (125 - 190 nm) from krypton dimers. Xe resonance emission (I_{Xe}') and emission from Xe*Kr $1(^3P_1)$ molecules (I_{Xe}'') overlap and form a strong narrow band at 147 nm (I_{Xe}).

Excited Kr atoms in their lowest metastable and resonant states ($^3P_0$, $^3P_1$, $^3P_2$ and $^1P_1$) are created by radiative cascades from highly excited states (and ionic states after recombination) or by

direct electron excitation. The $^3P_1$ and $^1P_1$ resonant states can in our case be considered as metastable because of the strong radiative trapping which results in their effective lifetimes being of the order of tens of microseconds. Since the radiative losses are quite weak, the metastable Kr atoms could either form Kr_2* molecules (1_u, 0^+_u states) in three body collisions (conversion rate $\boldsymbol{k}$) or transfer their energy to ground state Xe atoms (transfer rate $\boldsymbol{k_A}$), exciting them to 6p, 5d and possibly 7s states (see section 4.2). The exited Xe atoms relax radiatively (near-IR wavelength region) to the lowest resonant and metastable states of xenon. Kr_2* molecules, for their part, could either emit VUV radiation (the first and second continua) or transfer their excitation energy to ground state Xe atoms (transfer rate $\boldsymbol{k_M}$), exciting them to their lowest excited states.

If the total gas pressure and xenon concentration are low enough, the Xe-related VUV emission from Kr-Xe gas mixture discharges is concentrated near 147 nm as shown in Fig. 23.

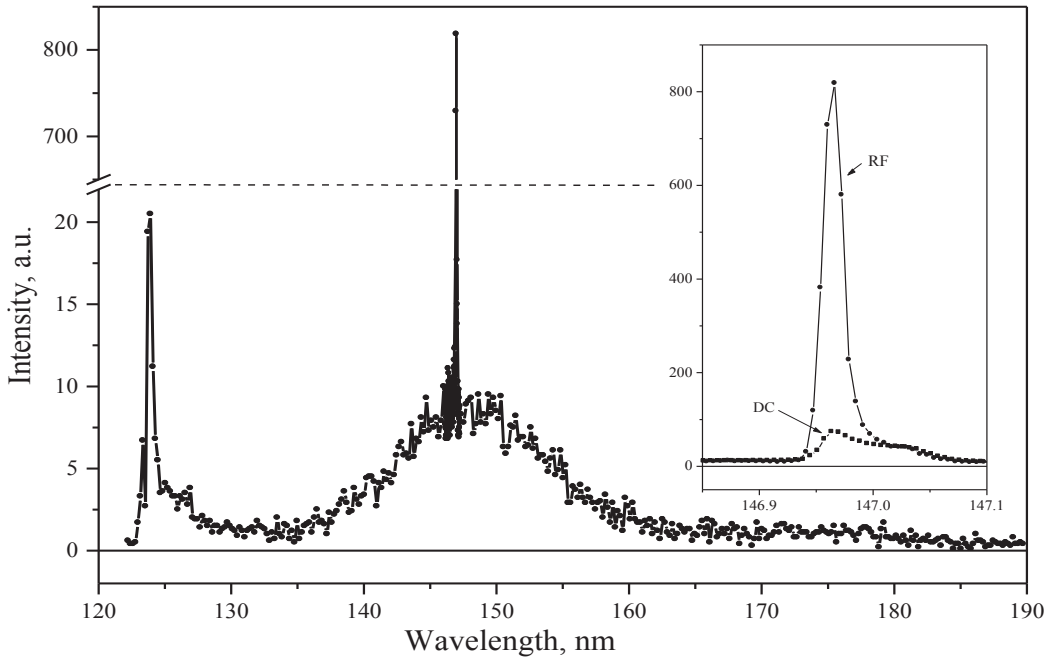

Fig. 23 A VUV emission spectrum from a RF gas discharge in 200 hPa Kr with 0.01 % Xe. The insert shows the region near the Xe resonance line at 146.97 nm from RF and DC discharges, demonstrating the very low self-absorption in the first case. The spectrum from the DC setup was scaled to have the same intensity as the RF spectrum in the long wavelength part of the shoulder, where absorption is minimal. The spectral resolution is 0.015 nm.

Therefore one has to conclude that the main final product resulting from energy transfer is the lowest pair of the excited Xe states (i.e.

the resonant $^3P_1$ and metastable $^3P_2$). These two states are mixed by electrons and emission from the resonant state is strongly self-absorbed. At the moderate Kr pressures (< 400 hPa) and small Xe concentrations (< 0.1 %) used in this study, the main emission is in part from Xe*Kr molecules in the weakly-bound state $1(^3P_1)$, which are created in three body collisions with two ground state Kr atoms. The other part comes from the transitions in free Xe* - Kr pairs which give a narrow band also near the atomic resonance line (see section 3.3.2).

To determine the energy transfer rate values we have used a steady state balance technique, which involves the following reactions:

1) $Kr^* + Xe \rightarrow Xe^{**} + Kr$ (atomic energy transfer channel), with rate $\boldsymbol{k_A}$
2) $Kr^* + 2Kr \rightarrow Kr_2^* + Kr$, with rate $\boldsymbol{k}$
3) $Kr_2^* + Xe \rightarrow Xe^* + 2Kr$ (molecular energy transfer channel), with rate $\boldsymbol{k_M}$
4) $Kr_2^* \rightarrow 2Kr + h\nu$, with lifetime $\boldsymbol{\tau}$.

Here Kr* and Xe* represent the four lowest excited states of krypton and xenon; Kr_2^* - krypton molecules in the lowest 1_u state; Xe** - xenon in the 5d, 6p or 7s configurations; Kr and Xe – ground state krypton and xenon atoms. It is also assumed that all energy acquired by Xe atoms in the $^3P_1$ and $^3P_2$ states is emitted only in the narrow band around 147 nm.

Applying the steady state condition to these four reactions, one obtains that the ratio of the integrated intensity I_{Xe} in the narrow band at 147 nm to the integrated intensity I_{Kr2} of the continuous emission of Kr_2^* does not contain the unknown population of the Kr metastable state which is the common energy source. Thus, to obtain the energy transfer rates (atomic and molecular channels), only the experimental dependence of the ratio on Kr gas pressure has to be known for a constant Xe admixture [1]:

$$\frac{I_{Xe}}{I_{Kr2}} = k_M \tau P_{Xe} + \left[\frac{k_A P_{Xe} \left(k_M \tau P_{Xe} + 1 \right)}{k} \right] \frac{1}{P_{Kr}^2} \qquad (1),$$

where $\boldsymbol{P_{Kr}}$ and $\boldsymbol{P_{Xe}}$ are the pressures of Kr and Xe. The first term in the sum is independent of the Kr pressure. This allows one to

calculate the molecular channel rate k_M if τ is known and then to use this rate in the second term, which is linear with $(P_{Kr})^{-2}$, to calculate the atomic channel rate k_A.

The fact that the ratio of the integrated intensities is directly involved in the calculations makes it necessary to take precautions to minimize the effect of self-absorption in the Xe band. That is why the discharge geometry and the type of excitation described in section 4.3.1 were chosen (compare the spectra from DC and RF discharges at the same gas pressures in the insert of Fig. 23).

This method of determination of the energy transfer rate from Kr atoms to Xe does not allow one to distinguish the contributions from each of the four lowest excited Kr states. However, electron mixing, which was estimated to be strong, is working in favour of the lower pair and besides, a big difference in population rates of these four states with a strong preference to the lower pair was established (see section 4.3.3).

Experimental data of the dependence of the band-to-continuum ratio on the Kr pressure are presented in the Fig. 24.

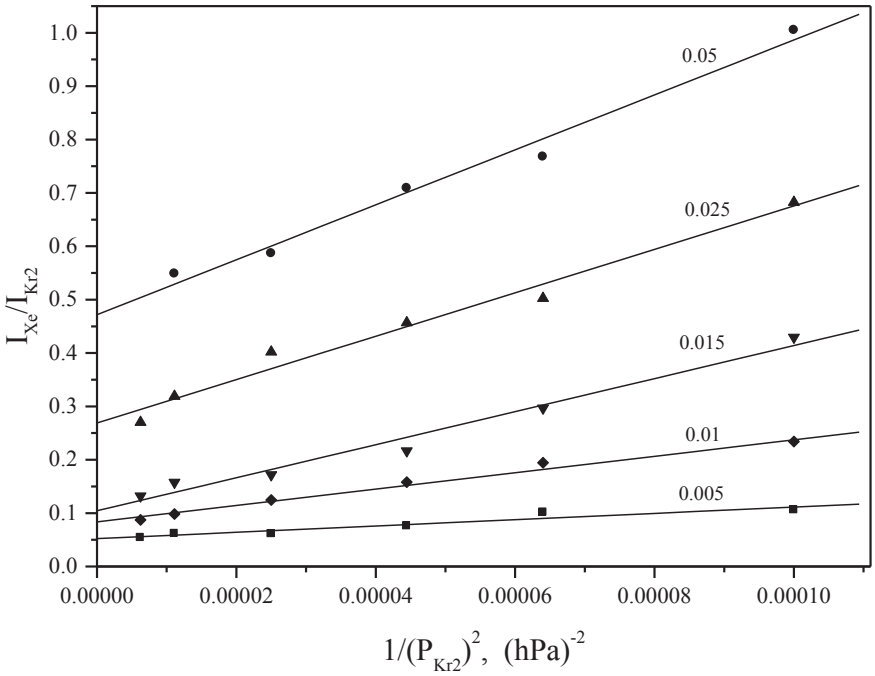

Fig. 24 The ratio of integrated intensity in the narrow band around the Xe resonant line at 146.97 nm to the integrated intensity of the Kr_2* continuum is shown for Kr – Xe mixtures in the Kr pressure range from 100 to 400 hPa for five different Xe admixtures with partial pressures from 0.005 to 0.05 hPa.

The analysis of the data, using Eqn. (1), gave the following energy transfer rates:
for the atomic channel: $\boldsymbol{k_A} = 1.7\times10^{6}\times P_{Xe}$ hPa^{-1}s^{-1} and
for the molecular channel: $\boldsymbol{k_M} = 3.9\times10^{7}\times P_{Xe}$ hPa^{-1}s^{-1}.
However, the presented $\boldsymbol{k_M}$ value might be the lower limit of the molecular channel energy transfer rate, and the actual value could be 2 to 3 times higher because of the possible shortening of the effective lifetime of the 1_u Kr_2 state (the radiative lifetime of 250 ns [16] was used in the calculations) by the collisions with electrons (for details see **Paper IV**).

4.3.3 IR emission studies.

The observations of the near IR emission from Kr – Xe mixtures allowed us to check the maximum Xe admixture for which direct Xe excitation would still be negligible in comparison with energy transfer from the Kr system. Our observations of Kr I radiative cascades in pure Kr and in mixtures with Xe showed that direct Xe excitation starts to play a noticeable role (i.e. when the difference in Kr radiative cascade intensities in pure Kr and in a Kr-Xe mixture become greater than a few percent) at Xe concentrations above 0.1 % when the Kr pressure is in the range of 80 – 400 hPa.

It was also established that, at low admixture concentrations and for both RF and DC discharges, the visible and near IR spectra in the range 400 – 1000 nm show no other spectral features besides Kr and Xe radiative cascades. The latter, together with the fact that at low Xe concentrations the lines of Kr radiative cascades have the same intensities as in pure Kr, suggests that there are no other strong energy transfer mechanisms which pump energy to Xe from ionic Kr or from excited Kr states other than from the four lowest excited states.

The dependence of the Xe 6p – 6s transition line intensities on Xe concentrations at constant Kr pressure allowed us to make an independent estimate of the atomic energy transfer rate. Using the same kinetic scheme as before (Fig. 22), one can estimate the fraction of the excitation energy that is transferred to the excited Xe states and afterwards emitted as Xe 6p - 6s transitions (I_X) from the ratio:

$$I_X \propto \frac{k_A P_{Xe}}{k_A P_{Xe} + kP_{Kr}^2 + \chi}, \qquad (2),$$

where P_{Xe} and P_{Kr} are the Xe and Kr pressures and χ is the radiative decay rate for the system of the four lowest Kr states. This ratio is based on the fact that the intensity of the Xe 6p – 6s transitions is proportional to the energy transferred to xenon per second in Kr* - Xe collisions, and that this energy is a fraction of the total Kr* energy loss, which is the sum of energy transfer, conversion and radiative decay.

Taking into account that at a constant Kr pressure the energy that is acquired by these Kr states per second does not change with Xe concentration if this stays lower than a critical value (approximately 0.05 %), one can calculate from equation (2) how the Xe 6p – 6s transition intensities change if the Xe pressure is halved:

$$\frac{I_X}{I_{X/2}} = \frac{k_A P_{Xe} + 2(kP_{Kr}^2 + \chi)}{k_A P_{Xe} + (kP_{Kr}^2 + \chi)} \qquad (3).$$

Here $I_{X/2}$ is the emission from a mixture with the half of the original Xe concentration ($\frac{1}{2} P_{Xe}$). Equation (3) shows that if the energy transfer to Xe is much stronger than the sum of the conversion rate and radiative decay, then the ratio is unity and the Xe transition intensities do not change at all. In the opposite case the ratio is two and for equality one obtains a ratio of 1.5.

In our experiments all Xe 6p – 6s lines showed a similar dependence on Xe pressure. As an example, the line at 823.16 nm, which was the most convenient for measurements, gave the following results for Kr pressure of 80 hPa and Xe admixtures of 0.025, 0.0125 and 0.00625 %: The ratios between the intensities of the line (averaged over five experimental points) for the adjacent pairs of admixtures are 1.81, 1.86 and approximately 2. For the latter, at low Xe concentrations, the experimental uncertainty becomes too large because of the low intensity of the Xe lines.

From equation (3) and the experimental intensity ratios we estimated the atomic energy transfer rate k_A. It was found that the k_A values obtained for different gas conditions are in a fairly good agreement and give an average atomic channel energy transfer rate $k_A = 1.6\times10^6\times P_{Xe}$ hPa^{-1}s^{-1}. This value is practically the same as was obtained in our VUV studies.

Finally, the IR observation of radiative cascades in Kr showed that the integrated intensity of the lines having the states $^3P_2$ and $^3P_1$ as the lower state is about four times higher than the integrated intensity of the transitions to the $^3P_0$ and $^1P_1$ states (see Fig. 25).

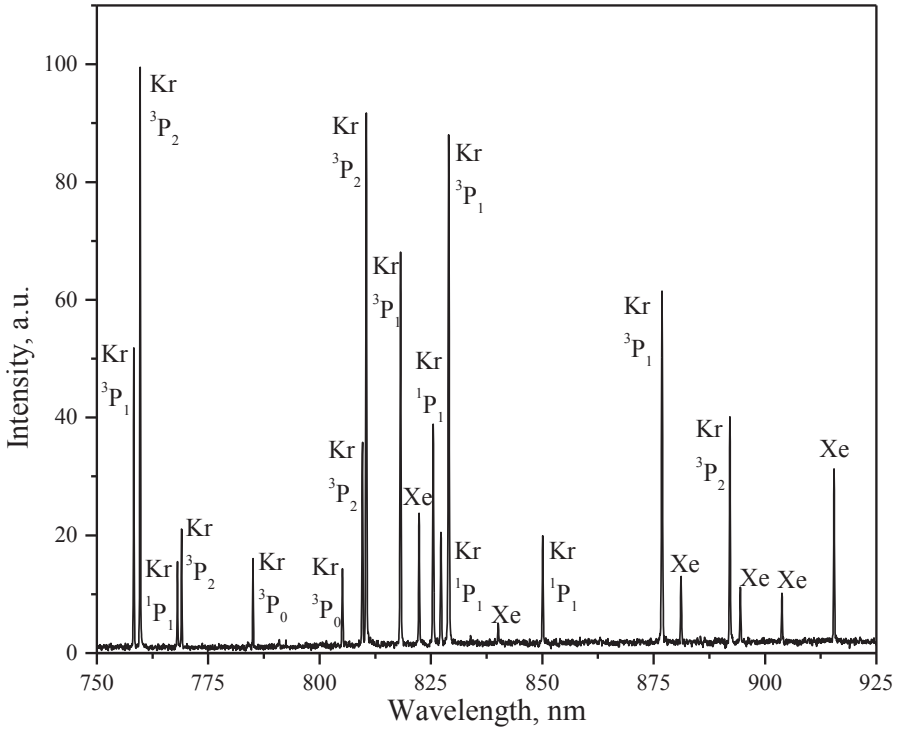

Fig. 25. Near-IR emission spectrum from a RF gas discharge in 160 hPa Kr with 0.1 % Xe. Krypton and xenon lines are marked with Kr and Xe. For all Kr lines the lower transition state, which belongs to the 5s or 5s` electron configurations, is indicated.

This suggests that the main part of the electron excitation energy, originating from krypton ionic states and being transferred to the four lowest excited states of krypton in radiative cascades is directed towards the lower pair of the krypton states. Direct electron excitation should also be more efficient for the lower pair than for the higher pair, since it has approximately 0.6 eV lower energy (see Fig. 19) and higher statistical weight. Taking into account that the electron mixing of the states is also in favour of the lowest pair, one can conclude that the Kr to Xe atomic channel energy transfer rate obtained in this study can most probably be ascribed to transfer from the $^3P_2$ and $^3P_1$ pair of states.

5. Energy transfer processes in argon-nitrogen mixtures.

Our search for an optimal rare gas mixture in attempts to create a bright and narrow VUV radiation source stimulated the research in a related area, namely the VUV emission from discharges in argon with a small admixture of nitrogen. At certain conditions these discharges produce intense and narrow N I lines at 149 nm and 174 nm as the result of a very strong Ar → N energy transfer. These atomic nitrogen transitions have metastable $^2D^o_{1/2,3/2}$ and $^2P^o_{3/2,5/2}$ atomic nitrogen states as their lower transition state. This is in contrast to the rare gas mixtures, where the narrow and intense VUV bands, discussed in chapter 3, originate from transitions to the ground atomic or molecular states, so these bands are usually affected by strong self-absorption. These facts suggest that one should consider Ar-N_2 mixtures not only as a promising medium for narrow band VUV sources but also as a possible candidate for an active medium for pulsed VUV lasers.

5.1 VUV emission from Ar-N_2 mixtures.

It is well known that gas discharges in Ar - N_2 mixtures emit UV light in molecular nitrogen bands (e.g. the molecular transition $C^3\Pi_u \rightarrow B^3\Pi_g$ at 337 nm). Mixtures of argon with a small admixture of nitrogen are used also in conventional narrow band sources which produce atomic nitrogen lines in the VUV region at 149 and 174 nm. An example of such VUV emission is shown in Fig. 26, where a spectrum from a DC discharge in 440 hPa of Ar with 0.01% N_2 is shown.

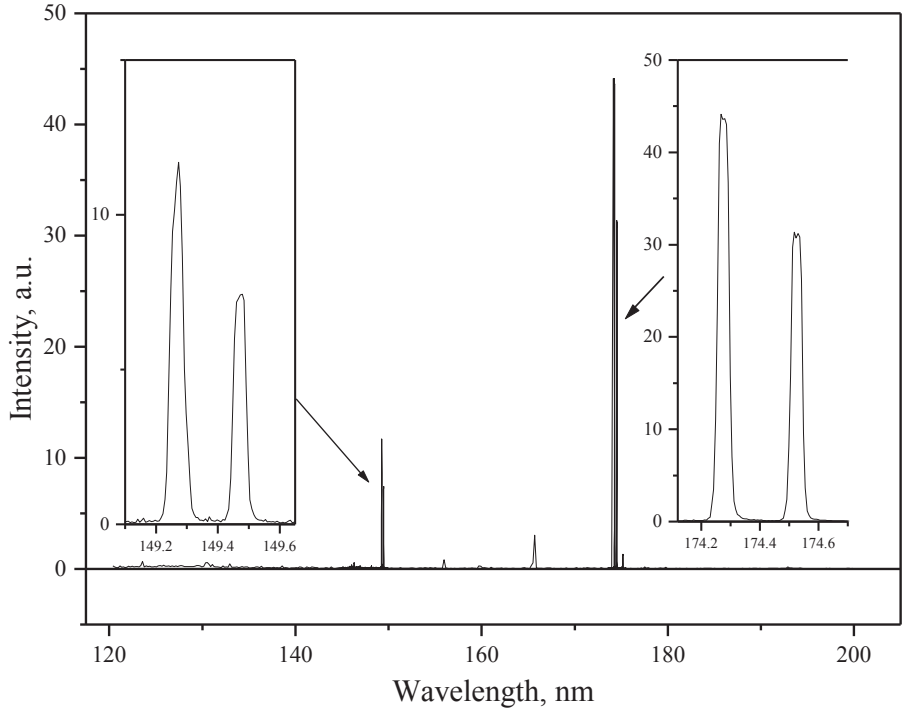

Fig. 26 A VUV emission spectrum from a DC discharge in 440 hPa of Ar with 0.01% N_2. The intensity of the lines around 149 nm is considerably (~ 6 times) reduced by lower detection efficiency in comparison with the lines around 174 nm.

The origin of these VUV lines is shown in Fig. 27 which presents a schematic diagram of energy levels of the lowest excited states of atomic nitrogen.

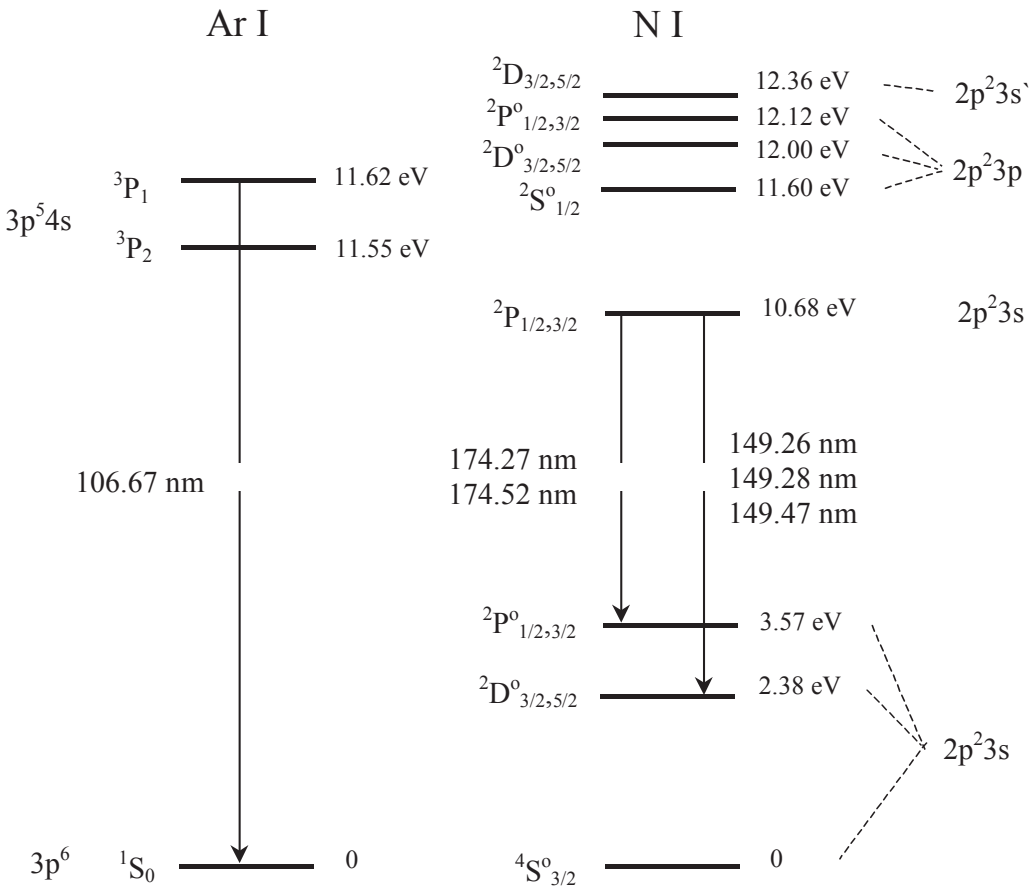

Fig. 27 A schematic diagram of the lowest excited states of Ar I and N I. VUV transitions are indicated with arrows and the wavelengths are shown.

The same figure contains also the two lowest excited states of Ar: the metastable $^3P_2$ and resonant $^3P_1$. Both states have long effective lifetimes (note that the resonant state is usually strongly self-absorbed when the total pressure is a few hPa or higher). Besides, there are nitrogen excited states with energy close to the energy of the $^3P_1$ and $^3P_2$ states of argon (see Fig. 27). These considerations suggest that a strong energy transfer could indeed exist from Ar I to N I.

5.2 Pulsed transverse discharge excitation: experiment and results.

The study of energy transfer processes in Ar – N_2 mixtures was conducted using time resolved VUV and UV spectroscopy, which provides a powerful tool in kinetic analysis. In this section we discuss details of pulsed discharge excitation and give examples of the experimental results (for details see **Paper V**).

Ar-N_2 mixtures with total pressures of 150 – 600 hPa and with N_2 concentrations of 0.125–1.5 hPa were excited in a pulsed transverse discharge with spark preionization. The excitation was performed by filling the gas mixtures into the discharge chamber of a modified commercial UV excimer laser Model MSX-250 of the MPB Technologies Inc. The discharges were formed between two electrodes of 250 mm length with a 7 mm gap between them. A primary capacitor (16.2 nF), charged to 12 kV, provided current pulses with a duration of less than 100 ns. One side of the chamber was equipped with a MgF_2 window and was used for VUV observations. The other side, containing a sapphire window, served for UV observations.

The time dependence of the emission intensity from the discharge afterglow was recorded for the following emissions: the VUV Ar_2 continuum at 126.0 nm, the VUV nitrogen atomic lines at 149.47 nm and 174.52 nm, and the UV N_2 band at 337.0 nm. To record smooth and reproducible decay curves, accumulation of 9000 pulses was usually performed for each wavelength setting. Fig. 28 shows an example of an Ar_2 continuum decay curve for an Ar – N_2 mixture with a total pressure of 150 hPa and a nitrogen concentration of 0.125 hPa.

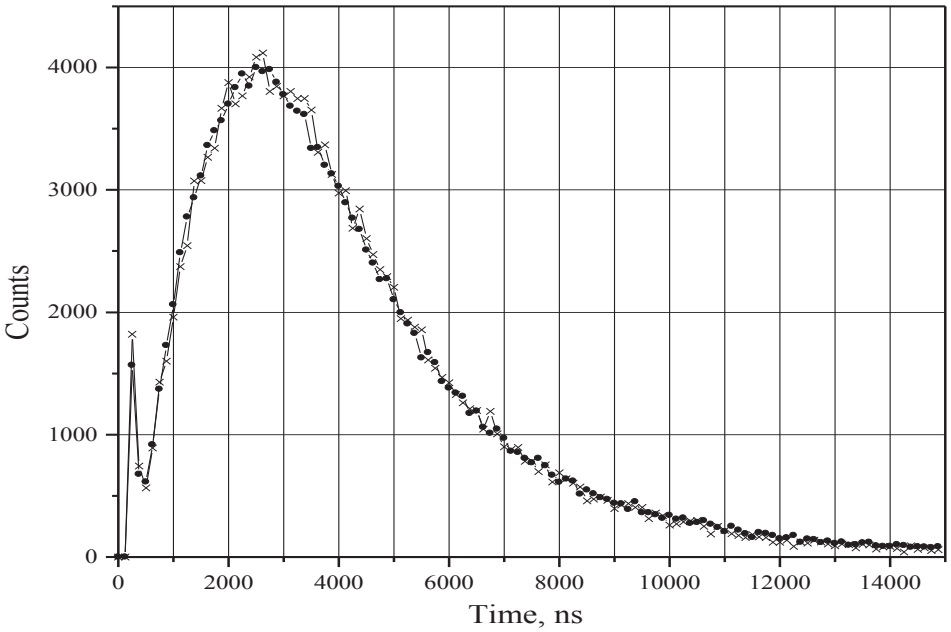

Fig. 28. Decay curves of the Ar_2 continuum at 126 nm from an Ar-N_2 mixture with a total pressure of 150 hPa and a nitrogen concentration 0.125 hPa. To show the reproducibility, two curves recorded with same conditions are given.

Note that no attempts to compare the relative intensities of the bands were made in this study and that all analysis is based on the time dependencies only.

Fig. 29 shows Ar_2 decay curves for pure Ar (150 and 300 hPa) and for Ar – N_2 mixtures with different N_2 concentrations.

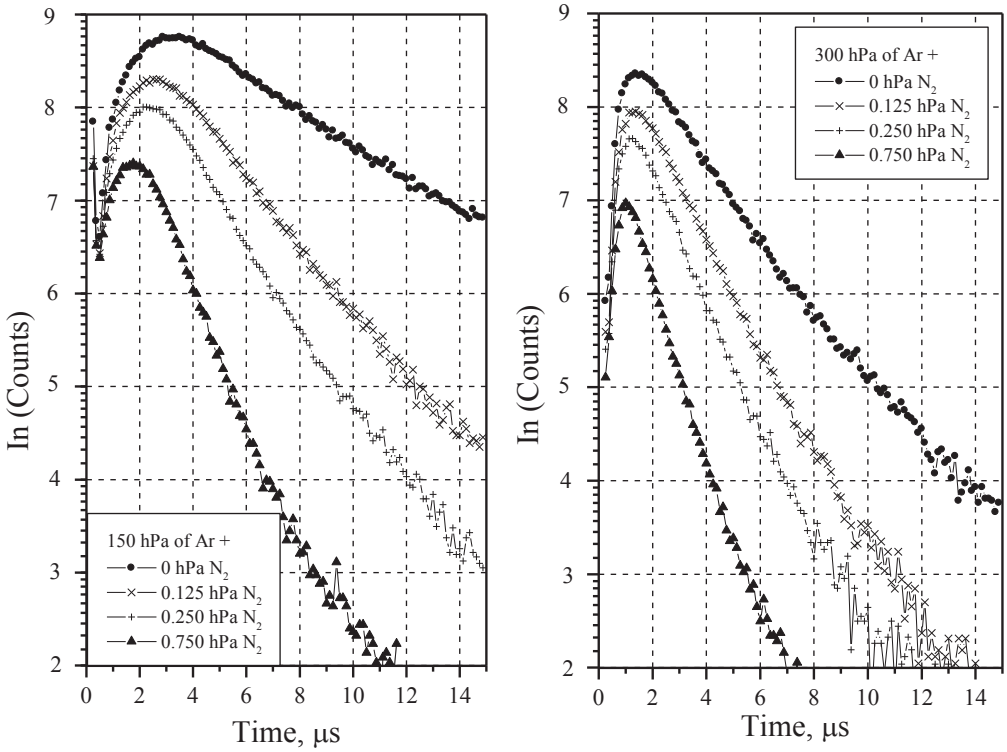

Fig. 29. Time dependence of the Ar_2 decay at 126 nm from pure Ar and Ar- N_2 mixtures at the total pressures of 150 and 300 hPa. The intensity is given in logarithmic scale.

As one can see from the figure, the higher Ar pressure or the higher N_2 concentration, the faster is the Ar_2 decay and the earlier appears the maximum of the emission.

Much information on the argon to nitrogen energy transfer processes can be obtained from a comparison of the decay curves for all three systems (Ar_2, N_2 and N) recorded at the same gas pressures. As an example, such a comparison is given in Fig. 30 for an Ar pressure of 150 hPa and two nitrogen concentrations.

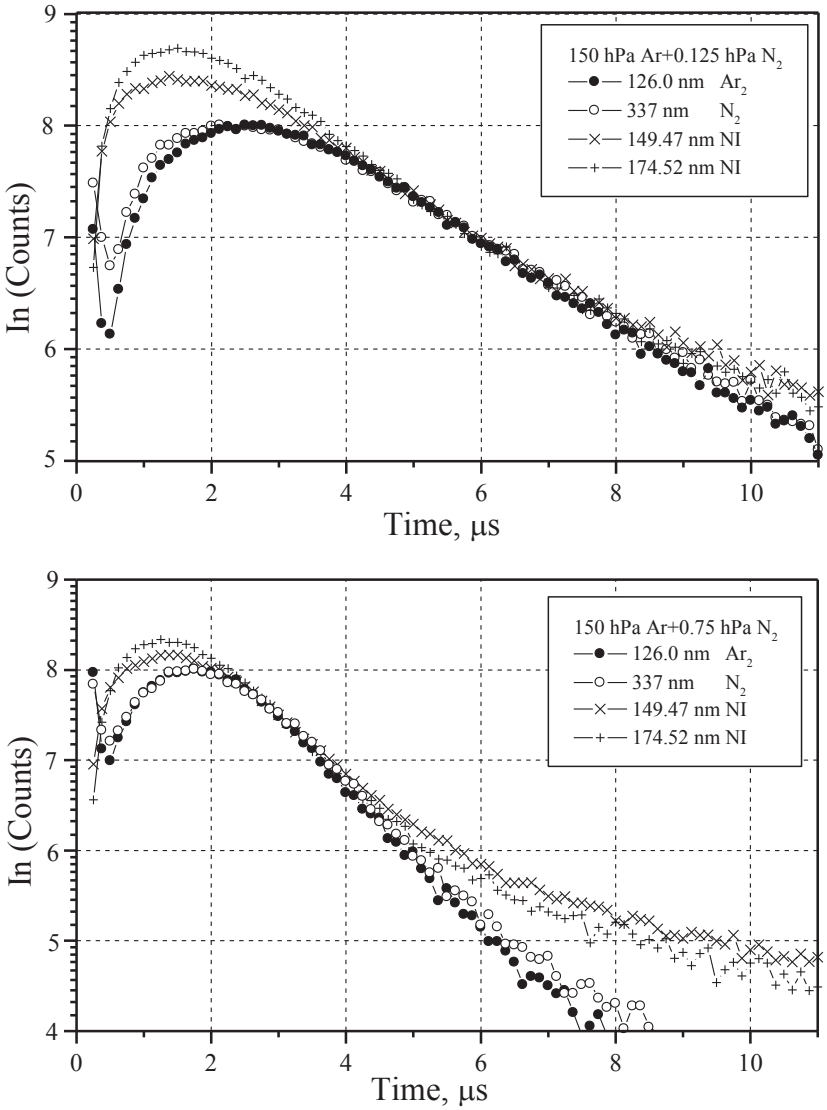

Fig. 30. Decay curves for the Ar_2 continuum at 126 nm, N_2 band at 337 nm and N I lines at 149.47 and 174.52 nm for two different Ar- N_2 mixtures. All curves were scaled in intensity to show in the best way the region where all curves have the same decay rate.

As one can see from the figure, the Ar_2 and N_2 decays look very similar. The maximum in atomic nitrogen emission appears about 1 μs earlier than in the molecular decays, but the decay rate after the maximum and until a certain time is similar for all three systems. However, for high Ar pressures and N_2 concentrations, the N_2 decay was found to be faster than the decay of Ar_2 and N (see PAPER V) since the decay rate of Ar_2* molecules is limited by the effective lifetime of the 1_u metastable state which is about 1 μs. This effective lifetime is determined by the radiative lifetime (~ 3 μs [16]) which is shortened by strong electron mixing with the resonant state 0^+_u.

5.3 Kinetic scheme of energy transfer processes in Ar- N_2 mixtures.

The analysis of the decay curves of Ar_2, N_2 and N showed that the Ar metastable $^3P_2$ state is the common source of excitation energy for three acceptors: argon dimers, nitrogen molecules and atomic nitrogen. The competition between energy transfer channels to these three acceptors is controlled by the conditions in the discharge volume, first of all by the partial pressures of the gases. The results also indicate that atomic nitrogen can acquire energy from the reabsorbed Ar resonant state $^3P_1$ and excited Ar_2 molecules in the 1_u state.

The scheme of energy transfer from Ar to atomic and molecular nitrogen can be summarized in the diagram, shown in Fig. 31.

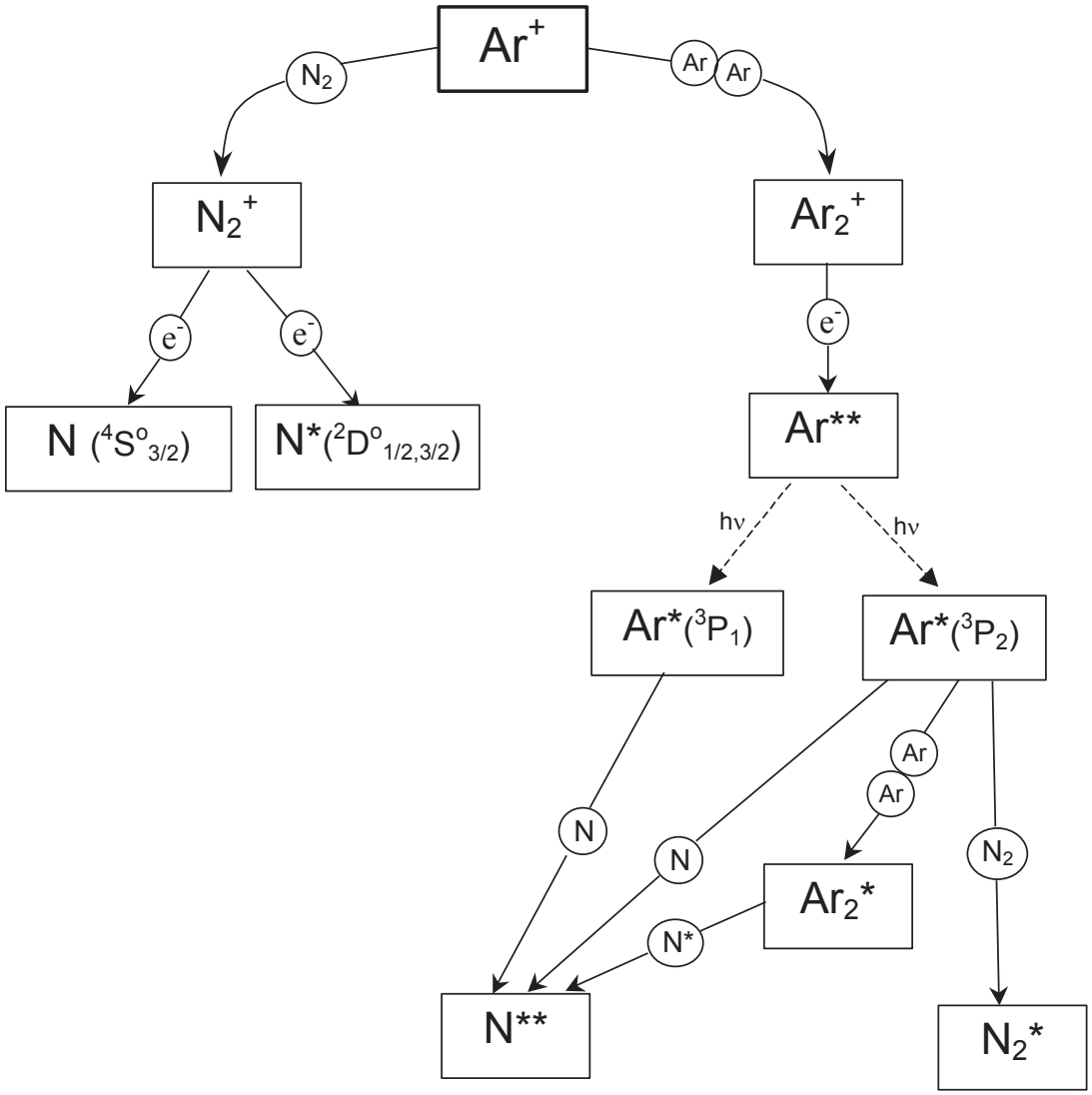

Fig. 31. A diagram of energy transfer processes in an argon-nitrogen mixture. The arrows contain a circle with a symbol of an electron (e^-), a nitrogen atom in the ground state (N), a metastable nitrogen atom (N*), nitrogen molecule (N_2) or argon ground state atom (Ar) to show which species participate in the reaction.

In this diagram the processes of nitrogen atomization are also given. The result of these processes are nitrogen atoms in their ground state $^4S^o_{3/2}$ and the lowest metastable states $^2D^o_{3/2,5/2}$. These are the atoms that participate later in energy transfer processes, acquiring energy from the lowest excited Ar states and from excited Ar_2 molecules.

6. Refrences.

1. A. Gedanken, J. Jortner, B. Raz, and A. Szoke. J. Chem. Phys. **57**, 3456 (1972).
2. O. Cheshnovsky, B. Raz and J. Jortner, J. Chem. Phys. **57**, 4628 (1972).
3. O. Cheshnovsky, B. Raz and J. Jortner, J. Chem. Phys. **59**, 3301 (1973).
4. M.V. Bobetic, J.A. Barker, J.Chem.Phys. **64**, 2367 (1976).
5. M.C. Castex, J. Chem. Phys. **66**, 3854 (1977).
6. D. Freeman, K. Yoshino, Y. Tanaka, J. Chem. Phys. **67**, 3462 (1977).
7. G. Novak, J. Fricke, J.Phys.B:At.Mol.Phys. **18**, 1355 (1984).
8. A.Z. Devdariani, A.L. Zagrebin and K.B. Blagoev, Ann. Phys. Fr. **14**, 467 (1989).
9. A.L. Zagrebin and N.A. Pavlovskaya: Opt. Spectrosc. (USSR) **69**, 320 (1990).
10. A.N.Zaidel, E.Ya.Shreider, *Vacuum Ultraviolet Spectroscopy*, Ann Arbor, London 1970.
11. F.M.Penning, *Electrical Discharges in Gases*, Philips' technical library 1957.
12. G. Gerasimov, B. Krylov, G.Zvereva, R. Hallin, A.Arnesen, F. Heijkenskjold, Optics and Spectroscopy, **81**, 857 (1996).
13. H.A. Koehler, L.J. Ferderber, D.L. Redhead, P.J. Ebert, Appl.Phys.Lett, **21**,198 (1972).
14. S. Neeser, M. Schumann, H. Langhoff, Appl.Phys.B, **63**, 103 (1996).
15. Y. Salomero, A. Briot, H. Brunet, H. Dijols, J. Galy, P. Millet, J.P. Montagne, *J.Chem.Phys*. **74**, 288 (1981).
16. A.A. Madej, B.P. Stoicheff, *Phys.Rev.A* **38**, 3456 (1988).

7. Comments on my participation

I had the main responsibility for the experiment and data analysis in the papers I and IV as well as for the numerical simulations and data analysis in paper II. In paper III, I gave a considerable contribution to apparatus development and experimental work and also participated in the data analysis. In paper V, I gave a substantial contribution to apparatus and software development and participated in the experimental work and data analysis.

Acknowledgments

I have had the pleasure to work within the Atomic and Excimer Physics group at the Department of Physics of Uppsala University during the last five years. It has been a wonderful time. First of all, I would like to thank my supervisors Professor Reinhold Hallin and Professor Arne Arnesen. I am very grateful to them for inviting me to Uppsala and giving me all possible support in my research. The trust in me they always showed was extremely stimulating.

I am deeply thankful to my colleagues Professor Gennadii Gerasimov and Dr. Boris Krylov, who introduced me into the field of excimer science and from whom I learned so much.

I would like to thank Filip Heijkensköld, whose expertise in experimental physics and electronics always makes instruments work as they should, and even better.

Warm thanks to Professor Alexander Devdariani from St.-Petersburg University and to Professor Leif Karlsson from Uppsala University for very helpful discussions and advice.

I am very grateful to Professor Gerry O'Sullivan and Dr. Padraig Dunne from University College Dublin for my exciting visit to Ireland and to all people at the Department of Experimental Physics of UCD for their hospitality.

I would like to thank the Swedish Institute for my first year scholarship and Uppsala University for providing me a position of a PhD student at the Department of Physics. The financial support of this work from the Swedish Research Council for Engineering Sciences (TFR), the Göran Gustafsson Foundation and the Carl Trygger Foundation for Scientific Research is gratefully acknowledged.

ACTA UNIVERSITATIS UPSALIENSIS
Comprehensive Summaries of Uppsala Dissertations from the Faculty of Science and Technology 715
Distributor: Uppsala University Library, Uppsala, Sweden

Andrei Morozov

VUV Emission and Energy Transfer Phenomena in Rare Gas Mixture Discharges.

Dissertation in Physics to be publicly examined in the Häggsalen, Ångströmlaboratoriet on May 23rd, at 10.15 a.m. for the Degree of Doctor of Phylosophy in Physics. The examination will be conducted in English.

ABSTRACT
Morozov, A., 2002. VUV emission and energy transfer phenomena in rare gas mixture discharges. Acta Universitatis Upsaliensis. *Comprehensive Summaries of Uppsala Dissertations from the Faculty of Science and Technology* 715. 57 pp. Uppsala ISBN-91-554-5318-X

VUV emission spectra of Xe-X (X = He, Ne, Ar and Kr) and of Kr-Y (Y = He, Ne and Ar) mixtures with low concentrations of the heavier gases (0.1 - 1 %) and moderate total pressures (50 - 200 hPa) are recorded near each of the two resonance lines of Xe and Kr in DC glow capillary discharges. A tentative identification of the emission structures is given.

Numerical simulations of absorption spectra from Kr-Xe mixtures close to the Xe resonance line at 146.96 nm are performed. It is shown that the absorption structures can result from bound-bound and bound-free transitions in XeKr molecules between the ground state and the weakly-bound $1(^3P_1)$ excited state. The depth of the excited state is estimated.

Simultaneous observations of the VUV and visible - near IR emission from DC and RF discharges in gaseous Kr with small Xe admixture concentrations are conducted. A scheme of energy transfer processes in Kr-Xe mixtures is proposed. The emission spectra are used for investigation of energy transfer from the lowest excited states of both atomic krypton and krypton molecules to the ground state xenon atoms. Values of energy transfer rates from the 1_u state of Kr_2* molecules and from the system of the four lowest Kr excited states to Xe ground state atoms are obtained.

Energy transfer processes in gaseous Ar with a small admixture of N_2 excited in a transverse pulse discharge are investigated and an energy transfer scheme is proposed. The results confirm that all emitting species have Ar metastable state $^3P_2$ as their common source of excitation energy. Evidences of strong energy transfer from $Ar_2*(1_u)$ molecules and the reabsorbed Ar state $^3P_1$ to atomic nitrogen are also obtained.

Key words: VUV spectra, excimers, energy transfer, rare gas discharges

Andrei Morozov, Department of Physics, Uppsala University, Box 530, SE-751 21, Uppsala, Sweden.

Paper I

INSTITUTE OF PHYSICS PUBLISHING JOURNAL OF PHYSICS D: APPLIED PHYSICS

J. Phys. D: Appl. Phys. **36** (2003) 1126–1134 PII: S0022-3727(03)57526-X

VUV emission spectra from binary rare gas mixtures near the resonance lines of Xe I and Kr I

A Morozov[1], B Krylov[2], G Gerasimov[2], A Arnesen[1] and R Hallin[1]

[1] Department of Physics, Uppsala University, Box 530, SE-752 21 Uppsala, Sweden
[2] Vavilov State Optical Institute, Birzhevaja Line 12, St Petersburg, 199034, Russia

E-mail: AndreiMorozov@hotmail.com

Received 17 December 2002, in final form 6 March 2003
Published 16 April 2003
Online at stacks.iop.org/JPhysD/36/1126

Abstract
Emission spectra of Xe–X (X = He, Ne, Ar and Kr) and of Kr–Y (Y = He, Ne and Ar) mixtures with low concentrations of the heavier gases (0.1–1%) and moderate total pressures (50–200 hPa) have been recorded near each of the two resonance lines of Xe and Kr in DC glow capillary discharges. The recorded intense emissions have narrow spectral profiles with FWHM of about 0.1 nm. The profiles are very similar in shape to profiles of known high resolution absorption spectra recorded at comparable gas pressures. A tentative identification of the emission structures is given, which involves transitions in heteronuclear molecules and quasimolecules between weakly-bound states.

1. Introduction

Binary rare gas mixtures with a small admixture of the heavier gas ($\leqslant 1\%$) emit under certain excitation conditions intense and narrow vacuum ultraviolet (VUV) bands around the resonance lines of the admixture atoms (see, e.g. [1–3]). Such discharges can therefore serve as VUV light sources, which are in a great demand from science and technology.

The intense and narrow emission has initially been interpreted to be of atomic origin [1–6]. Later, absorption studies [7, 8] of binary rare gas mixtures, performed with high resolution, have shown that absorption spectra near the resonance lines have a considerable number of discrete structures and that the intensity of the structures depend on both the host and admixture gas pressures, demonstrating that heteronuclear atomic pairs (bound or unbound) are responsible for the absorption structures. This suggests that the emission spectra may also have strong contributions from heteronuclear molecules (or quasimolecules).

High resolution VUV emission spectra of bands near the resonance lines of the admixtures with reliable identification of the structures have not yet been presented for binary rare gas mixtures. To our knowledge, only limited information exists on the band structures for some mixtures: Ne–Xe in [9] and Kr–Xe in [10–12]. In this paper we report emission spectra from capillary DC glow discharges of Xe–X and Kr–Y mixtures (X = He, Ne, Ar, Kr and Y = He, Ne, Ar) near the first and second resonance lines of Xe (146.961 and 129.559 nm) and Kr (123.584 and 116.487 nm). A spectral resolution of 0.015 nm, which is considerably higher than in the previous emission studies [1–6], allowed us to record the profiles of the short and long wavelength emission structures around the resonance lines, which definitely indicate a molecular or quasimolecular origin of these structures.

In our previous studies [10–12] we have presented a possible identification of such VUV spectra from Kr–Xe mixtures. It was shown that transitions between KrXe molecules in the weakly bound excited state $1(^3P_1)$ and the ground state could be responsible for the strong emission (and absorption) in the vicinity of the Xe resonance line at $\sim$147 nm, while transitions between the more strongly bound state $0^+(^3P_1)$ and the repulsive part of the ground state contribute to the broad low intensity continuum extending from the resonance line to longer wavelengths.

In this paper we extend our identification attempts to all VUV emission spectra which are reported here. The analyses of possible origins of the emission structures is based on the currently available data on the internuclear potentials of the atomic pairs. A review of the data is given in section 4.

Both the presented experimental spectra and tentative identification of the spectral structures may be useful in the development of intense narrow-band VUV radiation sources utilizing rare gas discharges.

2. Experimental set-up

The experimental set-up was described earlier in detail [11], so here we briefly outline only the main features. The gas mixtures were excited in DC glow discharges with currents of 20 mA inside a 600 mm long capillary of 1.4 mm inner diameter, which was made of fused silica. A fan was used to sustain a constant mixture circulation through the capillary to prevent separation of gases, which might occur in DC discharges. The mixtures of rare gases were prepared from high purity gases in a special volume, connected to the rest of the vacuum system. Both the discharge tube and the mixing volume were outgased at the pressure of 10^{-6} hPa before being filled with the working mixtures in order to reduce the impurity C I lines and CO bands.

The capillary was mounted inside a special volume which could be filled with liquid nitrogen to cool the excited gas. The emitted VUV radiation, after passing a MgF_2 window, was resolved spectrally with a 1 m normal incidence vacuum spectrometer with 0.83 nm mm^{-1} dispersion. The spectral resolution was 0.015 nm. A PM tube with a MgF_2 window operating in the photon counting mode was used as detector.

The range of the total pressures (50–200 hPa) and the admixture concentrations (0.1–1%) were chosen to demonstrate the emission profiles in the best way. Low partial pressures of the heavier gas admixture (equal to or less than 2 hPa) were used to reduce self-absorption, ensuring intense emission near the resonance lines.

3. Results

An example of VUV emission spectra from Ar–Xe gas mixtures is given in figure 1. A linear scale of intensity is used in the left chart since it is convenient to present intensity and width of the structures. However, to show the low intensity part of the spectral profile and to present several profiles with quite different intensity on the same chart a logarithmic scale is much more convenient (see the right-hand chart in figure 1). Therefore, in the following figures, a logarithmic scale of intensity is used.

The spectra from mixtures with krypton admixture near the first (123.584 nm) and second (116.487 nm) resonance lines of Kr are shown in figures 2 and 3, respectively. Each figure contains three charts with spectra from He–Kr (top), Ne–Kr and Ar–Kr (bottom) mixtures, showing the dependence of the emission profiles on the density of the species. All charts show spectra from mixtures with 50 hPa main gas pressure +0.25% Kr and 100 hPa main gas pressure +0.5% Kr. The charts for Ne and Ar also show spectra from 200 hPa main gas pressure +1% Kr. Since our experimental set-up could not support a stable DC discharge in 200 hPa of He, we give spectra from 50 hPa He +0.1% Kr for the helium mixtures. For convenience, the position of the resonance line is shown with a vertical arrow. The integration time of photon counting was the same (2 s) for all spectra around both resonance lines.

The spectra from mixtures with xenon admixture near the first (146.961 nm) and second (129.559 nm) resonance lines of Xe are shown in figures 4 and 5, respectively. Each figure contains four charts for He–Xe (top), Ne–Xe, Ar–Xe and Kr–Xe (bottom) mixtures. All charts show spectra from mixtures with 50 hPa main gas pressure +0.1% Xe, 50 hPa main gas pressure +0.25% Xe and 100 hPa main gas pressure +1% Xe. The position of the resonance line is shown again with a vertical arrow. A CO impurity band at about 147.9 nm

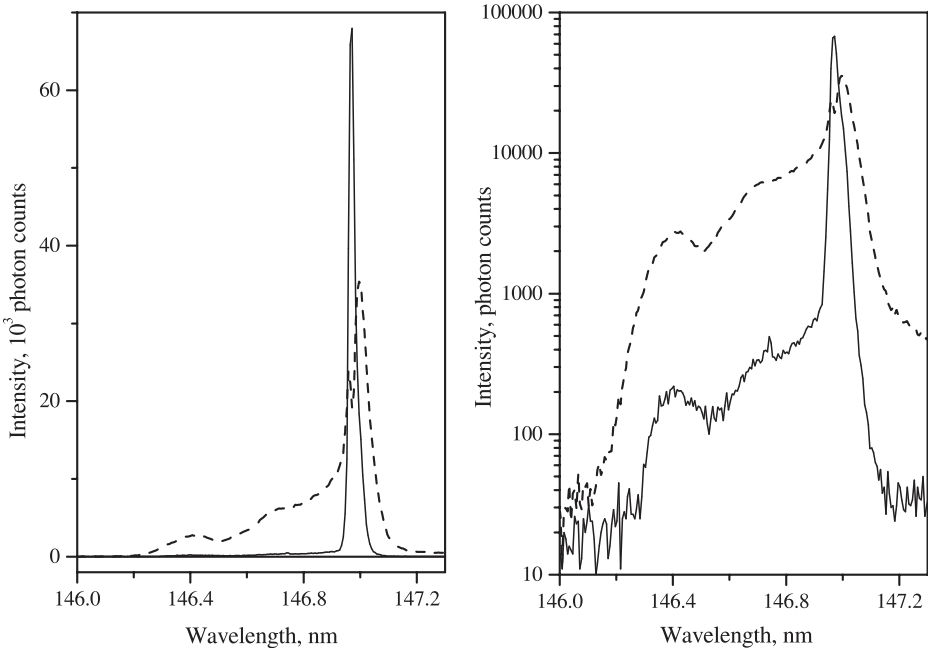

Figure 1. Emission spectra from Ar–Xe gas mixtures at two gas conditions: 100 hPa Ar +1% Xe (——) and 50 hPa Ar +0.1% Xe (- - - -). In the left-hand chart a linear scale of intensity is used. The right-hand chart shows the same curves in a logarithmic scale.

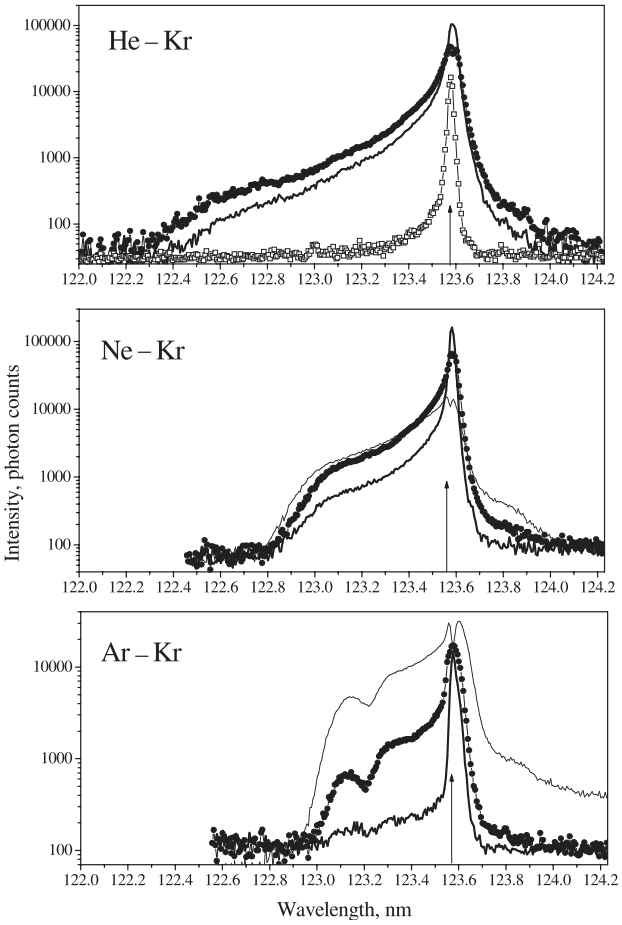

Figure 2. Emission spectra from binary mixtures containing small amounts of Kr with He (top), Ne and Ar (bottom) near the first resonance line of Kr I. The conditions are: 200 hPa main gas pressure +1% Kr (——), 100 hPa main gas pressure +0.5% Kr (· · · · · ·) and 50 hPa main gas pressure +0.25% Kr (——). The thin line with hollow squares shows the spectral profile from 50 hPa of He +0.1% Kr. The arrow marks the position of the atomic resonance line.

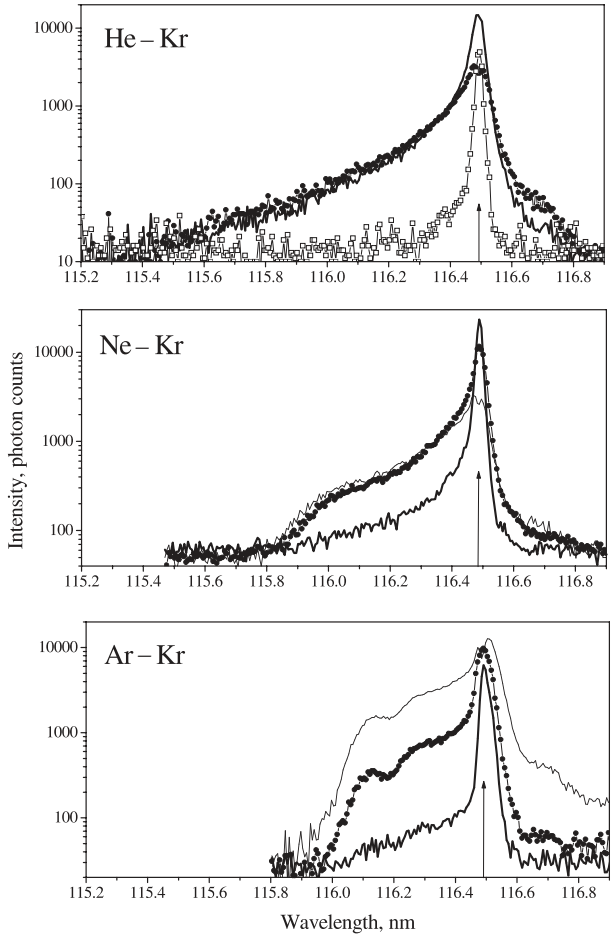

Figure 3. Emission spectra from binary mixtures containing small amounts of Kr with He (top), Ne and Ar (bottom) near the second resonance line of Kr I. The conditions are: 200 hPa main gas pressure +1% Kr (——), 100 hPa main gas pressure +0.5% Kr (· · · · · ·) and 50 hPa main gas pressure +0.25% Kr (——). The thin line with hollow squares shows the spectral profile from 50 hPa of He +0.1% Kr. The arrow marks the position of the atomic resonance line.

which was easily excited in the He–Xe and Ne–Xe mixtures did not allow us to record the long wavelength part of the emission profiles for these mixtures at the first resonance line. The integration time of photon counting was 1 s for the spectra recorded around the first resonance line and 5 s for the spectra around the second resonance line. Different integration times were used because the excitation of the Xe $^3P_1$ state is favoured in comparison with the $^1P_1$ state in DC discharges (see, e.g. [11] for details on Kr–Xe mixture emission).

The intensity of the spectral profiles around the second resonance lines is also reduced in comparison with the intensity of the corresponding profiles around the first resonance lines due to the lower transmittance of the MgF_2 windows (one at the capillary tube and one at the PM tube) at shorter wavelengths [13] and the grating efficiency, which decreases with decreasing wavelength in the spectral range of this study.

All emission profiles in figures 2–5 have common features. The spectra have highest intensity in the vicinity of the resonance line (±0.05 nm), and there are 'blue' and 'red' spectral wings on the short wavelength and long wavelength sides of the resonance lines. One can also see self-absorption at the wavelengths of the atomic resonance lines in the spectral profiles from the mixtures with the highest partial pressures of both gases. Most probably it is caused mainly by radiation absorption in the 4 mm long zone between the end of the capillary discharge and the capillary output window but also, to a certain degree, in the discharge volume itself.

For a mixture of two given gases the blue wings usually have a well-defined cut-off wavelength, where the intensity of the wing reaches the background intensity. This cut-off wavelength does not change much when varying the partial pressures of the gases, until the admixture concentration becomes so low that the wing intensity is too weak to be reliably detected above the background noise. Keeping the same admixture gas and changing the host gas from the heaviest to the lightest, one can note two features common for all mixtures. The lighter the main gas, the broader becomes the blue wing, and the fewer the number of structures that appear in the wing (see figures 2–5).

The red wing profiles are very different for the heavy (Ar and Kr as the host gas) and light mixtures (He and Ne as the host gas) as one can see in figures 2–5. The spectra

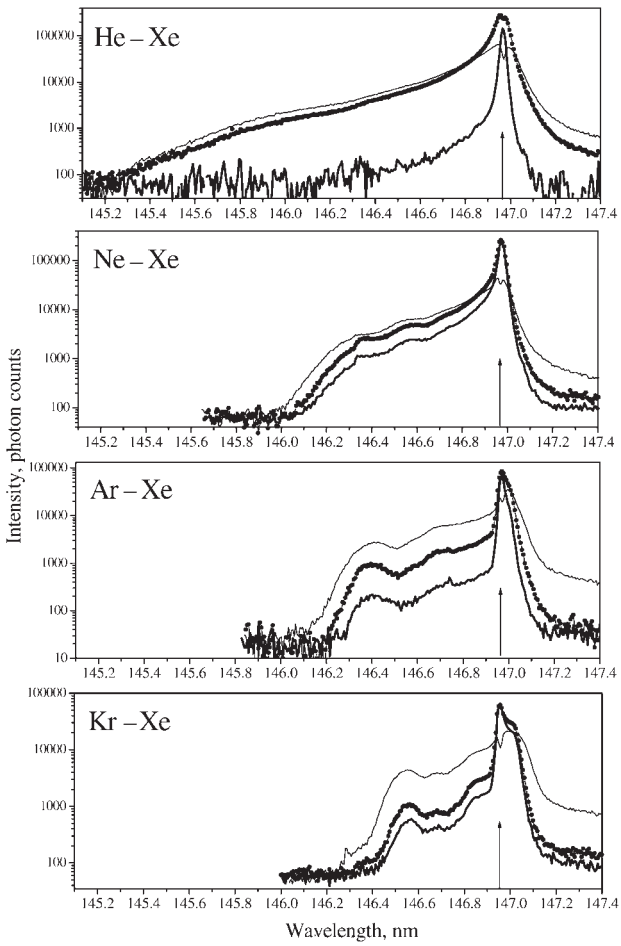

Figure 4. Emission spectra from binary mixtures containing small amounts of Xe with He (top), Ne, Ar and Kr (bottom) near the first resonance line of Xe I. The conditions are: 100 hPa main gas pressure +1% Xe (——), 50 hPa main gas pressure +0.25% Xe (· · · · · ·) and 50 hPa main gas pressure +0.1% Xe (——). The arrow marks the position of the atomic resonance line.

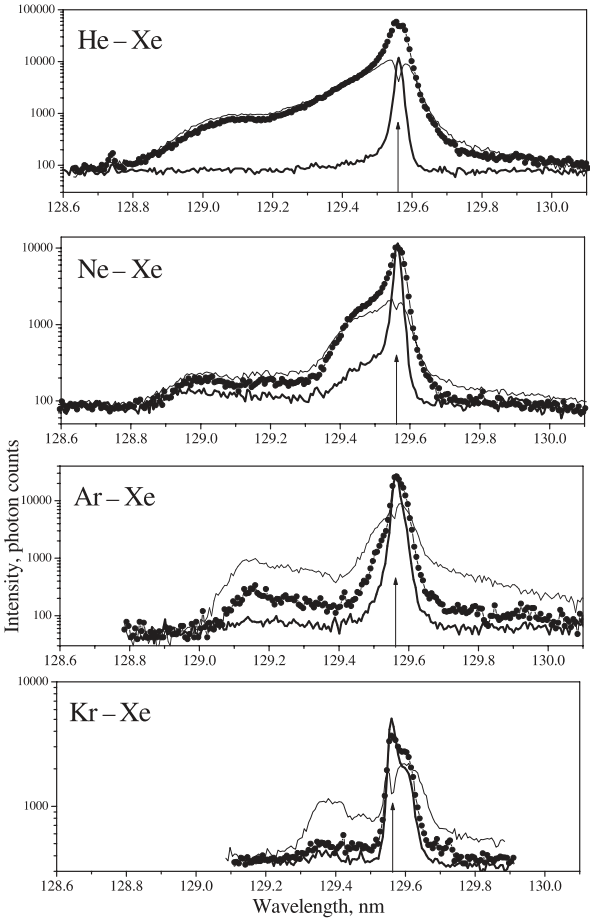

Figure 5. Emission spectra from binary mixtures containing small amounts of Xe with He (top), Ne, Ar and Kr (bottom) near the second resonance line of Xe I. The conditions are: 100 hPa main gas pressure +1% Xe (——), 50 hPa main gas pressure +0.25% Xe (· · · · · ·), 50 hPa main gas pressure +0.1% Xe (——). The arrow marks the position of the atomic resonance line.

from the heavy mixtures, unlike from the light mixtures, have a 'shoulder' immediately on the long wavelength side of the resonance line. Also, self-absorption appears not in the centre of the peak, but is shifted towards shorter wavelength. Another feature of the red wing for the heavy mixtures is that there is no definite cut-off wavelength of the wing: the higher the partial pressures, the longer the wing expands. In contrast, the red wings of the majority of the light mixtures have a definite length and decrease monotonously or have only one structure—the wing reaches background intensity in about 0.6 nm from the resonance line (note that for higher partial pressures of admixtures than used in the study, the red wings expand due to emission from homonuclear molecules of the admixture). The exceptions are the mixtures of Xe with He and Ne close to the first resonance line. In this case the red wing expands monotonously for at least 1.1 nm away from the resonance line, where it has small but non-zero intensity and is screened in our experiments by the impurity CO band.

For the purpose of spectral structure identification, the effect of cooling was investigated in mixtures with Kr admixtures. Spectra were recorded from mixtures of 1% Kr with Ne and Ar at the total gas pressure of 100 hPa with and without liquid nitrogen cooling of the outside wall of the capillary. Figure 6 demonstrates the effect of cooling on the spectral profiles around the first resonance line of krypton.

There is a considerable redistribution in the spectral profiles as a result of the cooling: the long wavelength part of the red wing increases its intensity while the intensity of the short wavelength side of the blue wing decreases, especially in the mixtures with neon. The spectral profiles near the second resonance line behave in a similar way. A comparison of the intensity of the spectra recorded from discharges with and without cooling should however be done with care since there are counter-working effects on the intensity: an increase of the density of admixture atoms with cooling increases the intensity, while a thermal lens, i.e. the defocusing effect in the capillary due to the temperature gradient across the discharge volume, is more effective in the cooled discharge, decreasing the intensity. A very strong influence of the wall temperature on the thermal lens effect was confirmed by passing visible laser light through the discharge capillary and observing the change of laser beam spot size.

Drastic changes of spectral profiles with cooling were observed in mixtures with Xe. However, the interpretation of

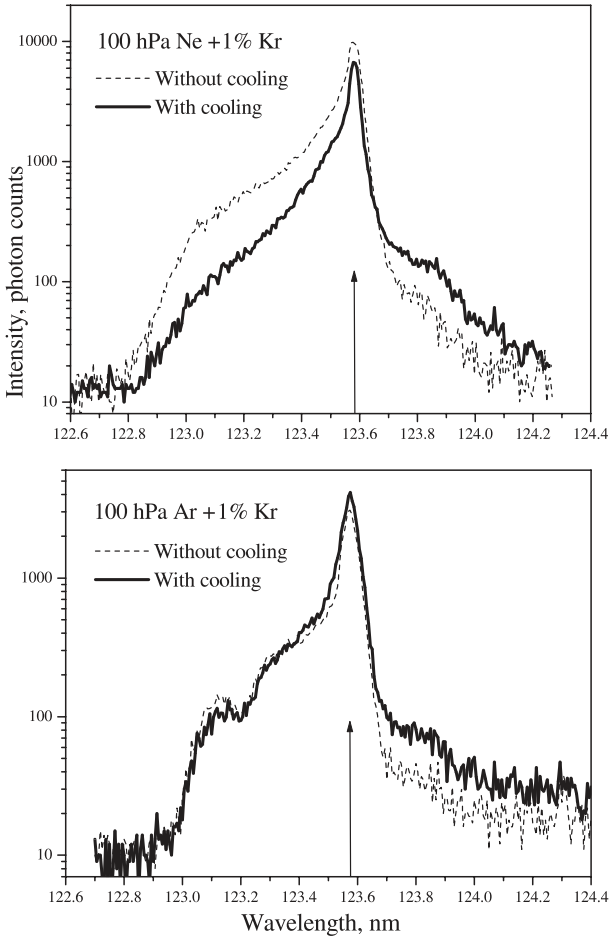

Figure 6. The effect of cooling on emission profiles near the first resonance line of krypton is demonstrated for Kr mixtures with Ne (top) and Ar (bottom). Dashed lines represent the case when no cooling is applied while solid lines show the spectral profiles from discharges when the outer wall of the capillary was cooled with liquid nitrogen.

these results is much more complicated since a considerable part of the xenon atoms freeze on the inner capillary wall. We could not observe the effect of cooling on mixtures with helium, since the discharge became very unstable after applying the liquid nitrogen.

4. Discussion

4.1. Comparison of intensities

All presented spectra were recorded with the same experimental set-up and in a short period of time, so the loss of transmittance of the optics from the first measurement to the last was found negligible. The integration time was the same for all mixtures with the same admixture near a given resonance line (2 s for all mixtures with Kr, and 1 s and 5 s for Xe mixtures close to the $^3P_1$ and $^1P_1$ resonance lines, respectively). A discharge current of 20 mA was kept constant for all investigated mixtures. Thus all possible precautions were taken to record spectra from all mixtures with the same admixture in similar conditions.

However, there are some factors that affect the intensity from the mixtures differently. First, it is the input power. The lighter the buffer gas, the more voltage is required to sustain a current of 20 mA. Thus the input power was highest in the mixtures with He (up to two times higher than in mixtures with Kr). Second, it is the geometrical factor that affects the observation of the radiation from the discharge channel. The lighter the buffer gas, the more visually uniform is the discharge channel. With He as buffer gas the discharge channel always filled the whole cross-section of the capillary, while for mixtures with 200 hPa of Kr the discharge channel filled only the central part of the capillary (broader channels were observed at lower pressures). Finally, there is the thermal lens effect. For lighter buffer gases when the gas temperature is very high due to higher input power, the defocusing lens effect is considerably stronger than for the mixtures with heavier host gases. All these factors affect the detected intensity, but there is not enough information to estimate their influence quantitatively. Nevertheless, we believe that in a first approximation all emission spectra for a given gas admixture close to the same resonance line could be directly comparable as if they were recorded at the same conditions. This is so because the more power that is applied the more photons are emitted but the lower is the fraction that reaches the registration system due to the increased effect of the thermal lens.

4.2. Internuclear potentials

Since heteronuclear atomic pairs might strongly contribute to the VUV emission, one has to discuss the internuclear potentials for these pairs before it is possible to analyse the origins of the observed emission structures. In the following paragraphs a review is given on the information that presently exist on internuclear potentials of the lowest excited states of the heteronuclear rare gas molecules which have Kr and Xe resonant atomic states as their origin.

The first attempts to estimate such potentials were made by Castex [7] for Xe*($^3P_1$) + Ar and Xe*($^3P_1$) + Kr on the basis of the analysis of high resolution absorption spectra and the parameters of the ground state potentials. Applying the quasistatic theory, parameters of potentials of the excited states were deduced. According to these calculations, the excited molecular states contributing to the absorption spectra close to the atomic resonance lines are weakly bound [7] with potential wells that are shallower than the wells of the corresponding ground state.

Later, semi-empiric calculations were performed for some excited states of the heteronuclear molecules [14, 15] which predicted the existence of pairs of bound states: the states $1(^3P_1)$ and $0^+(^3P_1)$ for Kr*Ar, Xe*Ar and Xe*Kr, and the states $1(^1P_1)$ and $0^+(^1P_1)$ for Kr*Ar (see, e.g. figure 7). Parameters of the potential curves for these states were also estimated [14, 15]. According to these calculations, the states $1(^3P_1, ^1P_1)$ have approximately the same equilibrium internuclear distance as the ground state and their potential well depths are of the same order as the well depth of the weakly bound ground state. The states 0^+ are usually deeper and have smaller equilibrium distances (this is especially characteristic for the heaviest atomic pairs). Parameters of the weakly bound states $1(^3P_1, ^1P_1)$ and $0^+(^3P_1, ^1P_1)$ for molecules of Kr (and Xe) with

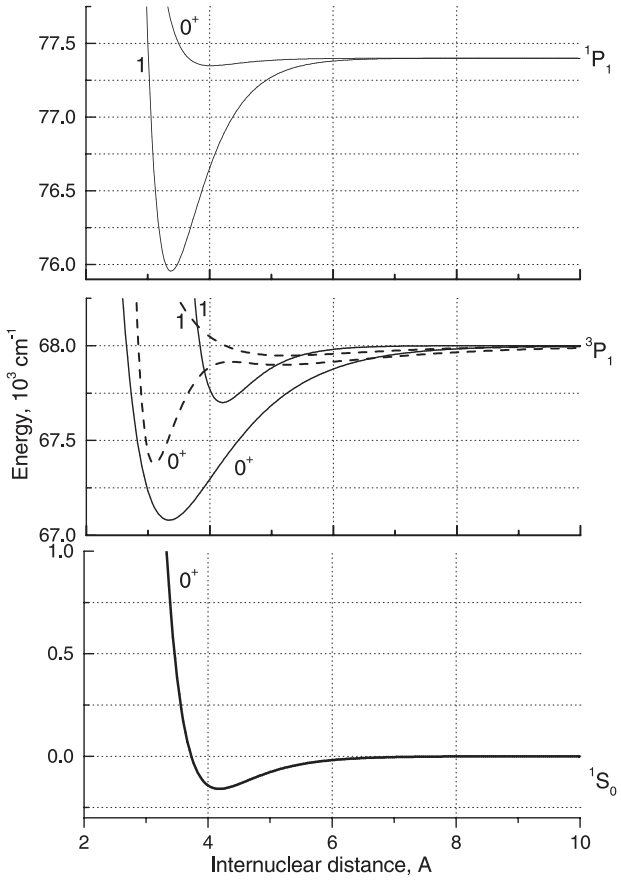

Figure 7. A scheme of potential curves for the excited states $1(^3P_1)$, $0^+(^3P_1)$, $1(^1P_1)$, $0^+(^1P_1)$ and the ground state of XeKr molecules. The curves for the states with the origin in the Xe state $^1P_1$ are given on the basis of [18]. Two sets of results are given for the states with the origin in the Xe state $^3P_1$: solid lines represent potentials which are based on the results of [14] (semi-empiric calculations), while the dashed lines give potentials according to [19] (laser spectroscopy).

He and Ne were estimated in another paper [16] using similar semi-empiric calculations. The depths of all states were found to be a few cm^{-1} for molecules with He and a few dozens of cm^{-1} for molecules with Ne.

Information on the potential curves of the rare gas dimers for a number of excited states was also supplied by laser spectroscopy of jet-cooled rare gas mixtures (e.g. see a review paper [17]). Thus, the internuclear potentials for the states $1(^1P_1)$ and $0^+(^1P_1)$ of Xe*Ar and Xe*Kr were obtained in [18]. For these molecules, in contrast to other atomic pairs, the $0^+(^1P_1)$ states were found to be weakly bound (111.8 cm^{-1} and 51.2 cm^{-1} for XeAr and XeKr, respectively) and to have equilibrium distances of 3.77 Å and 3.66 Å, respectively, which are approximately the same as the equlibrium distances of the ground states. According to the calculations in [18], the $1(^1P_1)$ states are more strongly bound (243.5 and 1444.6 cm^{-1}) and have approximately 0.5 Å shorter equilibrium distances (3.23 and 3.01 Å) than the states 0^+ (see figure 7).

A similar laser spectroscopic technique was used in [19] to obtain internuclear potentials for the states $1(^3P_1)$ and $0^+(^3P_1)$ of the Xe*Kr molecule (see figure 7). The results are in bad agreement with the predictions of the semi-empiric calculations [14, 15]: the weakly bound state $1(^3P_1)$ is found to be considerably shallower (only 52.2 cm^{-1} in contrast to ∼300 cm^{-1}) and to have considerably larger equilibrium distance (5.24 Å in contrast to ∼4 Å). The $0^+(^3P_1)$ state was found to have a double minimum. The parameters of the inner minimum (equilibrium at 3.09 Å, 624 cm^{-1} deep) are more or less similar to the parameters of the state 0^+ in the semi-empiric calculations [14, 15]. The outer minimum has an equilibrium distance of 5.1 Å (practically the same as the equlibrium of the state 1) and it is 101 cm^{-1} deep.

Ab initio calculations of internuclear potentials for the Xe*Ar molecules were presented in the paper [20] for a considerable number of the lowest excited states. However we do not take the results into account since the states $1(^3P_1, ^1P_1)$ were predicted to be completely repulsive, which disagrees with the experimental results [18] as well as with the results of the semi-empiric calculations [14].

As one can see, data on internuclear potentials of heteronuclear atomic pairs of rare gases is scarce. Moreover, there is a bad agreement between the semi-empiric calculations and the experimental results for the single molecule where results from both techniques are available. However, there are some general properties that are practically the same for all these atomic pairs. All molecules of Kr*Ar, Xe*Ar and Xe*Kr have pairs of excited states 1 and $0^+(^1P_1, ^3P_1)$. Each pair contains a weakly bound state with an equilibrium distance equal to or greater than that of the ground state, and a more deeply bound state with an equilibrium distance smaller than that of the ground state. These potential wells contain a considerable number of vibrational levels. Molecules with He and Ne have, according to the semi-empiric calculations [16], very weakly bound excited states. The potential wells of molecules with Ne hardly contain more than a few vibrational levels, while the molecules with He most probably contain none.

Using these general properties of the internuclear potentials and the results of high resolution absorption studies [7, 8] we will now make an attempt to build a general identification scheme for our emission spectra. This identification should be regarded only as an approximation, which will probably need adjustments when new data appear on the internuclear potentials.

4.3. Identification of the emission structures

When one compares our emission spectra (figures 2–5) with high resolution absorption spectra reported in [7, 8], one observes a striking similarity between the corresponding absorption and emission spectral profiles for all mixtures. This is demonstrated in figure 8, where two pairs of our emission and the corresponding absorption spectra from [8] are given for Kr–Xe mixtures near the first resonance line of Xe and for Ar–Xe mixtures near the second resonance line of Xe. This similarity suggests that transitions between the same states give rise to the main spectral features in both absorption and emission.

(I). Let us consider first the case of the heavy atom mixtures (Ar and Kr as the host gas). The authors of the absorption studies have suggested that the main contribution to the blue wing arises from Kr*X and Xe*Y molecules in bound–free [8] or in bound–free and bound–bound [7] transitions from the

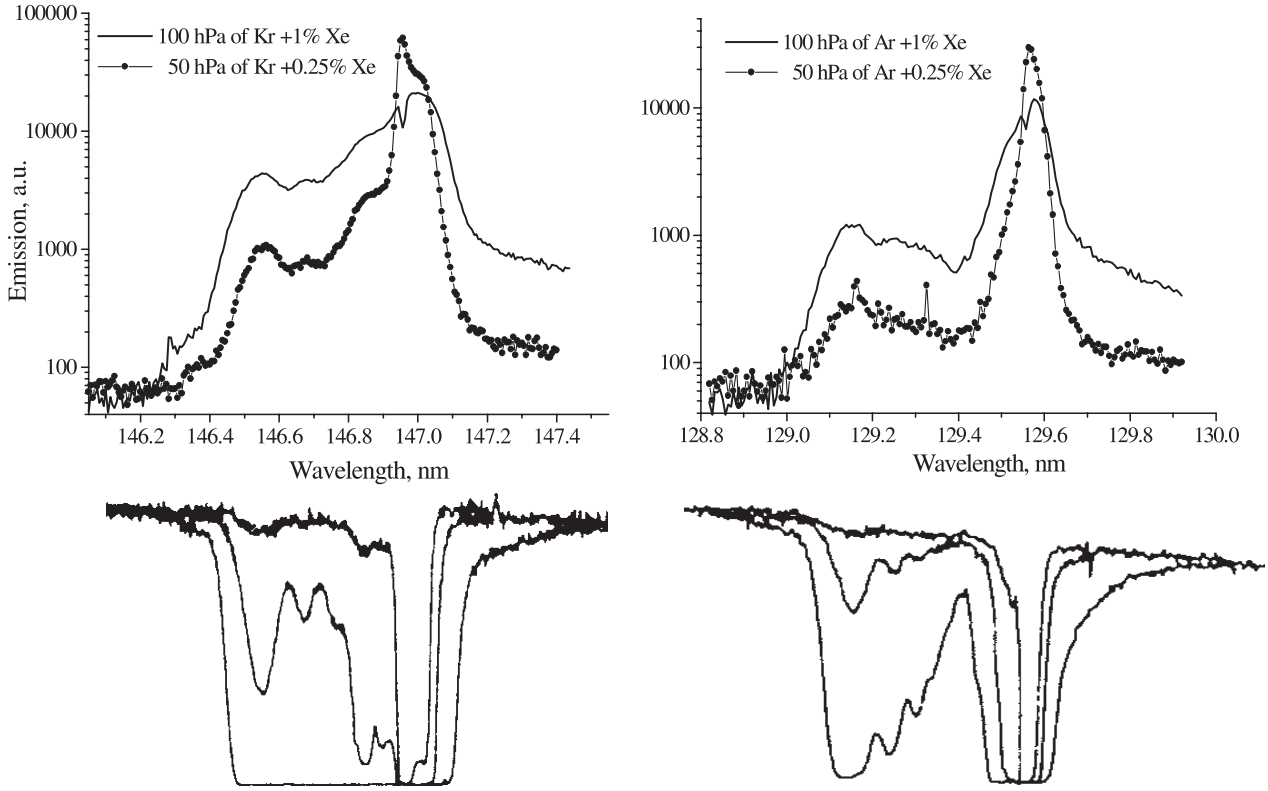

Figure 8. A comparison of emission (this paper) and absorption [8] spectral profiles is given for mixtures of Xe with Kr (left) and Ar (right). The top charts on both sides show the emission spectra, while the bottom charts present the corresponding absorption spectra (densitometer traces). Two emission profiles are given: 100 hPa main gas pressure +1 hPa of Xe (——) and 50 hPa main gas pressure +0.13 hPa of Xe (· · · · · ·). The absorption spectra from [8] were recorded with a Xe pressure of 0.13 hPa and main gas pressures of 8,215 and 650 hPa.

ground state. The identification was supported in particular by the character of the dependence of the absorption profile intensities with gas cooling and by the linear dependence of the absorption band intensities on the product of the pressures of the main gas and the admixture [7].

Therefore, if one assumes that the blue wing in absorption is mainly due to transitions between the vibrational levels of the ground state and the repulsive part of an excited state, then the most suitable candidate for the excited state is a weakly bound state due to the fact that the weakly bound states have larger equilibrium distances than the strongly bound states, and consequently, the repulsive part is situated closer to the region of the potential well of the ground state—see figure 9. Note that in this context the term 'weakly bound' is used for the states $1(^3P_1)$ of all heavy atomic pairs, as well as the state $1(^1P_1)$ of Kr*Ar and the state $0^+(^1P_1)$ of Xe*Kr and Xe*Ar since all these states exhibit similar properties (see previous section). Because of the similarity of the emission and absorption profiles, it is reasonable to expect that the same transitions give the main contribution to the blue wing in emission. This is supported by our results on the spectral temperature dependence (figure 6)—the short wavelength part of the blue wing reduces its relative intensity with cooling, the reason being that the shorter the wavelength becomes, the higher kinetic energy is required for an atomic pair to produce emission in the blue wing. Another experimental fact, namely that the number of emission structures in the blue wing is smaller for a lighter main gas than for a heavier main gas with the same admixture, is connected with the reduction of the number of vibrational levels in the ground state (see, e.g. [21]).

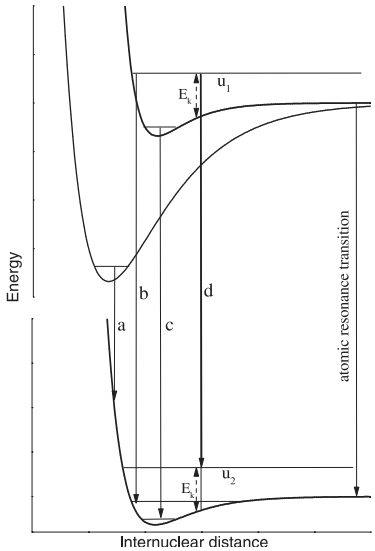

Figure 9. Examples of bound–free (a), free–bound (b), bound–bound (c) and free–free transitions (d) are given for a schematic diagram of potential curves for the two lowest excited states and the ground state of a heteronuclear rare gas molecule. The atomic resonance transition is also shown. Details on free–free transitions are given in section 4.3.

Concerning the emission in the red wing, it is convenient to start the identification with the well developed and extended

long wavelength part of the red wing. Because of its width (thousands of cm^{-1} in energy scale—see transitions type (a) in figure 9) it is reasonable to attribute it to the emission from highly situated vibrational levels of the strongly bound states to the ground state in Xe*X and Kr*Y heteronuclear molecules. We consider the contribution from excited Kr_2 and Xe_2 molecules to be small since the maximum concentration of the admixture in this study was 1% and therefore the number of homonuclear molecules, created in three-body collisions, should be about two orders of magnitude lower than the number of the heteronuclear molecules, and the total pressure is not high enough to support noticeable energy transfer to homonuclear molecules of admixture atoms from heteronuclear molecules (see results on Kr–Xe emission presented in [11]).

There are two other contributions to the red wing close to the resonance lines. One of them is from bound–bound transitions between vibrational levels of the excited weakly bound state and vibrational levels of the ground state of the heteronuclear molecule (see our earlier publications [10–12] concerning Kr–Xe emission). These are probably the transitions that form the intense shoulders close to the resonance lines in the emission profiles. Similar shoulders were observed in the absorption studies [7, 8] (see figure 8), and a bound–bound origin was suggested in [8]. However, the shoulders in the absorption studies appeared as diffuse structures even at the resolution of 0.001 nm, which is probably explained by an overlap of very closely situated vibrational components. A special attention should be given to Xe*Kr emission close to the first Xe resonance line. If the internuclear potential of the $0^+(^3P_1)$ state is indeed as predicted in [19] and has two minima, then bound–bound transitions from that state to the ground state could also give a considerable contribution (in comparison with the contribution from the state $1(^3P_1)$) to the emission in the vicinity of the resonance line and in the intense red shoulder.

Another contribution to the red wings, and possibly to some extent to the blue wing, arises from transitions in free atomic pairs (free–free transitions). In this case an emitting atom of the admixture is perturbed by a closely situated atom of the main gas, so that the wavelength of the transition will be defined by the energy difference between the potential curves of the excited and the ground states of the heteronuclear molecule at the given internuclear distance between the atoms, where the transition takes place (see, e.g. [22]). The transition (d) in figure 9 gives an example of the classical description of such a free–free $Xe(^3P_1) + Kr(^1S_0) \rightarrow Xe(^1S_0) + Kr(^1S_0)$ transition, where the system has total energy u_1 before and u_2 after the transition. Since the kinetic energy E_k of the system is conserved in the transition (the photon momentum is very small), the wavelength of the transition corresponds to the energy difference between the potential curves for the actual internuclear distance. Note that for free–free transitions the kinetic energy of the two-atom system is too high both in the excited and ground quasimolecular states to let the atoms form a stable molecule with discrete vibrational levels.

(II). The light mixtures (He and Ne as the host gas) have one feature which makes them very different from the heavy atom mixtures, namely that the states 1 and 0^+ are practically identical and both are very weakly bound [16]. As a consequence, the excited states hardly have any vibrational levels and free–free transitions are the dominating origin of the spectral red wings. The blue wings, as in the case of heavy atom mixtures, arise through a combination of free–bound and free–free transitions. The number of structures in the blue wing is smaller since the ground states contain just a few vibrational levels (compare the blue wings in figures 2–5).

5. Conclusion

VUV emission from all presented binary rare gas mixtures demonstrates narrow and intense emission close to the resonance lines of the heavier gas. This emission is especially intense close to the lower energy resonance lines.

The presented emission profiles show a remarkable similarity with the corresponding absorption spectral profiles. This suggests that the same transitions give the main contribution to both types of spectra.

The recorded spectral structures in both the short and long wavelength wings near the resonance lines can be attributed to transitions in heteronuclear molecules and quasimolecules between the excited states $1(^3P_1)$, $0^+(^3P_1)$, $1(^1P_1)$, $0^+(^1P_1)$ and the ground state. The short wavelength wings originate from free–bound and free–free transitions. The long wavelength wings have their origins in free–free and, for heavy mixtures which have Ar and Kr as the host gas, also in bound–bound transitions. The extended and low intensity part of the long wavelength wings observed in heavy mixtures have their origin in bound–free transitions between the states $0^+(^3P_1)$ and the ground state.

The data presented in this paper could be useful for the development of VUV radiation sources. However, a separate study is required to compare excitation dynamics in the different binary rare gas mixtures.

Acknowledgments

We gratefully acknowledge the support of this paper received from the Carl Trygger Foundation for Scientific Research and the Göran Gustafsson Foundation. The Swedish Institute through the Visby Program is acknowledged for two scholarships (B Krylov and G Gerasimov).

References

[1] Gedanken A, Jortner J, Raz B and Szoke A 1972 *J. Chem. Phys.* **57** 3456
[2] Cheshnovsky O, Raz B and Jortner J 1972 *J. Chem. Phys.* **57** 4628
[3] Cheshnovsky O, Raz B and Jortner J 1973 *J. Chem. Phys.* **59** 3301
[4] Novak G and Frike J 1985 *J. Phys. B: At. Mol. Phys.* **18** 1355
[5] Cook J D and Leichner P K 1985 *Phys. Rev.* A **31** 90
[6] Cook J D and Leichner P K 1991 *Phys. Rev.* A **43** 1614
[7] Castex M C 1977 *J. Chem. Phys.* **66** 3854
[8] Freeman D, Yoshino K and Tanaka Y 1977 *J. Chem. Phys.* **67** 3462
[9] Wieme W and Lenaerts J 1980 *J. Chem. Phys.* **72** 2708
[10] Gerasimov G, Hallin R, Krylov B, Volkova G, Heijkenskjold F and Morozov A 1997 *Proc. SPIE* **3403** 322

[11] Krylov B, Gerasimov G, Morozov A, Arnesen A, Hallin R and Heijkenskjold F 2000 *Eur. Phys. J.* D **8** 227
[12] Morozov A, Krylov B, Gerasimov G, Hallin R and Arnesen A 2000 *Eur. Phys. J.* D **11** 379
[13] Elliott D J 1995 *Ultraviolet Laser Technology and Applications* (San Diego: Academic)
[14] Zagrebin A L and Pavlovskaya N A 1990 *Opt. Spectrosc. (USSR)* **69** 320
[15] Zagrebin A L and Tserkovnyi S I 1995 *Chem. Phys. Lett.* **239** 136
[16] Devdariani A Z, Zagrebin A L and Blagoev K B 1989 *Ann. Phys. Fr.* **14** 467
[17] Yamanouchi K and Tsuchiya S 1995 *J. Phys.* B **28** 133
[18] Tsuchizawa T, Yamanouchi K and Tsuchiya S 1990 *J. Chem. Phys.* **92** 1560
[19] Pibel C D, Yamanouchi K, Miyawaki J, Tsuchiya S, Rajaram B and Field R W 1994 *J. Chem. Phys.* **101** 10242
[20] Spiegelmann F, Gadea F X and Castex M C 1990 *Chem. Phys.* **145** 173
[21] Bobetic M V and Barker J A 1976 *J. Chem. Phys.* **64** 2367
[22] Devdariani A Z 1999 *Opt. Spectrosc.* **86** 853

Paper II

Eur. Phys. J. D **11**, 379–385 (2000)

THE EUROPEAN PHYSICAL JOURNAL D

EDP Sciences

Identification of structures in absorption spectrum of Kr–Xe gas mixtures close to the Xe resonance line at 146.96 nm

A. Morozov[1,a], B. Krylov[2], G. Gerasimov[2], R. Hallin[1], and A. Arnesen[1]

[1] Uppsala University, Department of Physics, Box 530, 75121 Uppsala, Sweden
[2] Vavilov state Optical Institute, Birzhevaja Line 12, St. Petersburg, 199034, Russia

Received 15 December 1999 and Received in final form 20 February 2000

Abstract. The origins of spectral structures that appear close to the Xe resonance line at 146.96 nm in absorption spectra of Kr gas with an admixture of Xe are discussed in this paper. It is shown that these structures can result from bound-bound and bound-free transitions in the Xe–Kr molecule between the ground state and the $1(^3P_1)$ excited state, which both are weakly-bound. The depth of the excited state is estimated. An introduction of a hump on the $1(^3P_1)$ state internuclear potential is suggested.

PACS. 33.20.Ni Vacuum ultraviolet spectra – 33.20.Tp Vibrational analysis

1 Introduction

Recently increasing attention has been paid to vacuum ultraviolet (VUV) emission spectra of heteronuclear rare gas diatomic molecules [1, 2]. This is connected with a number of practical applications such as broad band radiation sources [3, 4], and with discussions of the possibility to achieve VUV laser generation using heteronuclear rare gas molecules [5]. However, while the understanding of the internuclear potentials of the ground and excited states of homonuclear dimers is well established and seems to be quite reliable (see *e.g.* [6, 7]), the situation for heteronuclear dimers is less satisfactory. Detailed data exist only for the ground states [8], and were obtained by fitting theoretical potentials to a compilation of experimental results. Some information on the lowest excited states has been obtained by Castex [9] from absorption experiments and by Novak and Fricke [10] from surface VUV emission results. Theoretical investigations of the lowest excited states have been performed by Zagrebin and co-workers [11, 12], who obtained fundamental information on the internuclear potential curves for the lowest excited states. Application of these data in an attempt to define the origins of the observed spectral structures in emission and absorption could contribute to further adjustments of the shape and parameters of the internuclear potentials.

In this paper we discuss only the XeKr molecule. A basic scheme of internuclear potentials for the ground and the lowest excited XeKr molecular states (these excited states have their origins in the atomic Xe states $^3P_1$ and $^3P_2$) is presented in Figure 1. The potentials are shown in the Morse form. All excited-state potentials in Figure 1 are based on calculations [11], which predict the existence of bound (well depth about 1000 cm^{-1}) and weakly-bound (well depths about or less then 500 cm^{-1}) excited states.

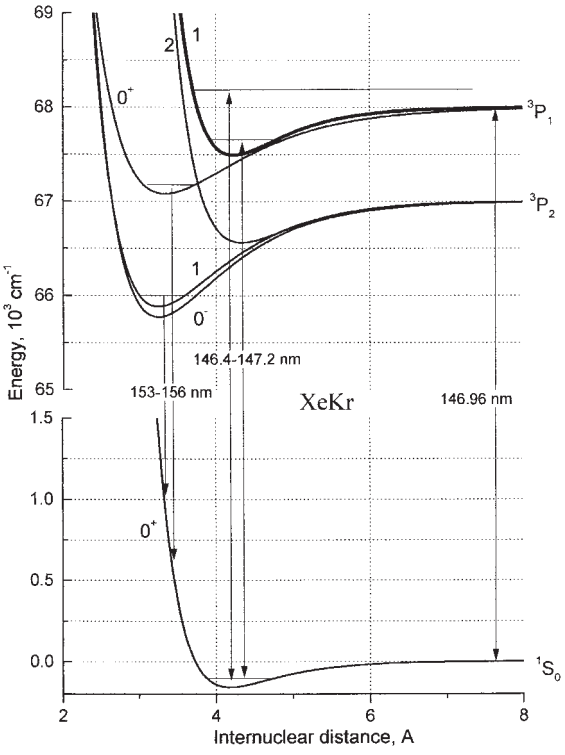

Fig. 1. Internuclear potentials for the ground and lowest excited states of the XeKr molecule. All curves are presented in the Morse form. Examples of bound and repulsive levels are shown by horizontal lines. Vertical arrows represent principal classes of transitions, including the atomic Xe^* resonance line and examples of bound-bound and bound-free transitions.

[a] e-mail: andreim@trym.fysik.uu.se

The weakly-bound states have equilibrium distances similar to that of the XeKr ground state, unlike the more strongly-bound excited states.

A Xe–Kr gas mixture emission spectrum shows a very intense and relatively narrow band around the Xe* resonance line at 146.96 nm (see [1]) with a width of 0.1–0.7 nm depending on the gas pressure. A reliable determination of the origins of this emission structure and detailed information on the internuclear potentials of the involved states would be useful for developing narrow band high intensity VUV radiation sources and for attempts to create a VUV laser working on molecular transitions in XeKr. In this article we present an attempt to analyse these potentials based on spectroscopic data.

We restrict our discussion to the state $1(^3P_1)$, since transitions from this state dominate the emission close to the Xe resonance line at 146.96 nm. This restriction is motivated by a number of facts: the atomic state $^3P_2$ is considerably shifted down in energy from the state $^3P_1$, so the transitions from the states $1(^3P_2)$ and $2(^3P_2)$ are situated at longer wavelengths; in addition the transition from the state $2(^3P_2)$ to the ground state is dipole forbidden. The relatively strongly-bound state $0^+(^3P_1)$ has an internuclear potential with a small equilibrium distance, so that emission from that state (similar in origin to the second continua of homonuclear dimers – see Fig. 1) appears as a broad continuum with maximum near 153 nm. Emission (absorption) from (to) this state close to 146.96 nm should also be small in comparison with emission (absorption) from (to) the state $1(^3P_1)$, because the weakly-bound state $1(^3P_1)$ has about the same potential well depth and equilibrium distance as the ground state, so the emission (absorption) from (to) this state will be more concentrated around the Xe* resonance line than for the $0^+(^3P_1)$ state. Moreover, due to the large difference in equilibrium distances between the ground and $0^+(^3P_1)$ states, their nuclear wave functions will have smaller overlap than the nuclear wave functions of the ground and $1(^3P_1)$ states.

However, it is quite difficult to identify the origins of the emission spectrum around 146.96 nm. No experimental emission data of high enough resolution (of the order of 0.001 nm) to be used as a detailed description of the bands have been published to our knowledge. Existing experiments show only general features, without the necessary details. Furthermore, for emission it is usually problematic to estimate relative populations of excited vibrational levels. In contrast to this, there are at least two high resolution experimental absorption studies performed by Castex [9] and Freeman *et al.* [13] (the resolution was 0.002 and 0.001 nm respectively) which describe absorption spectra around 146.96 nm in detail. Moreover, low resolution data (see *e.g.* our recently reported [1] results with a resolution of the order of 0.02 nm) show that emission and absorption spectra near the Xe resonance line at 146.96 nm exhibit remarkable similarity (Fig. 2), which indicates that corresponding spectral structures of both types of spectra have similar origins. The relative populations of the ground state vibrational levels are distributed according to Boltzmann statistics, and therefore easy to calculate. Furthermore, every emission spectrum around 146.96 nm from a Kr–Xe gas mixture light source is a combination of emission and self-absorption. This requires reliable and detailed information about the structure and origins of the absorption spectra in order to draw conclusions about the origins of the emission spectra. The discussion above indicates that elucidation of the origins of the emission spectral structures should be conducted after the origins of the absorption bands have been reliably established, which has not been done yet to our knowledge.

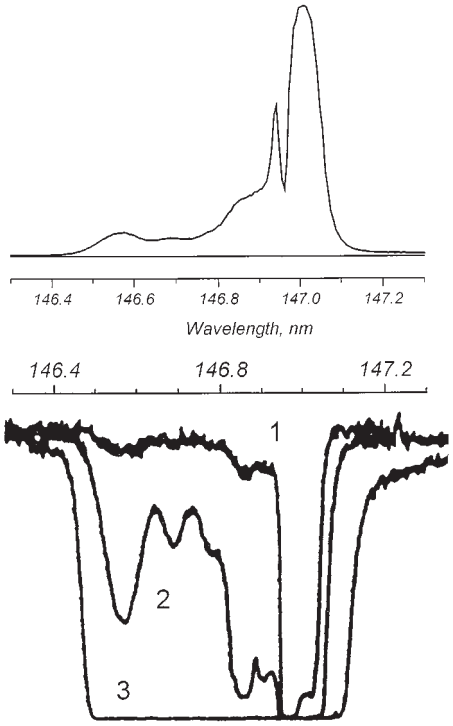

Fig. 2. An emission spectrum from a Kr–Xe gas mixture [1] (top spectrum) and absorption spectra recorded by Freeman *et al.* [13] (lower spectra) around the Xe I resonance line at 146.96 nm. The emission spectrum was obtained from a DC gas discharge (total gas pressure 120 hPa, Xe concentration 0.25%). Three absorption spectra are shown for the same Xe partial pressure 0.13 hPa and three different Kr pressures (1: 8 hPa, 2: 215 hPa, 3: 646 hPa).

In the next section we review the experimental absorption data to be used in the following discussion. These data will then be utilised to construct model internuclear potentials for the XeKr state $1(^3P_1)$ and to explain possible origins of the spectral structures. This will be done through qualitative analysis of the absorption spectra obtained by numerical simulations. These spectral simulations are obtained through calculations of the overlap of the nuclear wave functions of the ground state vibrational levels and bound or repulsive levels of the excited state (see Fig. 1). We do not expect the spectra obtained in this way to agree quantitatively with high resolution experimental spectra since model potentials have been used and rotational structure was beyond the scope of the present

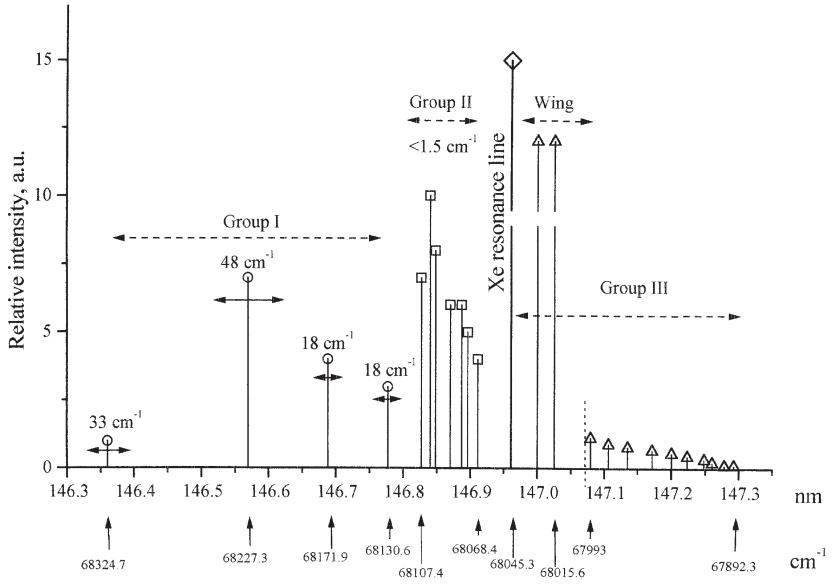

Fig. 3. A summary of experimental results obtained by Freeman *et al.* [13]. Vertical lines represent the positions (in nm and cm^{-1}) of spectral bands. Where it is available, the width of band is shown on top of the line. The Xe resonance line is marked with the diamond. Band group III (triangles) contains also the diffuse wing, adjoined to the resonance line: two of the most intense bands represent the maxima of the wing. Band group I (hollow dots) consists of four very broad and diffuse bands. Band group II (rectangles) is composed of seven very narrow bands with widths less than 1.5 cm^{-1}.

calculations. Our aim is, however, to be able to reproduce qualitatively all important spectral structures.

2 Review of available experimental data

According to Freeman *et al.* [13], three groups of discrete bands could be observed in the absorption spectra near the first resonance line of Xe I at 146.96 nm in Xe–Kr gas mixtures. In Figure 3 the results reported by Freeman in his Table I [13] are shown graphically: each observed band is represented by a vertical line at the appropriate wavelength, with the height proportional to the relative intensity of the band in its band group. The band's width is indicated if it was reported. The names of the absorption bands are the same as those used by Freeman [13].

As the first spectral feature, the broadened Xe I resonance line appears when only traces of Xe are added to Kr gas. On its long wavelength side the line has a wing containing three intensity maxima (146.961, 147.000 and 147.025 nm). At higher Xe concentration, more spectral features appear. The wing intensifies and broadens slightly towards long wavelengths but still exhibits a fairly sharp long wavelength edge. When $p(\mathrm{Xe}) \times p(\mathrm{Kr})$ reaches 0.4 torr^2 ($p(x)$ being the pressure of gas x), the sharp bands of band group II appear close to and on the short wavelength side of the resonance line (146.827–146.911 nm). All seven bands of this group have similar bandwidths of about or less then 1.5 cm^{-1} (0.003 nm). Here and onwards we use Freeman's pressure multiplication to show the relative intensities of band groups.

At slightly higher pressure, when $p(\mathrm{Xe}) \times p(\mathrm{Kr})$ is about 0.5 torr^2, the diffuse bands of band group I (146.360–146.777 nm, bandwidth from 18 to 46 cm^{-1}) appear on the short wavelength side of band group II. It was noted that band group I probably extends further towards longer wavelengths, but would be obscured by band group II.

Finally, at considerably higher pressure, when $p(\mathrm{Xe}) \times p(\mathrm{Kr})$ reaches 84 torr^2, with $p(\mathrm{Xe})$ at least 1.5 torr, band group III appears immediately to the long wavelength side of the fairly well-defined long wavelength edge of the broadened resonance line plus the wing. This group covers the range from 147.079 to 147.292 nm. No estimates were made of the bandwidth of the bands of that group.

In the Castex paper [9] only seven absorption bands were reported. The pressure and temperature dependencies of the blue satellite (Freeman's band groups I and II) and the red satellite (Freeman's wing) were discussed. The author reported that the blue satellite exhibits a strong temperature dependence, while the intensity of the red satellite changes only slightly with temperature. By analysing the pressure dependence the author drew the conclusion that Xe–Kr atomic pairs, bound or unbound, are responsible for the absorption around the Xe resonance line.

3 Computational technique

In the adiabatic approximation, the following formula is used to estimate the relative absorption probabilities W_{12} between a ground level 1 and an excited level 2 (bound or repulsive):

$$W_{12} \propto p_1 \left| \int \Psi_1(r) \mu_{12} \Psi_2(r) r^2 \mathrm{d}r \right|^2, \qquad (1)$$

where μ_{12} is the dipole transition moment, $\Psi(r) = P(r)/r$ are the radial parts of the nuclear wave functions for the ground and excited levels, and $P(r)$ are solutions of the radial Schrödinger equation:

$$\frac{\mathrm{d}^2 P}{\mathrm{d}r^2} + \frac{2m}{\hbar^2} \left[E - V(r) \right] P(r) = \frac{l(l+1)}{r^2} P(r). \qquad (2)$$

p_1 represents the relative population of a ground state vibrational level, which was calculated from the Boltzmann

distribution, and E is the energy – the eigenvalue for a bound level or the energy of a repulsive level.

In our calculations the dependence of the dipole transition moment on the internuclear distance is ignored, since no data on this dependence has been found in the literature. However, the dependence of the dipole transition moment on internuclear distance for heavy homonuclear inert dimers (see data on Ar_2, Kr_2 and Xe_2 in [14]) is relatively minor in comparison with the oscillations of the nuclear wave functions. It is therefore reasonable to conclude that in the case of heteronuclear dimers this simplification will not cause overly large deviations between the calculated and experimental spectra.

Nuclear wave functions for bound vibrational levels and for repulsive levels were calculated numerically. The code used to determine energy eigenvalues and nuclear wave functions is based on the method described by Hajj [15]. It is an iterative technique that determines the eigenvalue and produces the corresponding wave function by solving the Schrödinger radial equation (Numerov method). In the case of repulsive levels, the wave functions were normalised to a delta function in energy. The ground and excited state internuclear potentials were defined in numerical form or as mathematical functions.

We have tested the method on numerical calculations of eigenvalues for Morse potentials when these could also be determined analytically. A comparison of the results showed excellent agreement.

Results on simulations of absorption spectra for bound-bound and bound-free transitions are presented in this paper. For bound-bound transitions, the total absorption spectrum was obtained as the sum of the intensities of all possible transitions between vibrational levels of the excited and ground states with the weight factors $W_{12} = \exp\{-E/kT\}$ (see Eq. (1)), where E is the ground state vibrational level energy and T is the temperature. The spectrum is composed of a large number of transition lines, which makes it difficult to analyse it or compare it with experimental spectra. In experimental absorption spectra all these lines are broadened and superimposed due to limited resolution of the spectrometer and because of the presence of the rotational structure which "blurs" the spectrum. Therefore an additional simple recalculation of the absorption spectra was applied to imitate the limited resolution and rotational "blurring", the latter being beyond the scope of our calculations: the intensity $I(\lambda)$ at a succession of wavelengths λ in the range 146.0–147.4 nm, where each wavelength was separated from the next by a sufficiently small step to keep all spectral details, was calculated as the sum of all neighbouring transition line intensities I_i, multiplied by a Gaussian weight factor determined by the wavelength difference between the current wavelength λ and the transition line wavelength λ_i:

$$I(\lambda) = \sum_i I_i \exp\left[-\left(\frac{\lambda - \lambda_i}{\Delta/\sqrt{\ln 2}}\right)^2\right]. \qquad (3)$$

The HWHM of the Gaussian Δ was selected to be not less than the wavelength resolution of the experimental spectrum used as a model, and large enough to imitate rotational "blurring" of the spectrum.

For bound-free transitions, the total absorption spectrum is a sum of transition probability continua: each of them was obtained for a given ground vibrational level and a set of excited repulsive levels in the energy range from 5 to 400 cm^{-1} above the $^3P_1$ Xe^* atomic state with a step of 0.1 cm^{-1}. Each continuum also has a Boltzmann weight factor determined by the ground state vibration level energy.

4 Results and discussion

All calculations in this work were performed with the XeKr ground state taken in the Morse form:

$$V(r) = D\left[1 - \exp\{-\alpha(r - R_m)\}\right]^2 - D, \qquad (4)$$

where

$$\alpha = \frac{\ln(2)}{R_m - R_0}.$$

The following values of the parameters for the ground Morse potential were used: well depth $D = 159$ cm^{-1}, equilibrium distance $R_m = 4.18$ Å and zero-potential distance $R_0 = 3.73$ Å. The same values are used in the multiparameter potential of Lee [16]. By choosing these values for the simple Morse potential we obtain a quite good approximation for the more realistic, but very complex potential of Lee: the potentials are in very good agreement in their lower repulsive parts and around the equilibrium point. However, the Morse curve approaches the atomic origin faster than the potential of Lee, which gives 14 vibrational levels while the potential of Lee has 18 levels according to Bobetic and Barker [8]. We believe that the use of the Morse potential for the ground state is justified since we chose to use a Morse potential for the excited state.

The first spectral feature to identify is the most intense structure, namely the diffuse wing with several maxima located to the long wavelength side of the resonance line (Fig. 3). We have tried to demonstrate that this structure can be explained in the frame of bound-bound transitions between the ground state and the excited state $1(^3P_1)$ (Fig. 1). The result of our spectral simulation is presented in Figure 4. The excited state was taken in the Morse form with the following parameters: $D = 170$ cm^{-1}, $R_m = 4.4$ Å, $R_0 = 4.0$ Å. R_m and R_0 were taken directly from Zagrebin's calculations [11]. The value of $D = 500$ cm^{-1} given in [11] has lately been corrected to 300 cm^{-1} [17]. However, the proposed value of $D = 300$ cm^{-1} is too large according to our spectral simulations: the resulting spectral structure expanded much farther to the long wavelengths than in the experimental spectra. Therefore a more suitable value of 170 cm^{-1} was chosen and used instead. The position and width of the calculated structure as well as the location of the maximum are in rather good agreement with the experimental

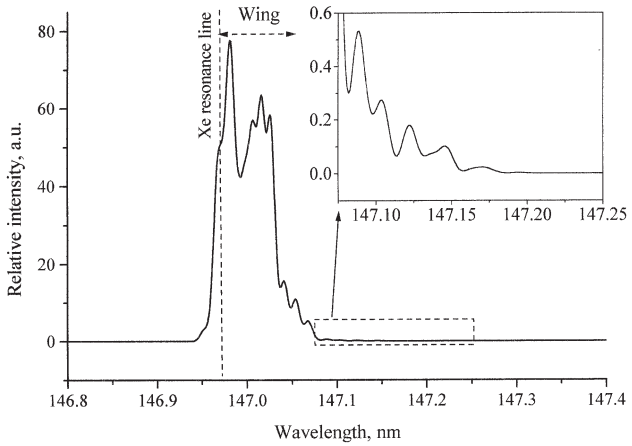

Fig. 4. Calculated absorption spectrum consisting of all possible transitions between bound vibrational levels of the ground state and the excited state $1(^3P_1)$. Both states have internuclear potentials in the Morse form. The inset shows the long wavelength spectral structure.

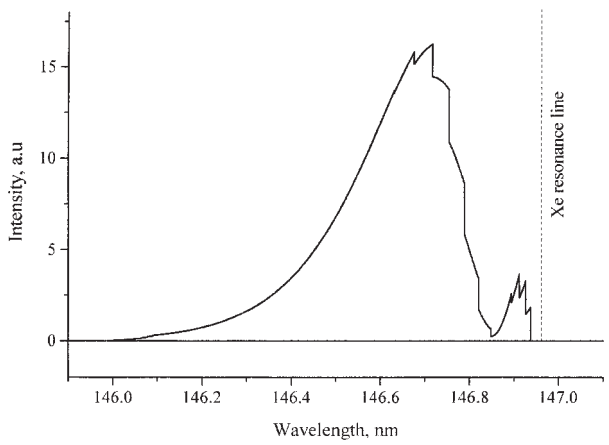

Fig. 5. Calculated absorption spectrum consisting of all possible transitions from ground state vibrational levels to the repulsive part of the excited state $1(^3P_1)$ from 5 cm^{-1} to 400 cm^{-1} above the $^3P_1$ Xe^* atomic state.

spectrum (compare the wing in Figs. 3 and 4). Of course, with the model potentials used and the assumptions that were made, one cannot expect detailed agreement. However, this calculations demonstrate that the wing can indeed have its origin in bound-bound transitions in XeKr molecules. This differs from the explanation that it is the broadened Xe atomic resonance line (transitions in free atomic pairs), which was proposed by Castex [9]. The temperature dependence of the wing, that was considered to be a proof of its atomic origin [9], will be discussed at the end of this section.

In Figure 4 an area directly adjoined to the long wavelength edge of the wing is expanded in a special window. One can see a number of peaks with much weaker intensities than the wing described above. We suggest that this structure (note that there is nothing similar on the short wavelength side of the resonance line) corresponds to the band group III (Fig. 3). It is quite possible that in a model using potentials which give a larger number of vibrational levels (*e.g.* the multiparameter potential of Lee [16]), this structure will intensify and expand slightly to longer wavelength. If this assignment of the origin of the band group III is correct, and this group does result from bound-bound transitions, the distance between the resonance line and the band with the longest wavelength gives the minimal depth of the excited state: 153 cm^{-1}. Observation of the emission spectrum around the resonance line [1] has shown that the relative intensity of the emission spectrum at the wavelengths of the band group III increases considerably with decreasing gas temperature. This could be explained by assuming that this band group originates from bound-bound transitions from the lowest excited vibrational levels, for which the relative populations increase considerably with gas cooling.

We now discuss the diffuse band group I. Within the framework of Morse-Morse potentials, the source of this group is very unlikely to be bound-bound transitions. Considering the band group I location, which is shifted significantly to shorter wavelength from the resonance line, and the large widths of the bands (see Fig. 3), the natural conclusion is that this group originates from bound-free transitions. In Figure 5, a calculated spectrum is shown. This spectrum is composed of the sum of all transitions from ground state vibrational levels to repulsive levels with energies given by the repulsive part of Morse potential of the state $1(^3P_1)$ (see Fig. 1). The following parameter values for the $1(^3P_1)$ state were used: $D = 170$ cm^{-1}, $R_m = 4.4$ Å and $R_0 = 3.7$ Å. The positions of maxima of the calculated structures and their widths are very sensitive to the Morse parameters of the excited state, especially on R_0. The spectrum shown in Figure 5 was obtained for the excited state with the same D and R_m as in our discussion of the wing (band group III) and only R_0 has been adjusted to achieve a total width of the structure close to the width observed in the experiments. Note that the "teeth" on the spectral profile are due to the fact that the total spectrum is a sum of partially overlapping continua where every "tooth" is in the place where the next continuum starts. Each continuum was obtained for transitions from a certain ground state vibrational level to an unbound level of the excited state with energy ranging from 5 to 400 cm^{-1} counted from the $^3P_1$ Xe^* atomic level. This range was taken because no spectral structures have been seen further than 400 cm^{-1} towards shorter wavelengths. Furthermore, energies less then 5 cm^{-1} give wave functions with very slow oscillations, which result in calculational difficulties, but do not provide much additional information. To summarise the results on band group I, we believe that the position and width of band group III as well as the number and widths of its maxima can be simulated through bound-free transition between potentials mentioned above (only small changes of the parameter values are required). However, the numerical fitting to experimental spectra would require considerable effort, which makes no sense until reliable and detailed data are obtained for one of the potentials (the ground or excited

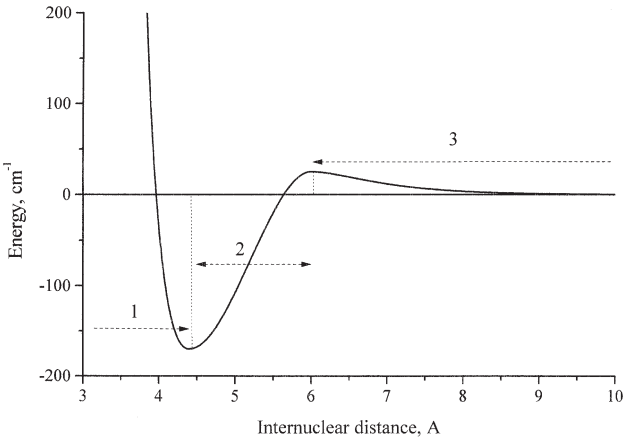

Fig. 6. The $1(^3P_1)$ state internuclear potential, containing a hump. The potential is composed of three parts: part 1: ordinary Morse potential for internuclear distances from 0 to equilibrium distance. Part 2: third degree polynomial. Part 3: Morse potential with negative sign from the hump maximum (corresponds to the equilibrium distance) and towards infinity.

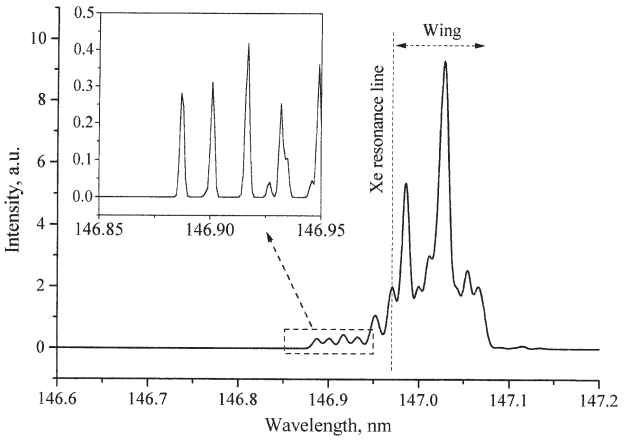

Fig. 7. Calculated absorption spectrum consisting of all possible transitions between vibrational levels of the ground state and the state $1(^3P_1)$ containing the hump. The inset shows the short wavelength spectral structure composed of relatively intense and narrow lines.

state) and for the dependence of the dipole transition moment on the internuclear distance.

We find the identification of the band group II to be the most problematic. It consists of seven sharp and intense bands, especially in comparison with the weak band group III. We believe that such narrow bands could not be observed in bound-free transitions between two Morse potentials: the slope of the repulsive part is too sharp, which will result in broad structures in the spectra. On the other hand, the bands are too intense to be assigned to bound-bound transitions between two Morse potentials, which still could explain the wing (compare Figs. 3 and 4). The problem could be solved by a considerable change of the shape of the excited state internuclear potential. Two different cases are discussed in the following paragraphs.

I. The band group II is assumed to originate in bound-free transitions with a non-Morse excited state. We have found that transitions between the ground Morse potential and a purely repulsive excited potential could result in sufficiently sharp bands. However, for the excited Xe* atomic state $^3P_1$ there are only two possible XeKr states: 0^+ and 1. The state $0^+(^3P_1)$ is bound (emission from this state appears with a broad maximum around 153 nm), and the state $1(^3P_1)$ has to be weakly bound (as discussed above) to explain the wing and the band groups III. There is, however, a compromise: the weakly-bound state $1(^3P_1)$ potential could have a "hump" (see Fig. 6). This potential has both a bound part at small internuclear distances and a slightly sloping repulsive part after the hump at large distances. We have constructed a model potential of that type in the following way: the potential consists of a Morse curve for small internuclear distances up to the equilibrium distance ($D = 170$ cm^{-1}, $R_m = 4.4$ Å, $R_0 = 4.0$ Å), then a 3rd degree polynomial until the hump maximum is reached and then a long-distance tail of another Morse potential taken with negative sign ($D = -25$ cm^{-1}, $R_m = 6.5$ Å, $R_0 = 6.0$ Å). This potential was numerically tested and it was found that the bound-free transitions from the ground state vibrational levels $\nu = 7$ and 8 give very narrow bands with FWHM less then 1.5 cm^{-1} as the band group II has. Bands from levels $\nu = 6$ and 9 gave narrow peaks with low intensity broad shoulders. The rest of the vibrational levels gave relatively low intensity broad structures. This demonstrates the possibility that all 7 observed bands could have the same origin (after a slight modification of the excited state potential) in bound-free transitions from the ground state to an excited state with a hump.

One should note that it is possible to apply the same considerations if we assume that the band group II originates from bound-free transitions between the weakly bound ground state and the excited state $0^+(^3P_1)$ if we introduce the same hump as for the $1(^3P_1)$ state.

II. The band group II could also result from bound-bound transitions in the case of a non-Morse excited state. An absorption spectrum corresponding to transitions between vibrational levels in the bound parts of the ground potential and the humped excited state potential described above is shown in Figure 7. There are sufficiently intense bands at the wavelengths of band group II, and still, as for Morse potentials, there are the wing and the weak structure where band group III is situated. However, the question of the width of the bands is still open: how could bands situated far from the centre of the wing (wavelength of band group II) be narrow while the centre of the wing is totally diffuse (according to Freeman *et al.* [13]). The answer might be given if also the rotational structure is taken into account, but this is beyond the model used in this work.

Analysis of rotational structure should also help to determine which alternative gives rise to, or dominates, the experimental spectra, that is whether the band group I originates from bound-bound or bound-free transitions.

One should note that the introduction of the hump for the $1(^3P_1)$ state to explain the band group II will not

lead to drastic changes in the remaining spectral ranges. This is connected with the fact that the humped potential described above has the same depth and equilibrium distance as the Morse potential used to calculate the bound-repulsive spectrum between two Morse potentials. Moreover, we inherited the repulsive part of the "humped" potential directly from the Morse potential. The result is that the bound-bound spectrum between the humped excited state and the ground state taken in the Morse form (see Fig. 7) still shows the diffuse wing with the right width and the low-intensity structure at the wavelength of the band group III. The shape of the wing will be different but as we pointed out, we do not expect detailed agreement. The diffuse structure at the place of the band group I will not change drastically either – the further from the resonance line the more similar the structure becomes to the one presented in the Figure 5.

Finally we consider the temperature dependence of the intensity of long and short wavelength structures around the resonance line in the absorption spectra. Castex [9] reported that the short wavelength satellite (corresponding to Freeman's band groups I and II) has a strong temperature dependence – its intensity increases with cooling of the absorbing gas, while the intensity of the long wavelength wing depends only slightly on the gas temperature. The explanation [9] was that the long wavelength satellite, corresponding to Freeman's wing, is due to transitions in free pairs (atomic line broadening), which has a very weak temperature dependence in comparison with bound-free transitions which give the short wavelength satellite. However, another explanation of the temperature dependence can be given by assuming a bound-bound origin of the long wavelength satellite. The intense part of the long wavelength satellite is composed mainly of all transitions with small differences in vibrational quantum number ν between the ground and excited state vibrational levels ($\nu = 0, \pm 1$ are dominating). This means that all, low as well as high, ground state vibrational levels contribute to the satellite. Decreasing the temperature and thereby increasing the relative population of lower vibrational levels in accordance with the Boltzmann factor, we only change the shape of the satellite, increasing some and decreasing other closely situated components without a considerable change of the total intensity. On the other hand, the dominant part of the short wavelength satellite, which is situated far from the resonance line, receives its main contribution from transitions starting from vibrational levels close to the bottom of the ground state potential well. For example, a change of temperature from 300 K to 165 K will result in an increase of the relative population of the vibrational level $\nu = 0$ with respect to the level $\nu = 14$ from 2:1 to 4:1, which causes a considerable growth of the absorption intensity in this structure.

5 Conclusion

We have demonstrated by numerical simulation that all spectral structure in the absorption spectrum around the Xe resonance line at 146.96 nm in Kr gas with an admixture of Xe can be explained by bound-bound and bound-free transitions between the ground XeKr state and the weakly-bound excited state $1(^3P_1)$. This explanation is supported by the dependence of the absorption and emission spectra on gas temperature. The depth of the potential well for the excited state $1(^3P_1)$ is estimated to be 170 cm^{-1}. To explain the part of the short wavelength structure that contains a number of narrow bands, we suggest the following modification of the excited state $1(^3P_1)$ potential: the weakly-bound state potential may have a hump with a maximum height of about 25 cm^{-1} at an internuclear distance near 6 Å.

We thank Professor A. Devdariani from St. Petersburg University and Professor L. Karlsson from Uppsala University for very useful advice and discussions. We are grateful to Dr. Zagrebin from St. Petersburg University for sending the results of his latest calculations. This project has been supported by the Swedish Research Council for Engineering Sciences (TFR) and Uppsala University.

References

1. B. Krylov, G. Gerasimov, A. Morozov, A. Arnesen, R. Hallin, F. Heijkenskjold, Eur. Phys. J. D **8**, 227 (2000).
2. T. Efthimiopoulos, D. Zouridis, A. Ulrich, J. Phys. D: Appl. Phys. **30**, 1746 (1997).
3. S. Kubodera, M. Kitahara, J. Kawanaka, W. Sasaki, K. Kurosawa, Appl. Phys. Lett. **69**, 452 (1996).
4. J. Wieser, D.E. Murnick, A. Ulrich, H.A. Huggins, A. Liddle, W.L. Brown, Rev. Sci. Instrum. **68**, 1360 (1997).
5. P.J.M. Peters, H.M.J. Bastiaens, in *Gas Lasers – Recent Developments and Future Prospects*, edited by W.J. Witteman, V.N. Ochkin (Kluwer Academic Publishers, 1996).
6. J.A. Barker, R.O. Watts, J.K. Lee, T.P. Schafer, Y.T. Lee, J. Chem. Phys. **61**, 3081 (1974).
7. W.C. Ermler, Y.S. Lee, K.S. Pitzer, N.W. Winter, J. Chem. Phys. **69**, 976 (1978).
8. M.V. Bobetic, J.A. Barker, J. Chem. Phys. **64**, 2367 (1976).
9. M.C. Castex, J. Chem. Phys. **66**, 3854 (1977).
10. G. Novak, J. Fricke, J. Phys. B: At. Mol. Phys. **18**, 1355 (1985).
11. A.L. Zagrebin, N.A. Pavlovskaya, Opt. Spectrosc. (USSR) **69**, 320 (1990).
12. A.Z. Devdariani, A.L. Zagrebin, K.B. Blagoev, Ann. Phys. Fr. **14**, 467 (1989).
13. D. Freeman, K. Yoshino, Y. Tanaka, J. Chem. Phys. **67**, 3462 (1977).
14. A.A. Madej, B.P. Stoicheff, Phys. Rev. A **38**, 3456 (1988).
15. F.Y. Hajj, J. Phys. B: At. Mol. Phys. **13**, 4521 (1980).
16. J.K. Lee, D. Henderson, J.A. Barker, Mol. Phys. **29**, 429 (1975).
17. A.L. Zagrebin, private communications.

Paper III

Eur. Phys. J. D **8**, 227–239 (2000)

THE EUROPEAN PHYSICAL JOURNAL D

Energy transfer studies in krypton-xenon mixtures excited in a cooled DC discharge

B. Krylov[1], G. Gerasimov[1], A. Morozov[2], A. Arnesen[2], R. Hallin[2,a], and F. Heijkenskjold[2]

[1] Vavilov State Optical Institute, Birzhevaja Line 12, St. Petersburg, 199034 Russia
[2] Uppsala University, Department of Physics, Box 530, 751 21 Uppsala, Sweden

Received 12 May 1999 and Received in final form 27 August 1999

Abstract. The VUV spectrum of gaseous mixtures of krypton with a small amount of xenon added was investigated in the range 115–200 nm. The mixtures were excited in a capillary DC discharge where the capillary could be cooled by using liquid nitrogen. The mixed molecule band around the Xe I resonance line at $\lambda = 147$ nm and the mixed molecule continuum to the long wavelength side from the line were analysed. The band around $\lambda = 147$ nm was identified as transitions between a weakly bound excited state and the weakly bound ground state of XeKr molecules. When cooling the capillary wall, the appearance of the Xe_2 continuum was observed. The effect is ascribed to energy transfer between molecular states as a consequence of radiation trapping in the band around $\lambda = 147$ nm. The role of the mixed molecule in the formation of the VUV spectrum of the gas mixture is discussed and underlined.

PACS. 33.20.Ni Vacuum ultraviolet spectra – 33.50.Hv Radiationless transitions, quenching

Introduction

The main part of the research on rare-gas excimers has been centered around the homonuclear species Ar_2^*, Kr_2^* and Xe_2^* and the interest in the VUV fluorescence of rare gases is to a large extent connected with the development of VUV light sources, including lasers. Not so many publications are devoted to the excitation processes and optical spectra of heteronuclear rare-gas excimers like the XeKr molecule.

The lowest excited states of the Xe*Kr molecules are built up by the same Xe atomic states, *i.e.* the resonant $^3P_1$ and the metastable $^3P_2$ states, as the lowest excited states of the Xe_2^* molecule (Fig. 1). Therefore transitions from excited states of XeKr and Xe_2 to the weakly bound ground states give overlapping VUV continua. This is the reason why the identification of the XeKr molecule spectrum was a debated topic in many previous studies.

Like the spectra of other rare gas mixtures, the Xe–Kr VUV spectrum is intriguing because of the manifestation of energy transfer processes between the rare gases (from a light gas to a heavier one). The authors of [1,2] studied, among others, gaseous krypton-xenon mixtures excited with a pulsed electric discharge (70–640 torr total pressure, 0.001–0.1% of xenon) [1] and with an α-source (1000 torr total pressure, 0.0025–2.5% of xenon) [2]. They reported that small amounts of another rare gas admixture, *e.g.* Xe in Kr, acted as a very efficient electronic energy acceptor. This led to a gradual disappearance

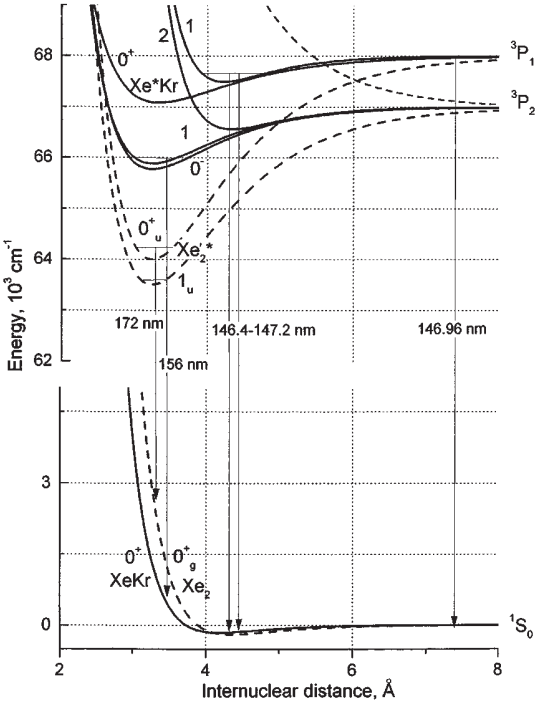

Fig. 1. Morse potential curves for the lowest XeKr and Xe_2 (dashed curves) electronic states. Potential curve parameters and references are listed in Table 1. See also comments in Section 3. The main optical transitions discussed in the work are indicated.

[a] e-mail: reinhold.hallin@fysik.uu.se

of the molecular continuum of the host gas and to the appearance of the resonance atomic line and the molecular continuum of the admixture. The relative contributions of two energy transfer mechanisms involving atom-atom and molecule-atom energy transfer were estimated. The authors [1,2] underlined that molecule-atom energy transfer is a resonant process for a wide range of excitation energies and that this process is characterised by a large ($\sim 10^{-14}$ cm^2) cross section.

Also, a spectroscopic study of krypton-xenon mixtures with α-particle excitation [3] (total pressure 100–500 torr, 0.001–10% of xenon) verified that energy transfer from krypton atoms and molecules to xenon is very efficient. The spectra of mixtures with only a few percent of xenon were very similar in shape and intensity to those of pure xenon. In contrast to [1,2], where the reaction constants were obtained from measurements of spectral intensity ratios, reaction rates and a kinetic scheme of the transfer phenomena were determined from measurements of the time constants governing the decay of the main krypton and xenon emissions in the VUV.

Many additional details of the kinetic scheme of the energy transfer processes, including reaction rates, were obtained with pulsed electron-beam excitation and time-of-flight techniques in the publications [4,5] (total pressure 25–900 torr, 0.1–10% of xenon, time-dependent and time-independent measurements). In particular, the transfer rates to the excited mixed molecule $(KrXe)^*$ were obtained.

The results of the recent work [6] obtained with a pulsed discharge excitation (total pressure 5–140 torr, 0.4–50% of xenon), have elucidated the nature and the position of the emission maximum in the region of 156 nm. It is definitely ascribed to transitions in the Xe^*Kr molecule as the analogy of the second continuum of homonuclear inert-gas molecules. The relaxation constants of Xe^*Kr and Xe_2^* molecules with Kr as buffer gas were estimated and found to have similar values for both excimer systems.

Interesting results were also obtained when excimers formed in aggregates of condensed phases were investigated [7–10]. For example, in [8] solid layers of Kr were bombarded with thermal Xe atoms in the metastable $^3P_2$ state. From the observed VUV emission, the potential parameters for the $Xe(^3P_2) + Kr(^1S_0)$ excimer system were deduced.

Semiempirical calculations of the $Xe(^3P_1,^3P_2)$–$Kr(^1S_0)$ interaction potentials, the radiative lifetimes of the XeKr lower excited states and the VUV spectra of the heteronuclear molecules were performed in [11–13].

Part of the cited works also contains a considerable amount of data about other inert gas mixtures (xenon-argon, krypton-argon and others) which might be useful for understanding krypton-xenon spectra.

In this paper we present spectra of krypton-xenon mixtures obtained in uncooled and cooled capillary DC discharges. The spectra show that the role of mixed XeKr molecules has not been adequately taken into account in the previous publications. Intense formation of excited XeKr molecules begins at very low partial densities of xenon and takes place in a xenon concentration range up to more than 1%. These molecules were often not included in the kinetic models or were included only passively as a final emitting product. We have tried to analyse carefully the participation of the mixed molecules in the energy transfer processes. The result forces us to consider the mixed molecules as a necessary component of the kinetic models.

Furthermore, the spectra recorded at relatively high both total and partial xenon pressures have demonstrated that the spectral intensity distribution depends strongly on the gas temperature.

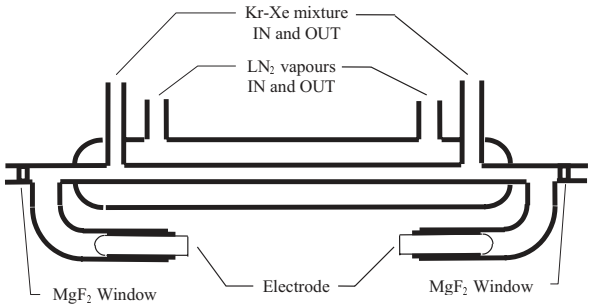

Fig. 2. Scheme of the gas discharge tube used for the experiments.

1 Experiment

Spectra have been recorded in the range 115–200 nm from a DC capillary discharge at total gas pressures of 30–300 torr and with 0.01–1% xenon admixture to the krypton gas. The gas inside the capillary could be cooled down to the temperature of condensation.

The discharge tube (see Fig. 2) was made of fused silica with windows of magnesium fluoride to allow detection of the VUV spectrum down to 115 nm. Two cold tungsten electrodes were melted into side branches of the tube. The DC discharge (10–50 mA) took place in a capillary tube of 0.30 m length and 1.5 mm inner diameter and the tube was connected to a vacuum system to be evacuated and filled with gas. An initial pressure of less than 2×10^{-7} torr was achieved before filling the system. The distance between the magnesium fluoride windows and the capillary ends could be changed but was usually about 10 mm.

It is a well-known phenomenon for a DC discharge in a gas mixture that the gas can be separated by the running discharge so that one of the gaseous components is collected near the anode while the other component gathers around the cathode. To prevent this separation, a flow of the gas mixture through the capillary was maintained with a specially designed fan.

The capillary was surrounded by a concentric tube also made of fused silica. The volume inside this tube was flushed with cold nitrogen vapour in order to cool the capillary walls. The capillary wall temperature was adjusted by changing the inlet pressure of the vapours and measured with a copper-constantan thermocouple within the

range 100–400 K. To prevent unnecessary evaporation of liquid nitrogen, the outer wall was thermally isolated.

Krypton-xenon mixtures were prepared in a special volume, connected to high pressure gas bottles containing high purity krypton and krypton-xenon mixtures (1% and 0.1% of Xe). It took about one hour to prepare a homogeneous gas mixture.

The spectra were recorded using a 1 m normal-incidence vacuum spectrometer with 0.417 nm/mm dispersion. The spectral resolution, determined by the widths of the entrance and exit slits, was 0.015 nm. A pm-tube with a magnesium fluoride window and a cesium-tellurium photocathode, operating in the photon counting mode, was used as detector. The photon counting time per channel was in the range 0.1–0.5 s and the peak count rate reached 8×10^4 counts per second. The main part of the wavelength region 115 to 200 nm was usually recorded with 640 channels per spectrum, *i.e.* with a recording system spectral resolution of 0.125 nm. However, several narrow spectral ranges, including in particular the atomic lines of xenon and krypton and lines of impurities, were usually recorded with higher spectral resolution, down to 0.02 nm or better. No corrections for changes in window transmission, grating efficiency and detector efficiency within the investigated wavelength range have been made for the spectra shown in this article.

The krypton, xenon and krypton-xenon molecular continua and the resonance lines of atomic krypton ($\lambda_1 = 116.487$ nm, $\lambda_2 = 123.584$ nm) and xenon ($\lambda_3 = 129.559$ nm, $\lambda_4 = 146.961$ nm) were observed in the spectra. Besides, the resonance line of impurity hydrogen ($\lambda = 121.567$ nm) and groups of carbon lines ($\lambda_1 = 156.1$ nm, $\lambda_2 = 165.7$ nm) were observed. The intensities of the impurity lines decreased as the discharge was cooled. We also examined the effect of the impurities on the intensities of the continua. According to our observations, a change of intensity caused by the impurities cannot have been more than a few percent after conditioning of the capillary tube.

2 Results of the experiment

When a small quantity of xenon (less than one percent of the total pressure) was added to krypton, the VUV emission spectrum changed in the same manner as in the above cited works, namely that the intensity of the krypton continuum decreased with increasing xenon partial pressure, and an intense peak of narrow-band radiation arose in the immediate vicinity of $\lambda = 147.0$ nm. Figure 3 illustrates the aforesaid: as an example, the spectra of pure krypton and krypton with an admixture of 0.1% of xenon are shown at a total pressure of 300 torr and a discharge current of 20 mA.

The narrow-band radiation at $\lambda = 147.0$ nm was in previous works completely ascribed to the atomic resonance line of xenon ($\lambda = 146.96$ nm). However, this identification is not correct in many cases. In reality, even at relatively low pressures of the "krypton-small amount of xenon" mixture, a structure of nonatomic origin appears

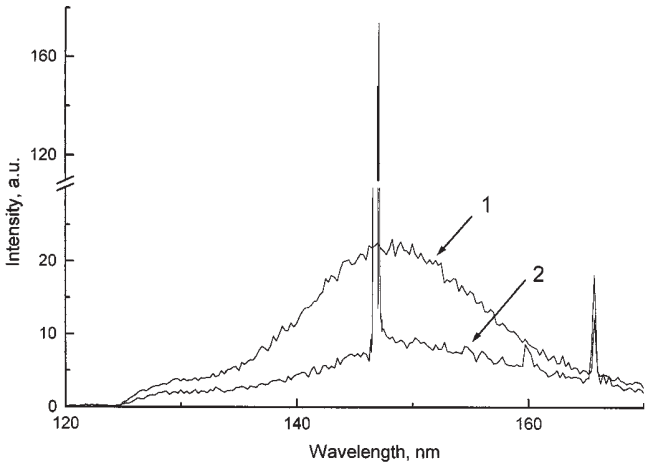

Fig. 3. Emission spectra from the capillary gas discharge showing the change of the spectral intensity distribution when a small quantity of xenon is added to krypton. 1 – pure krypton; 2 – krypton with an admixture of 0.1% of xenon. The total pressure was 300 torr and the discharge current 20 mA (no cooling).

near the xenon resonance line. Spectra of this mixture in the wavelength interval 146.5–147.3 nm, at the total pressure 30 torr and with different concentrations of xenon (0.05%, 0.25%, 1%), are shown in Figure 4. The figure demonstrates that at a concentration of xenon of 0.05%, corresponding to a partial pressure of 1.5×10^{-2} torr, the emission profile is already clearly asymmetric and a "shoulder" appears on the long wavelength side directly adjacent to the peak position of the atomic line which coincides with the peak of the absorption profile at higher xenon pressures. The shoulder is shifted from the atomic line by 0.06 nm. As the xenon concentration increases to 1% (0.30 torr), self-absorption becomes stronger and the upgrowing shoulder seems to be the main emission component. Also, with increasing xenon pressure, a relatively broad emission structure with several maxima, at least three, appears on the short wavelength side in the band 146.4–146.95 nm. This structure becomes more clearly defined at higher total pressures of the mixture, for example at the pressure 90 torr (Fig. 5).

If one compares the spectra in Figures 4 and 5, it is evident that the intensity of the atomic line and the components to the left and right of $\lambda = 146.96$ nm depend both on the partial pressure of xenon and on the total pressure of the mixture. The dependence on the krypton pressure is demonstrated more distinctly in Figure 6 where spectra recorded at the same xenon pressure of 0.15 torr and different total pressures (30, 60, and 300 torr) are presented.

Figures 4–6 also demonstrate the influence of self-absorption (in the emitting volume and in the gas layer between the discharge column and the exit window) on the spectrum. With increasing pressure, the absorption band becomes deeper and more asymmetric (wider to the long wavelength side) and the absorption profile seems

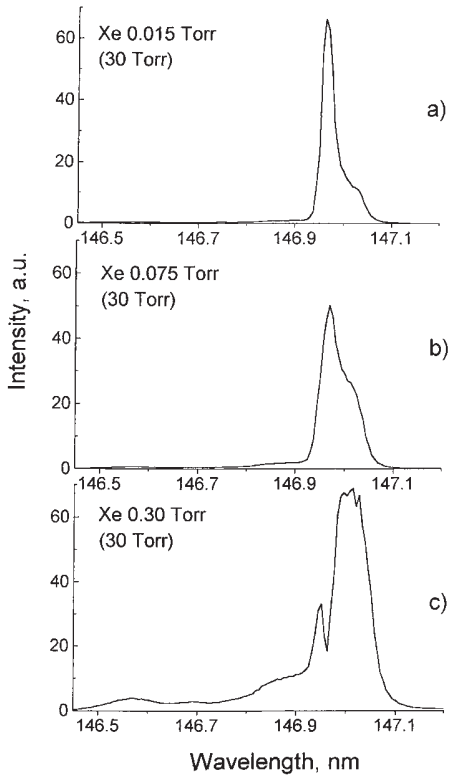

Fig. 4. Spectrum of narrow-band radiation of the krypton-xenon mixture near the xenon resonance line. The total pressure was 30 torr, the discharge current 20 mA and different concentrations of xenon: (a) 0.05%, (b) 0.25%, (c) 1%. The figure demonstrates that even at low pressures a structure of nonatomic origin appears near the xenon resonance line. The spectral resolution was 0.015 nm.

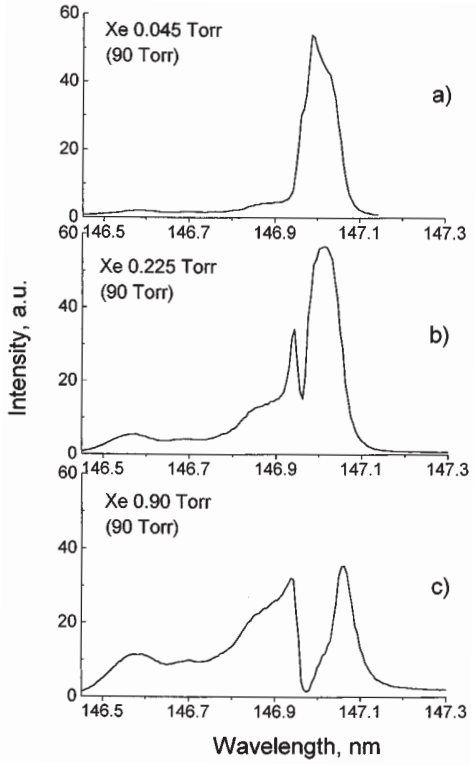

Fig. 5. Spectra of the krypton-xenon mixture near the xenon resonance line obtained at the total pressure 90 torr. The other specifications are the same as in Figure 4. The molecular structure is clearly defined. The influence of self-absorption on the spectrum in the vicinity of $\lambda = 147.0$ nm is distinctly seen.

to consist of two components (Fig. 5c), one appearing at the same wavelength as the emission "shoulder". The intensity of the absorption band depends both on the xenon pressure (Figs. 4 and 5) and on the krypton pressure (Fig. 6). The dependence on the krypton pressure indicates that the self-absorption also includes molecular absorption.

It should be pointed out that the emission peak at 147 nm in Figure 3 (spectrum 2) has a profile similar (actually, more self-absorbed) to the profile presented in Figure 6, spectrum 3. The total pressure in both cases is the same (300 torr), but the xenon partial pressure in Figure 3 is twice higher.

The influence of self-absorption on the emission spectrum is best shown in Figure 7a. Absorption maxima appear instead of emission maxima when the mixture Kr–Xe (0.25%) at 90 torr was replaced by the mixture Kr–Xe (1%) at 300 torr. Figure 7b shows densitometer traces of absorption spectra of Kr–Xe mixtures [14] (see also [15]) obtained at the xenon pressure 0.1 torr (all curves) and at the krypton pressures 6, 162, and 486 torr (curves 1, 2, and 3, respectively) in a 20 cm long cooled (160 K) absorption cell. It is evident from Figure 7 that the structure of the emission and absorption spectrum is the same: the peak positions in emission and absorption coincide

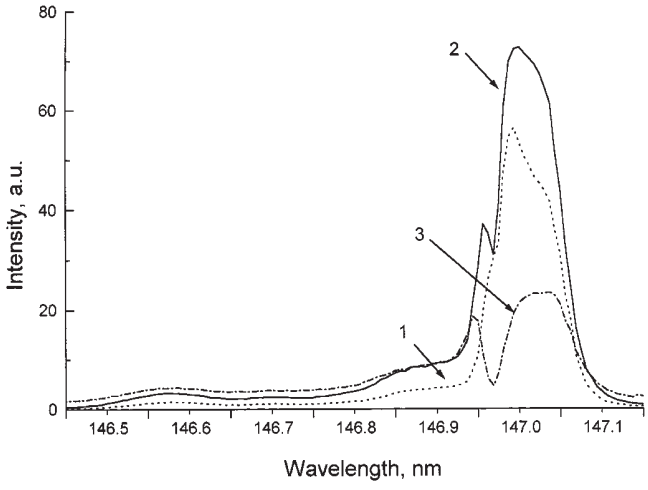

Fig. 6. The spectrum of the Kr–Xe mixture around $\lambda = 147.0$ nm and its dependence on the krypton pressure. The xenon pressure was constant, 0.15 torr. The total pressures were: (1) 30 torr; (2) 60 torr; (3) 300 torr. The discharge current was 20 mA. The spectral resolution was 0.015 nm.

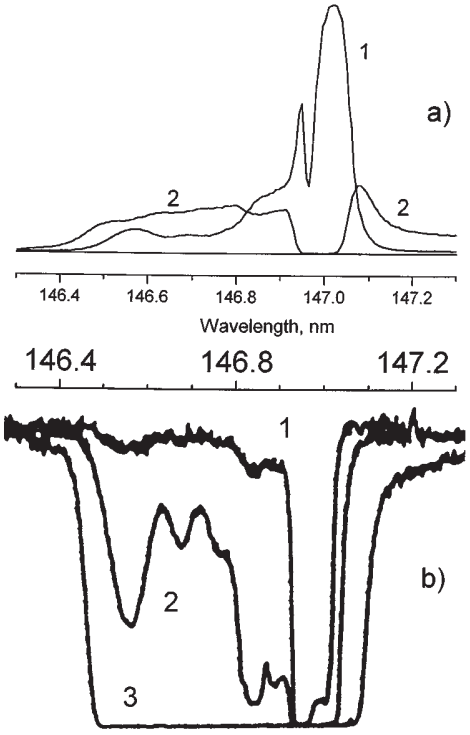

Fig. 7. Comparison of the emission (a) and absorption (b) spectrum of the krypton-xenon mixture around $\lambda = 147.0$ nm. The emission spectra (a) have been recorded at the total pressure 90 torr, 0.25% of Xe (curve 1) and 300 torr, 1% of Xe (curve 2). The absorption spectra (b) were recorded (densitometer traces are presented) in [14] at the xenon pressure 0.1 torr (all curves) and at the krypton pressures 6, 162, and 486 torr (curves 1, 2, and 3, respectively). As is evident, the structure of the emission spectrum and that of the absorption spectrum (peak positions, relative intensities and widths) is similar. See also specifications and comments in text.

precisely, and the relative intensities and widths are similar. The spectra obtained in [14] at high spectral resolution ($\sim$ 0.001 nm) showed that the resonance line is associated with two groups of discrete bands on its short wavelength side and with one group of bands on the long wavelength side (altogether more than 20 bands were observed). These bands appear as a result of bound-bound or bound-free transitions within the heteronuclear diatomic van der Waals molecules [14]. Figure 7 therefore allows identification of the emission spectra observed in the vicinity of $\lambda = 146.96$ nm on the basis of the results obtained in [14], namely: the xenon atomic line and bands of Xe*Kr molecules spanning the atomic line are seen, more or less self-absorbed by xenon atoms and mixed molecules.

The conclusion is that transitions in Xe*Kr molecules give a considerable contribution to the narrow-band radiation around $\lambda = 147.0$ nm that is crucial for the interpretation of the spectra. The identification of this band as well as the atomic xenon line and its use for measurements of molecule-atom energy transfer cross-sections therefore has to be done with care. It should be noted also that the appearance of the molecular structure in the range 146.40–146.95 nm is a good indicator that the strong molecular

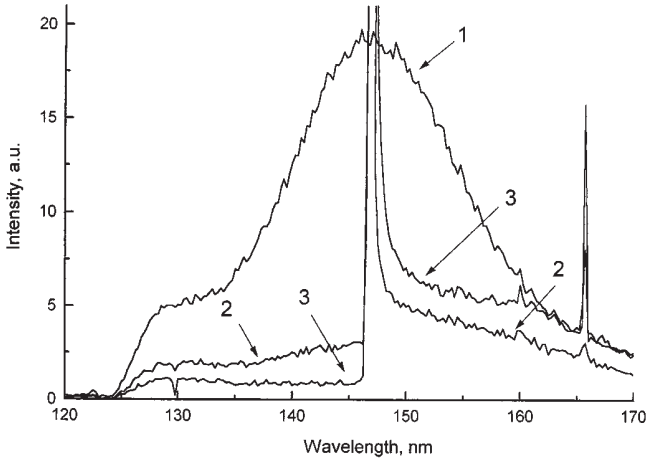

Fig. 8. Continua of krypton (curve 1) and krypton-xenon mixtures (curves 2 and 3). The total pressure was 300 torr (all curves), the Xe concentration 0.25% and 1.0% (curves 2 and 3, respectively). The continuous emission intensity in the mixture spectra is not equal on both sides of the band at 147.0 nm. The difference in intensities depends on the partial pressure of xenon. An explanation of the asymmetry is given in the text.

emission peak has arisen close to the xenon resonance line on the long wavelength side.

As can be seen in Figure 3 the krypton continuum goes down in intensity when xenon is added to krypton. However, the decrease in the intensity is not equal on both sides of the band at 147.0 nm: the long-wavelength side retains its intensity more than the short-wavelength side. The difference in intensities depends on the partial pressure of xenon (Fig. 8; total pressure 300 torr, 0.25% and 1.0% Xe). The short-wavelength continuum almost disappears when the mixture contains 1% (3 torr) of xenon. The explanation for the asymmetry is that an additional molecular continuum has appeared in the spectral region from the atomic line at 147.0 nm to approximately 190 nm. The extension of the continuum indicates that this is either the mixed molecule or the xenon molecule continuum. As was recently shown [6], each of these continua can appear as the dominant emission depending on the gas mixture. It was also verified in [6] that an emission maximum at $\lambda \approx 156$ nm is due to the mixed molecules and is an analogy of the krypton or xenon second continuum (see Fig. 1).

The maximum at 156 nm appeared in our spectra at "high" pressures of both krypton and xenon but was not clearly defined in spectra of the uncooled discharge (Fig. 9, spectrum 2; 300 torr, 1% Xe), and the maximum of the xenon second continuum was not seen. However, the spectrum changed completely when the capillary wall was cooled (Fig. 9, spectra 3 and 4). With decreasing wall temperature, an intense growth of the band at 156 nm was observed and, in addition, the xenon second continuum appeared and grew faster than the mixed molecule continuum (Fig. 9, spectrum 3). At a wall temperature close to the temperature of gas condensation, the second continuum from xenon molecules dominates the spectrum (Fig. 9, spectrum 4).

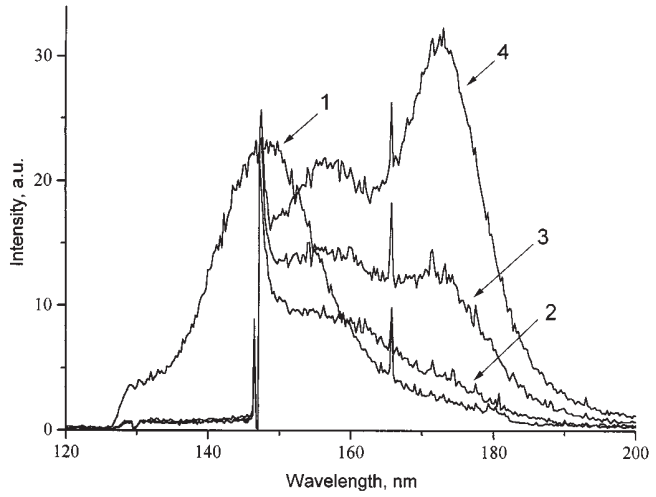

Fig. 9. Spectrum of a krypton-xenon mixture (curves 2–4) at the total pressure 300 torr, 1% of Xe, and its dependence on the gas temperature. The curves 2–4 show the change of the spectrum as a result of discharge capillary wall cooling from "no cooling" (curve 2) to a temperature close to the temperature of gas condensation (curve 4). With decreasing wall temperature, both the mixed molecule and the xenon continua grow, but the xenon continuum grows faster than the mixed molecule continuum (the atomic resonance line is self-absorbed more than in Fig. 8 because the distance between the discharge capillary and the exit window was longer than the usually used 10 mm). The krypton continuum (curve 1) is shown for comparison: the pressure was 300 torr, the discharge current 20 mA (without cooling).

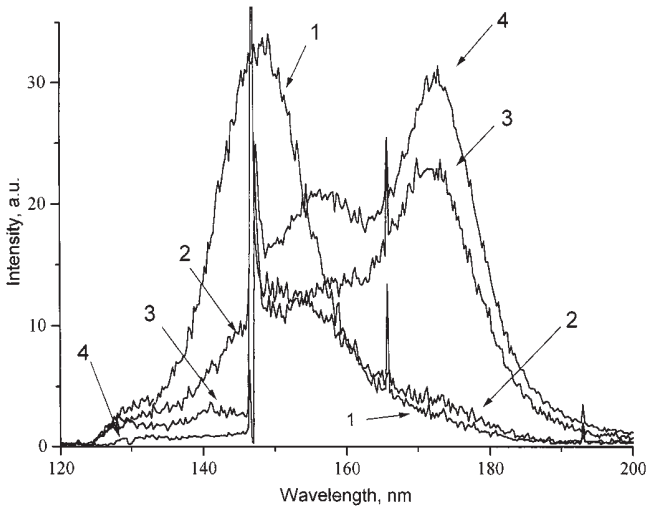

Fig. 10. Spectra of krypton (1) and krypton-xenon mixtures (2–4) at the lowest possible capillary wall temperature (close to the temperature of gas condensation). The curves (2–4) show how the intensities of the continua change with increasing xenon concentration: (1) 0%; (2) 0.1%; (3) 0.25%; (4) 1.0%. The total pressure was 300 torr, the discharge current 20 mA.

A similar growth of the mixed molecule and xenon continua was observed at room temperature in [2] (total pressure 1000 torr) and in [3] (total pressure 500 torr) when the xenon concentration was increased two orders of magnitude up to 2.5% and 1%, respectively.

Figure 10 exhibits the spectra of mixtures cooled close to the condensation temperature at 300 torr and different xenon concentrations (0.1%, 0.25%, 1%, spectra 2, 3 and 4 respectively). It is evident from the spectra that the growth of the band around 156 nm and, especially, the xenon second continuum occurs at relatively high xenon concentrations. A comparison of the krypton-xenon spectra 3 and 4 in Figure 10 with the spectrum of cooled (down to approximately the same temperature) krypton (spectrum 1) shows that, if we deal with energy transfer processes, they should be very effective.

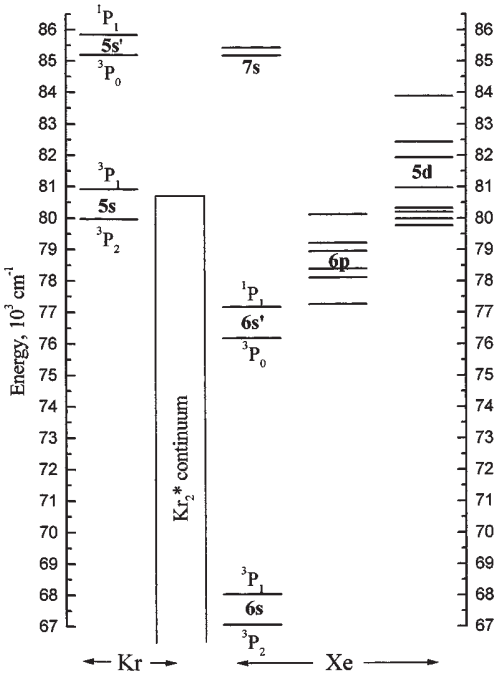

Fig. 11. Energy-level diagram for the lowest excited states of atomic krypton and xenon. The photon energy from the Kr_2^* continuum is also indicated.

3 Interpretation of the spectra and mechanisms of energy transfer

A simplified energy-level diagram for the lowest excited states of atomic Kr and nearby atomic Xe levels is shown in Figure 11.

Studies of electronic energy transfer processes in Kr–Xe mixtures were made in [1–5,16] using different methods for the excitation of the mixtures over a wide range of Kr host gas pressures and added Xe gas concentrations. Most of the results were obtained in time-resolved measurements from decay curves of atomic and molecular VUV emissions. We have tried to collect the most important processes for the discussion of our results and represent them in Figure 12. Reaction rates were taken from the previously cited works and also from [17–26,29,36].

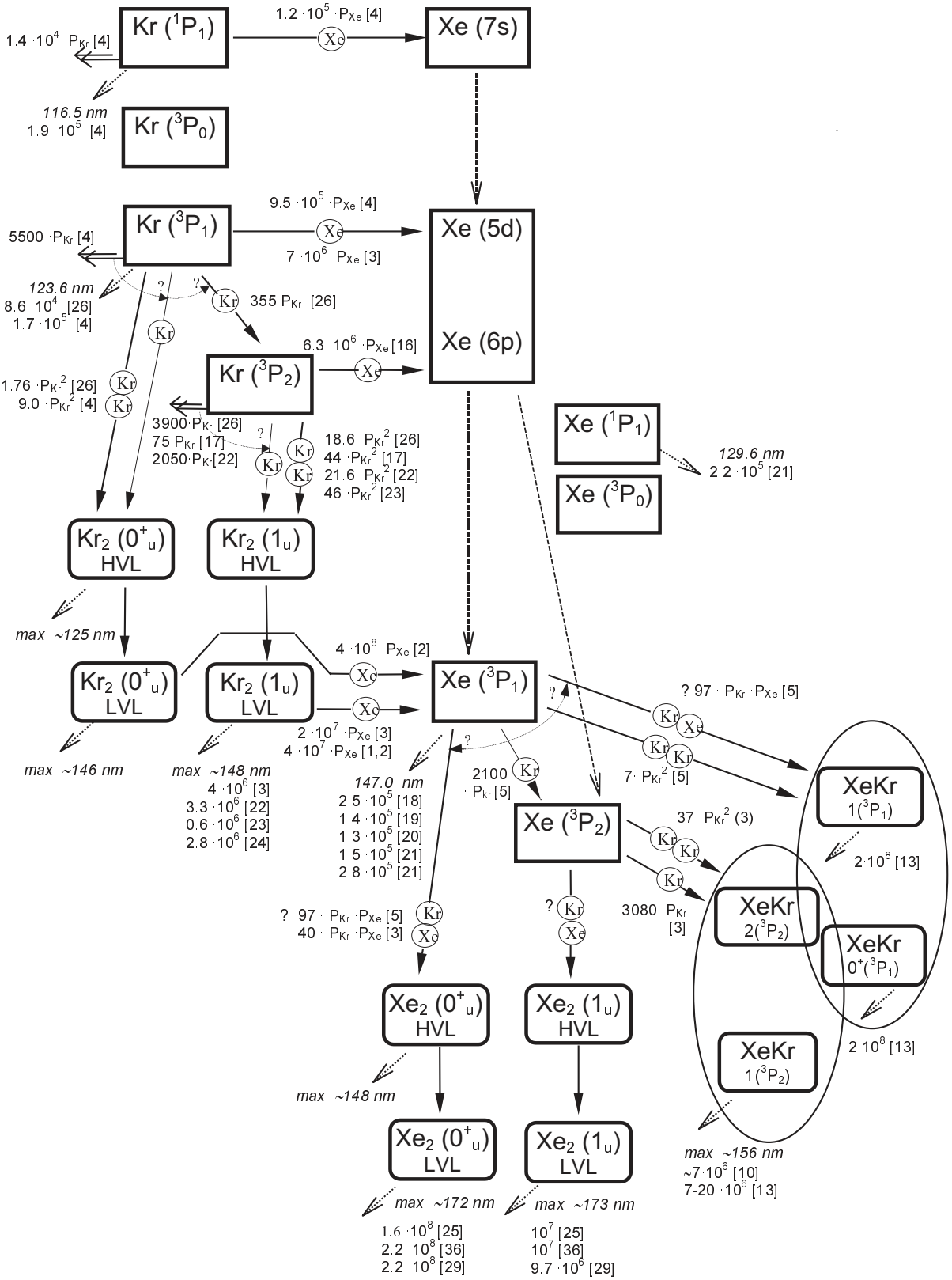

Fig. 12. Diagram of energy transfer processes in a "krypton-small amount of xenon" mixture, according to literature data. Reactions with a participation of electrons were not included. Rates are given in s^{-1}, $torr^{-1}s^{-1}$ and $torr^{-2}s^{-1}$. References are indicated to the publications listed at the end of the article. HVL (LVL) means high (low) vibrational levels. See also comments in Section 3.

However, some comments concerning the block diagram in Figure 12 should be made. Higher excited states of krypton atoms, not included in the diagram, have rather short ($10^{-7} - 10^{-8}$ s) radiative decay times, and therefore they can not act as efficient energy donors at low xenon concentrations. In contrast to the higher states, the lowest excited krypton states, included in the diagram, have rather long ($10^{-5} - 10^{-6}$ s) lifetimes since the optical transitions from the $^3P_0$ and $^3P_2$ levels are dipole forbidden or because of trapping of resonant radiation from the $^1P_1$ and $^3P_1$ states. The lifetime of trapped resonance radiation in krypton for atomic densities of 10^{16} cm^{-3} and higher is determined, according to [27,28], by the pressure broadening of the resonance line. Under such conditions, the decay constant $\beta(r)$ for a cylindrical tube with radius r is independent of the pressure and is given by $\beta(r) = (1/\tau_N)[0.205(\lambda/r)^{1/2}]$ [27,28], where τ_N is the natural lifetime of the upper state and λ is the wavelength of the resonance radiation. An experimental rate value of resonant radiation escape for the Kr($^1P_1$) state at $\lambda = 116.5$ nm, 1.9×10^5 s^{-1} ($r = 1$ cm) is given in [4] and two values are given for the Kr($^3P_1$) state at $\lambda = 123.6$ nm: 8.6×10^4 s^{-1} ($r = 5$ cm) [3,26] and 1.7×10^5 s^{-1} (r = 1 cm) [4].

A value of the quenching rate (that is, the constant of the reaction corresponding to the destruction of a Kr state by binary collisions with ground state Xe atoms) for the Kr($^1P_1$) resonant state has been found only in [4] (1.2×10^5 torr^{-1}s^{-1}); thus a comparison with other works is not possible. However, the quenching rate for the Kr($^3P_1$) resonant state, obtained from the Kr($^3P_1$) state decay curves (9.5×10^5 torr^{-1}s^{-1}) [4], can be compared with the result (7×10^6 torr^{-1}s^{-1}) deduced from the decay curves of the second krypton continuum at 145 nm [3]. The quenching rate of the Kr($^3P_2$) metastable state (6.3×10^6 torr^{-1}s^{-1}), measured by the flowing afterglow technique, has been taken from [16]. The fairly good correlation between the quenching rates obtained in [3,4,16] is worth noticing.

After energy is transferred from the Kr($^1P_1$, $^3P_{1,2}$) states to excited states of XeI, radiative cascading populates the lower-lying states of XeI, eventually the Xe($^3P_1$, $^3P_2$) levels [1–5] (the role of the Xe($^1P_1$) and Xe($^3P_0$) states has not been published, as far as we know).

The rate of molecule-atom energy transfer from the krypton molecular 1_u state, resulting in direct excitation of the xenon atomic state $^3P_1$, was measured in [3] from the decay curves of the second krypton continuum at 145 nm (2×10^7 torr^{-1}s^{-1}). This high rate is in agreement with theoretical predictions [1,2] ($\sim 10^7$ torr^{-1}s^{-1}) and with estimates of the molecule-atom energy transfer cross-sections [1,2] made with a one order of magnitude uncertainty on the basis of spectroscopic experimental data ($\sim 10^{-13}$ cm^2 and $\sim 10^{-14}$ cm^2 for the $Kr_2^*(0_u^+)$ and $Kr_2^*(1_u)$ states respectively, that is $\sim 4\times10^8$ torr^{-1}s^{-1} and $\sim 4 \times 10^7$ torr^{-1}s^{-1}).

It should be pointed out that the products of two-body collisions of Kr($^3P_1$, $^3P_2$) atoms with ground-state Kr atoms usually have no definite identification in the cited literature and that there is a strong discrepancy between the measured values of the rate. We suppose that the mentioned process is, mainly, a two-body conversion of excited atoms in excited molecules.

One might consider energy transfer from krypton atoms and molecules to xenon atoms as the "first" stage of energy transfer in the kinetic model shown in Figure 12. For the lowest xenon concentrations used the result of this stage is the accumulation of excitation energy in the Xe($^3P_1$) level. This conclusion was made on the basis of the spectroscopic results [1–5] which, at the lowest Xe concentrations, showed, besides the Kr emissions, only the high intensity Xe emission at 147 nm. At low Xe concentrations, quenching of the Kr atomic states by Xe ground-state atoms is not as effective as the two- and three-body reactions with Kr atoms (Fig. 12), and the main channel of energy transfer is the molecule-atom channel. One may speculate that the assumption about a selective "initial" population of the Xe($^3P_1$) level is less valid for higher Xe concentrations when atom-atom energy transfer becomes equally or more efficient than molecule-atom energy transfer and the lowest Xe states are populated through radiative cascading (according to the data collected in Fig. 12, the two energy transfer channels become equally efficient when the Xe pressure reaches $P_{Xe} \cong 5 \times 10^{-6} P_{Kr}^2$). In this connection we can indicate the ratio between the Xe($^3P_1$) and Xe($^3P_2$) state populations after a cascade from the atomic Xe($6p$) states (Fig. 12), obtained in [29]: ~ 90 percent of the number of initially excited Xe($6p$) states decay through the Xe($^3P_1$) state and ~ 10 percent bypass to the Xe($^3P_2$) state. This branching ratio did not vary with pressure in the range 75–7500 torr [29]. Hence it might be reasonable to assume a strong population of the Xe($^3P_1$) state in our whole range of Xe pressures and therefore not take the "initial" population of the Xe($^3P_2$) state into account.

The next step of energy transfer is the depopulation of the Xe($^3P_1$) and Xe($^3P_2$) states. Direct measurements of collisional depopulation of the Xe($^3P_1$) state in Kr–Xe mixtures was performed only in [5] as far as we know. According to time-dependent intensity measurements of the xenon resonance line [5], the Xe($^3P_1$) state is depopulated by collisions with both Xe and Kr ground-state atoms. The rate $2100P_{Kr}$ torr^{-1}s^{-1} was assigned to represent a collisional transition to the Xe($^3P_2$) metastable state. The rate $7P_{Kr}^2$ torr^{-2}s^{-1} was assigned to represent the formation of (KrXe)* molecules, while the rate $97P_{Xe}P_{Kr}$ torr^{-2}s^{-1} represents either the formation of the $Xe_2^*(0_u^+)$ states or (XeKr)* molecules. Unfortunately there is no direct information in [5] about the spectral resolution, so therefore we do not know whether the resonance line at $\lambda = 147.0$ nm was recorded together with or without the molecular structure around this line (Figs. 4–7).

The action of Kr ground-state atoms on the metastable Xe($^3P_2$) states was checked in [3] by carrying out a kinetic study of the 173 nm xenon second continuum. The two- and three-body rates of Xe($^3P_2$) state depopulation have been estimated, $3080P_{Kr}$ torr^{-1}s^{-1} and $37P_{Kr}^2$ torr^{-2}s^{-1},

Table 1. Parameters of the Morse potential curves presented in Figure 1 (see comments in Sect. 5). D_m is the depth of the potential well, R_m is the equilibrium internuclear distance, R_0 is the left zero value point of the Morse potential curve.

	KrXe						Xe_2		
	$1(^3P_1)$	$2(^3P_2)$	$0^+(^3P_1)$	$1(^3P_2)$	$0^-(^3P_2)$	$0^+(^1S_0)$	0^+_u	1_u	0^+_g
D_m, cm^{-1}	440 [13]	580 [11,13] *	920 [13]	1120 [11,13]	1230 [11]	159 [15]	4000 [21]	3500 [21]	196 [35]
R_m, Å	4.34 [11]	4.23 [11]	3.55 [13]	3.25 [13]	3.25 ***	4.18 [15]	3.2 [21]	3.2 [21]	4.36 [35]
R_0, Å	3.84 [11]	3.76 [11]	2.86 [13] **	2.65 [13]	2.65 [13]	3.7 [15]	2.5 [21]	2.5 [21]	3.89 [35] ****

* We used the ratio of the depths of the $1(^3P_1)$ and $2(^3P_2)$ states as in [11] and took D_m for the $1(^3P_1)$ state from [13].
** Slightly corrected (5.5 a_0 instead of 5 a_0) to get a crossing point between the $0^+(^3P_1)$ and $1(^3P_1)$ states as in [11] and [13].
*** We have taken the same R_m as for the $1(^3P_2)$ state (like in Fig. 3 in [11]).
**** The same value has been obtained from the absorption spectrum analysis in [37].

respectively. The authors did not indicate products of these reactions, however, so we believe that the mentioned processes are mainly two- and three-body conversion of excited atoms into excited Xe*Kr molecules.

Also the rate $(40 \pm 10)P_{Kr}P_{Xe}$ $torr^{-2}s^{-1}$ was derived in [3] from the decay of the 173 nm continuum, and was attributed to three-body formation of Xe_2^* molecules from $Xe(^3P_1)$ atoms. Notice that in [1,2] the formation of the Xe_2^* molecules was ascribed to three-body conversion of the $Xe(^3P_2)$ atoms.

It should be underlined that the scheme of processes indicated in Figure 12 does not include (for simplicity reasons) reactions with participation of electrons. In our case the electron density n_e is $\sim 10^{14}$ cm^{-3} [30]. Therefore, reactions having a rate $\sim n_e \times 10^{-9}$ s^{-1} or more should be taken into account. Collisions of excited atoms or molecules with electrons resulting in mixing of the level populations are most important in our case. If the separation in the energy between two levels is of the order of 1000 cm^{-1} or less, the mixing has the rate $\sim n_e \times 10^{-7}$ s^{-1} [31,32]. Therefore it is expected, for instance, that there is a strong mixing of the $^3P_1$ and $^3P_2$ atomic states in both Kr and Xe (Fig. 11) in the discharge channel.

From the results of [3,5] (Fig. 12) it follows that the mixed molecules Xe*Kr are the main product of depopulation of the $Xe(^3P_1, ^3P_2)$ states through collisions with atoms in any "krypton-small amount of xenon" mixture, at least at Xe concentrations $< 7\%$. The same conclusion could be drawn from general considerations; if the Kr/Xe concentration ratio is $> 100/1$ (as in our case), Xe atoms could compete with Kr in depopulation of the $Xe(^3P_1, ^3P_2)$ states only if they have a collisional cross section two orders of magnitude higher than Kr atoms which is unlikely. The aforesaid is in accordance with our spectra observed at Xe concentrations $< 0.1\%$. However, at Xe concentrations $> 0.1\%$, a total pressure ~ 300 torr and low gas temperature, the Xe_2^* continuum becomes the main feature of the VUV spectrum of the mixture (Figs. 9 and 10). Similar results were obtained at higher total pressures than in our discharges and at room temperature in [2,3]. The conclusion is that it is appropriate to look for an additional energy transfer processes.

The Morse potential curves for XeKr molecules (Fig. 1) will be used in the interpretation of the spectra depicted in Figures 3–10. These potential curves are derived from semiempirical calculations for the excited states [11,13] and data for the ground state presented in [15]. The restricted experimental results for the $1(^3P_1)$ state obtained in [8] were taken into account in the calculations [11–13]. For convenience, the Morse potentials of Xe_2 are also shown in Figure 1. The parameters used in the construction of the Morse potentials are presented in Table 1. For XeKr potentials we tried to use the data of [13] as the basic data but this publication contains the full sets of the Morse parameters only for the $0^+(^3P_1)$ and $1(^3P_2)$ states. Therefore it was necessary to combine the results of [11,13]. Sometimes the potential curves presented in [11,13] were used to derive a parameter. We consider the XeKr potentials shown in Figure 1 realistic but not very accurate.

A significant feature distinguishes the potential curves for Xe*Kr molecules from the curves for the Kr_2 or Xe_2 dimers, namely, according to the cited works [11–13], that there are "additional" bound excited electronic states. In reality, these are weakly bound states: the potential curves of the $1(^3P_1)$ and $2(^3P_2)$ states have shallow minima. These minima are situated at larger internuclear distances than the minima of the $0^+(^3P_1)$ and $1(^3P_2)$ states and at about the same internuclear distance as the weakly bound ground state $0^+(^1S_0)$. On the basis of the works [11,13] one can estimate the depths of the $1(^3P_1)$ and $2(^3P_2)$ wells to be some hundred cm^{-1}.

As underlined above, the atomic-molecular emission spectrum around $\lambda = 147.0$ nm (Figs. 4–6) is similar to the absorption spectrum of the Kr–Xe mixture close to the Xe resonance line (Fig. 7). This similarity indicates that both the emission and absorption spectra correspond to transitions between the same sets of upper and lower states. On the other hand, the structure of the Kr–Xe spectrum around the resonance line $\lambda = 147.0$ nm, that is the width and the presence of maxima and minima,

is quite different from that in pure Xe or Kr (see *e.g.* [33,34]). If we take the last two points into account, a comparison of the spectra (Figs. 4–7) with the potential curves (Fig. 1) indicates that molecular structure near $\lambda =$ 147.0 nm, in absorption and in emission, is quite probably caused by transitions between the weakly bound ground state $0^+(^1S_0)$ and the weakly bound excited state $1(^3P_1)$.

The following remarks about the identification of the spectrum around $\lambda = 147.0$ nm can now be made. The depths of the $0^+(^1S_0)$ and $1(^3P_1)$ states are so small that each of them has a more or less uniform density distribution over the vibrational levels when it serves as the initial electronic state of the discussed transitions, and, consequently, the same set of molecular transitions and similar spectra may be observed in absorption and in emission. The width of the molecular spectrum from the resonance line at $\lambda = 147.0$ nm to the short wavelength side is ≈ 0.6 nm, corresponding to ≈ 300 cm^{-1} in energy. This value exceeds by a factor of 2 the depth of the ground state well (≈ 160 cm^{-1}) estimated in [35]. One may therefore conclude that the spectrum on the short wavelength side of $\lambda = 147.0$ nm partially originates from free-bound transitions between the repulsive part of the $1(^3P_1)$ state and the well of the $0^+(^1S_0)$ state. The presence of the very broad molecular bands on the short wavelength side in the range 146.3–146.8 nm [14] (part of them are seen in Fig. 5) supports this conclusion. We may also conclude that the minimum of the potential curve of the ground state $0^+(^1S_0)$ is situated at a larger internuclear distance than the minimum of the $1(^3P_1)$ state. The width of the molecular spectrum from the resonance line at $\lambda = 147.0$ nm to the long wavelength side indicates that the well depths of the $1(^3P_1)$ and $0^+(^1S_0)$ states should be about the same. These facts are the starting points for the identification of the spectrum around $\lambda = 147.0$ nm. The previous analysis has shown that all details of the spectrum, including the strong peak on the long wavelength side (which was assigned as the atomic line wing in [14,15], can be considered as transitions between vibrational levels of the $1(^3P_1)$ and $0^+(^1S_0)$ states.

It is now possible to interpret the spectra in Figures 3, 8–10 and, in particular, give an explanation of the appearance of the Xe_2 continuum. At low xenon concentrations, the emissions related to the xenon admixture concentrate around the xenon resonance line $\lambda = 146.97$ nm (Figs. 3–6). The long wavelength low intensity "non-krypton" continuum, originating from transitions in Xe*Kr molecules from the lower vibrational levels of the $0^+(^3P_1)$ or $1(^3P_2)$ states, becomes distinguishable only at Xe concentrations $\approx 0.1\%$ (Fig. 3). If the total pressure is low enough, the integral intensity of the band around $\lambda = 147.0$ nm exceeds significantly the integral intensity of the mixed molecule continuum from the strongly bound states. For instance, at a total pressure of 100 torr and 0.1% Xe admixture, the ratio of the two intensities is about 10 according to our spectra. Making this estimate, we did not take self-absorption in the band into account. In reality the ratio is higher. The aforesaid indicates, firstly, a high population of the $1(^3P_1)$ mixed molecule state, and, secondly, that the band around $\lambda = 147.0$ nm is the main channel of radiative losses of the mixed molecules.

When the Xe concentration or the total pressure increases, the ratio between the integral intensity in the band around $\lambda = 147.0$ nm and the intensity of the mixed molecule continuum goes down. Partially this can be connected with a more rapid growth of the continuum intensity than of the band intensity, but the main reason is growing self-absorption in the band around $\lambda = 147.0$ nm since the detection of the light with the spectrometer is done along the discharge capillary and through the gas layer between the discharge channel and the exit window. Therefore, the decreasing ratio of the integral intensities observed in the spectra does not mean that the main part of the Xe*Kr emission from the emitting volume begins to concentrate in the continuum. One should remember that with a long and narrow emitting volume as in our case, the radiative losses that are not along the capillary but in the lateral direction are most important. It is obvious that the relative intensity of the band around $\lambda = 147.0$ nm is much higher at the inner capillary wall than what we obtain in the spectra observed along the capillary. Consequently, the band around $\lambda = 147.0$ nm is not so strongly trapped in the uncooled capillary as it seems from the spectra observed along the capillary.

This conclusion is also confirmed by the following: the spectra in Figures 3 and 8 and the spectra 1, 2 in Figure 9 show a significant difference between the integral intensity of the Kr–Xe mixture spectrum and the integral intensity of the pure Kr spectrum. But, in accordance with the scheme of the processes (Fig. 12), these integral intensities should not differ significantly because energy, transferred from the Kr molecules to the Xe atoms and, further, to the mixed molecules, should be emitted in the VUV range indicated in the figures.

Cooling of the capillary walls with liquid nitrogen vapours increases the gas density in the capillary and, what is more important in our case, increases the concentration of the XeKr ground state molecules, especially near the inner capillary wall. A well-known formula of statistical mechanics was used in [32] for estimates of the molecular concentrations in weakly bound ground states. For the XeKr mixture this formula gives, at a total pressure of 300 torr, 1% of Xe and a gas temperature of 110 K, a relative density ratio $N_m/N_a \approx 3\%$, where N_m and N_a are the concentrations of ground state XeKr molecules and Xe atoms respectively. However, since the condensed phase should be taken into account, this could be an underestimate when the gas temperature approaches the temperature of gas condensation and the density of the weakly bound molecule grows much more rapidly than the formula predicts. A growth of the XeKr molecule density leads to increasing self-absorption and trapping of the band around $\lambda = 147.0$ nm emitted in the lateral direction. Consequently, the efficient lifetime of the Xe*Kr $1(^3P_1)$ state increases and the probability of excitation transfer from the Xe*Kr $1(^3P_1)$ state grows.

The spectra in Figures 9 and 10 indicate that excitation energy is transferred to the Xe*Kr states and to the

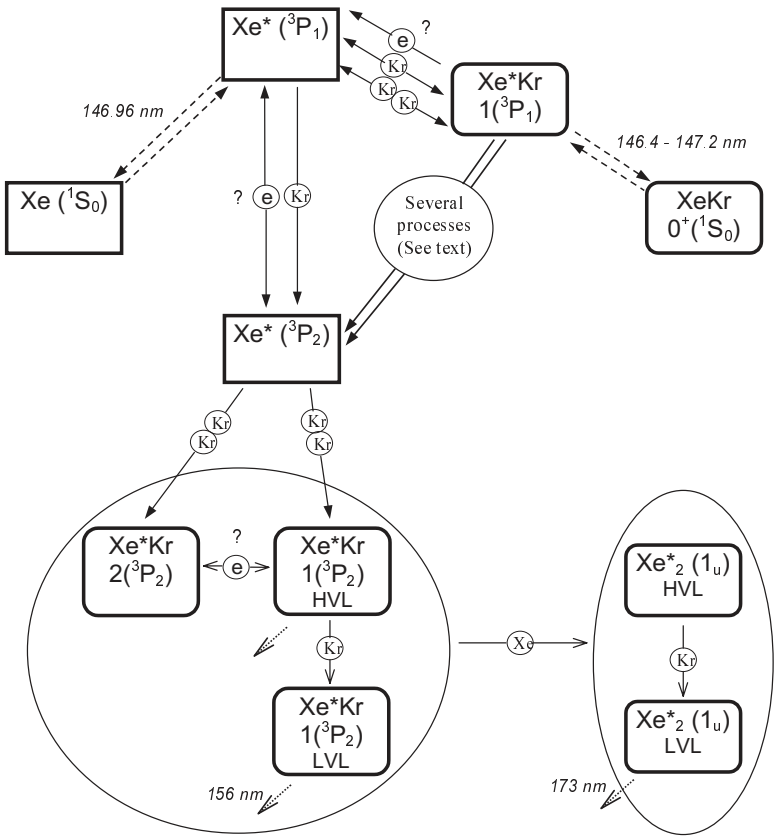

Fig. 13. Simplified scheme of energy transfer processes in a "krypton-small amount of xenon" mixture, in accordance with the results of this work (see details and comments in text). It is supposed that "initially", after energy transfer from Kr to Xe, excitation is mainly concentrated in the Xe*($^3P_1$) state (see Fig. 12). Reactions of atomic and molecular state mixing by electrons are marked by the sign "?" because it is assumed that energy transfer processes take place not only in but also outside the discharge channel. HVL (LVL) means high (low) vibrational levels.

Xe_2^* states emitting the continua with maxima at 156 nm and 173 nm. One should remember that Xe_2^* molecules, as has been supposed above, will not appear as a result of a three-body conversion of the excited Xe atoms in competition with three-body conversion to mixed molecules.

According to our analysis of the spectra, the trapping of the band around $\lambda = 147$ nm leads to an increase of excitation transfer to the Xe*($^3P_2$) state (Fig. 13). A number of processes may contribute. Firstly, an increasing efficient lifetime of the Xe*Kr 1($^3P_1$) state will lead to an increase of the efficient lifetime of the atomic precursor, Xe*($^3P_1$). In this case, mixing of the Xe*($^3P_1$) and Xe*($^3P_2$) states assisted by collisions with electrons and atoms gives a higher efficiency of excitation transfer to the Xe*($^3P_2$) state in a cooled capillary than in an uncooled capillary.

Secondly, the trapping of the band around $\lambda = 147.0$ nm leads to a growth of excitation transfer to the Xe*Kr(0$^+$($^3P_1$)) molecule *via* mixing of the 1($^3P_1$) and 0$^+$($^3P_1$) states (see Fig. 1) by electrons, and/or can initiate the following two reactions:

$$Xe^*Kr(1(^3P_1),\ 0^+(^3P_1)) + Xe(^1S_0) \rightarrow Xe_2^*(0_u^+) + Kr(^1S_0). \quad (1)$$

The $Xe_2^*(0_u^+)$ and Xe*Kr(0$^+$($^3P_1$)) molecules can be formed only in the upper vibrational states and therefore, to emit the second continua at 156 nm and 173 nm, they must relax (in collisions with the atoms) to their lowest vibrational levels. The natural lifetimes of these upper vibrational levels are very short (nanoseconds) which raises the question if relaxation to the lowest vibrational levels is possible at our total pressures. In this connection we refer to results reported in [29] where the observation of the temporal behaviour of the second Xe_2^* continuum was carried out in pure Xe. It was shown that a contribution of the $Xe_2^*(0_u^+)$ state to the second continuum shows up at Xe concentrations $> 4 \times 10^{19}$ cm^{-3}. This result is not in full agreement with the vibrational relaxation rate for the $Xe_2^*(0_u^+)$ state, 7×10^{-11} cm^{3}s^{-1}, obtained in [36]. We therefore believe that the latter value of the relaxation rate is too high since relaxation from the highest vibrational levels was not investigated in [36]. We have derived an estimate for this rate from the results of [29] to be $< 10^{-11}$ cm^{3}s^{-1}. Another result obtained in [36], the rate for $Xe_2^*(0_u^+)$ vibrational relaxation in collisions with Ar, is 6×10^{-12} cm^{3}s^{-1} which indicates an upper limit of the rate for $Xe_2^*(0_u^+)$ vibrational relaxation in collisions with Kr. In [6] relaxation constants of Xe_2^* and Xe*Kr molecules with krypton as a buffer gas were estimated to be 2×10^{-12} cm^{3}s^{-1} for both excimer systems. The listed results give reasons to believe that, at the total pressures used in our experiments, the relaxation from the upper to the lowest vibrational levels of both the $Xe_2^*(0_u^+)$ and Xe*Kr(0$^+$($^3P_1$)) molecular states is unlikely.

In accordance with [29], one can assume that the main part of the $Xe_2^*(0_u^+)$ molecules, being in their upper vibrational levels, dissociate along the repulsive potential

curves forming the two atomic $Xe^*(^3P_2)$ and $Xe(^1S_0)$ states (the single repulsive curve shown in Fig. 1 symbolises the $1g$, $0g^-$, and $2u$ repulsive states). The ratio 0.29 between the relaxation and dissociation rates was obtained in [29]. According to our estimates derived from the results of [29], the dissociation rate for the $Xe_2^*(0_u^+)$ molecule is $\approx 3 \times 10^{-11}$ cm^{3}s^{-1}. The same type of dissociation of the $Xe^*Kr(0^+(^3P_1))$ molecules can occur *via* the $Xe^*Kr(2(^3P_2))$ weakly bound state.

Hence, the growing trapping of the band around $\lambda = 147.0$ nm leads, in different ways, to an increase of excitation transfer to the $Xe^*(^3P_2)$ state. The $Xe^*(^3P_2)$ atoms, appearing as a result of a dissociation or a mixing, are then converted in a three-body process into $Xe^*(^3P_2)Kr$ molecules, which have longer (approximately one order of magnitude) radiative lifetimes than $Xe^*(^3P_1)Kr$ molecules. By analogy with conversion of the $Xe^*(^3P_1)$ state, one can assume that a significant part of the $Xe^*(^3P_2)$ atoms will be converted into weakly bound $Xe^*Kr(2(^3P_2))$ molecules (the optical transitions from the $2(^3P_2)$ state to the ground state are forbidden). Therefore, the two reactions

$$Xe^*Kr(1(^3P_2), 2(^3P_2)) + Xe(^1S_0) \rightarrow Xe_2^*(1_u) + Kr(^1S_0) \quad (2)$$

can be efficient. A total pressure of 300 torr is undoubtedly enough for collisional relaxation of both $Xe^*Kr(1(^3P_2))$ and $Xe_2^*(1_u)$ molecules to the lowest vibrational levels and the subsequent emission of the continua around 156 nm and 173 nm.

If we apply the aforesaid to an interpretation of the spectra 2, 3 and 4 in Figure 9, we conclude, first of all, that the growth of the total intensity of the continuous emission of the mixture with cooling is a result of trapping of the band around $\lambda = 147.0$ nm emitted in the direction to the capillary wall. Secondly, the intensity of the continuum at 173 nm grows faster than that at 156 nm because the Xe concentration increases under cooling and the efficiency of the reactions (2) grows. Thirdly, one may draw the conclusion from spectra 2, 3, 4 that the rate of the reaction (2) is of the same order of magnitude as the radiative decay of the mixed molecules taking part in the reaction. Figure 10 shows that a certain level of Xe concentration is necessary to obtain "the effect of cooling" (spectra 3 and 4 in comparison with spectrum 2). Firstly, the Xe concentration should be high enough for effective trapping of the band around $\lambda = 147.0$ nm. Secondly, the Xe concentration should also be high enough for a successful competition with the radiative decay of the $Xe^*Kr(2(^3P_2))$ molecules.

As a summary of this chapter, we want to make the following remarks.

- As mentioned above, a spectrum similar to the spectrum 4 in Figure 9 was observed in [2,3] at room temperature and total pressures of 1000 torr [2] and 500 torr [3] when the xenon concentration increased up to 2.5% and 1%, respectively. The lateral dimensions of the cells used for excitation of the mixture in [2,3] were $\leq$ 1 cm and 10 cm, respectively. That is: higher total pressure and Xe concentration are necessary to observe the Xe_2^* continuum at 173 nm in cells with small dimensions. One might suppose that the results from [2,3] confirm that the effect of trapping of the emission in the band around $\lambda = 147.0$ nm plays an important role for the interpretation of our results.
- The intensity of the Kr_2 continuum grows under cooling (spectrum 1 in Fig. 10 and spectrum 1 in Fig. 9). This effect was investigated in [32]. It should be pointed out that the integral intensity of the Kr–Xe spectrum under cooling (spectrum 4 in Fig. 10) is higher than the intensity of the Kr_2 continuum (spectrum 1 in Fig. 10). To understand this, we have to take into account that excitation is transferred from Kr to Xe through two channels, the "molecule-atom" channel as well as the "atom-atom" channel. The difference in the intensities can be connected with the growth of the "atom-atom" channel contribution at higher Xe pressures.
- In reality it is not possible to separate the emission from the $Xe^*Kr(1(^3P_1))$ molecules and from the uppermost vibrational levels of the $Xe^*Kr(0^+(^3P_1))$ state. When talking about $Xe^*Kr(1(^3P_1))$ emission, we also mean emission from the uppermost vibrational levels of the $Xe^*Kr(0^+(^3P_1))$ state.
- In this work a contracted discharge was used, having a narrow diameter ($\approx$ 0.5 mm) discharge channel along the axis of the discharge capillary. The molecular self-absorption and trapping of the band around $\lambda = 147.0$ nm takes place mainly in cold layers close to the inner capillary wall. A growth of the trapping with cooling leads to a consequent increase of the concentration of excited molecules (and atoms) in these layers. This in turn means that the processes of energy transfer described above and, consequently, also the emission of the continua may occur predominantly near the inner capillary wall, that is outside the discharge channel.
- Only the "main route" of excitation transfer from the trapped $Xe^*(^3P_1)$ state has been discussed in this paper. A simplified scheme of energy transfer processes starting from the $Xe^*(^3P_1)$ state is shown in Figure 13.

A number of observations remain to be interpreted. In particular, a rather intense structure of molecular origin has been observed near the Kr resonance lines. Possibly, Kr^*Xe molecules can also be the starting point of energy transfer from Kr to Xe.

4 Conclusion

The results of the work extend the understanding of the mixed molecule role in generating the VUV spectrum from a mixture of "krypton-small amount of xenon". The creation of excited mixed molecules Xe^*Kr is the basic channel of energy transfer from the atomic xenon state $Xe^*(^3P_1)$ which is a result of energy transfer from krypton to xenon. A strong emission peak from a weakly bound

excited Xe^*Kr state is observed around $\lambda = 147.0$ nm together with continuous emission from a more strongly bound excited Xe^*Kr state. Mixed molecule emission determines the spectrum of the mixture until emission in the band around $\lambda = 147$ nm becomes strongly limited by self-absorption. In our case this occurs when the discharge capillary wall is cooled down to temperatures close to the temperature of gas condensation. With cooling, the $Xe_2^*(1_u)$ molecule emission becomes the main feature of the spectrum. However, the mixed molecules work as an important link in the energy transfer processes, even when their contribution to the spectrum is small.

This work was supported by the Swedish Research Council for Engineering Sciences (TFR) and by Carl Tryggers Stiftelse for Vetenskaplig Forskning. Two of us, B.K. and G.G., would like to thank the Department of Physics, Uppsala University, for its hospitality. We also thank Dr. Alexei Utkin at the Department of Computational Physics, St. Petersburg State University, for the software used in our data acquisition system.

References

1. A. Gedanken, J. Jortner, B. Raz, A. Szoke, J. Chem. Phys. **57**, 3456 (1972).
2. O. Cheshnovsky, B. Raz, J. Jortner, J. Chem. Phys. **59**, 3301 (1973).
3. Y. Salamero, A. Birot, H. Brunet, H. Dijols, J. Galy, P. Millet, J.P. Montagne, J. Chem. Phys. **74**, 288 (1981).
4. J.D. Cook, P.K. Leichner, Phys. Rev. A **31**, 90 (1985).
5. J.D. Cook, P.K. Leichner, Phys. Rev. A **43**, 1614 (1991).
6. N.A. Kryukov, M.A. Chaplygin, Opt. Spectrosc. **82**, 510 (1997).
7. E.T. Verkhovtseva, A.E. Ovechkin, Opt. Spectrosc. **47**, 117 (1979).
8. G. Nowak, J. Fricke, J. Phys. B: At. Mol. Phys. **18**, 1355 (1985).
9. A.G. Belov, A.D. Klementov, S.A. Pendyur, I.Ya. Fugol, E.M. Yurtaeva, Opt. Spectrosc. **61**, 601 (1986).
10. P. Laporte, P. Gurtler, E. Morikawa, R. Reininger, V. Saile, Europhys. Lett. **9**, 533 (1989).
11. A.L. Zagrebin, N.A. Pavlovskaya, Opt. Spectrosc. **69**, 320 (1990).
12. A.Z. Devdariani, A.L. Zagrebin, Opt. Spectrosc. **72**, 309 (1992).
13. A.L. Zagrebin, S.I. Tserkovnyi, Chem. Phys. Lett. **239**, 136 (1995).
14. D.E. Freeman, K. Yoshino, Y. Tanaka, J. Chem. Phys. **67**, 3462 (1977).
15. M.C. Castex, J. Chem. Phys. **66**, 3854 (1977).
16. J.E. Velazco J.H. Kolts, D.W. Setser, J. Chem. Phys. **69**, 4357 (1978).
17. R. Turner, Phys. Rev. **158**, 121 (1967).
18. Y. Salamero, A. Birot, H. Brunet, J. Galy, P. Millet, J. Chem. Phys. **80**, 4774 (1984).
19. P.R. Timpson, J.M. Anderson, Can. J. Phys. **70**, 380 (1979).
20. W. Wieme, M. Vanmarcke, Phys. Lett. A **72**, 215 (1979).
21. Y. Salamero, A. Birot, H. Brunet, J.N. Foulquier, J. Galy, P. Millet, M. Rouzaud, J.L. Teyssier, J. Phys. B: At. Mol. Opt. Phys. **21**, 2015 (1988).
22. P.K. Leichner, R.J. Ericson, Phys. Rev. A **9**, 251 (1974).
23. R. Boucique, P. Mortier, J. Phys. D: Appl. Phys. **3**, 1905 (1970).
24. T. Oka, K.V.S. Rama Rao, J.L. Redpath, R.F. Firestone, J. Chem. Phys. **61**, 4740 (1974).
25. J.W. Keto, R.E. Gleason, T.D. Bonifield, G.K. Walters, F.K. Soley, Chem. Phys. Lett. **42**, 125 (1976).
26. Y. Salamero, A. Birot, H. Brunet, J. Galy, P. Millet, J.P. Montagne, J. Phys. B: At. Mol. Opt. Phys. **12**, 419 (1979).
27. A.V. Phelps, Phys. Rev. **114**, 1011 (1958).
28. R. Turner, Phys. Rev. **140**, A426 (1965).
29. P. Moutard, P. Laporte, J.-L. Subtil, N. Damany, H. Damany, J. Chem. Phys. **88**, 7485 (1988).
30. G. Gerasimov, B. Krylov, G. Zvereva, R. Hallin, A. Arnesen, F. Heijkenskjold, Opt. Spectrosc. **81**, 857 (1996).
31. C.W. Werner, E.V. George, P.W. Hoff, C.K. Rhodes, IEEE J. Quantum Electrn. **QE-13**, 769 (1977).
32. G. Gerasimov, B. Krylov, A. Loginov, G. Zvereva, R. Hallin, A. Arnesen, F. Heijkenskjold, Appl. Phys. B **66**, 81 (1998).
33. R.E. Huffman, J.C. Larrabee, Y. Tanaka, Appl. Opt. **4**, 1581 (1965).
34. Y. Tanaka, K. Yoshino, D.E. Freeman, J. Chem. Phys. **59**, 5160 (1973).
35. M.V. Bobetic, J.A. Barker, J. Chem. Phys. **64**, 2367 (1976).
36. T.D. Bonifield, F.H.K. Rambow, G.K. Walters, M.V. McCusker, D.C. Lorents, R.A. Gutcheck, J. Chem. Phys. **72**, 2914 (1980).
37. M.-C. Castex, J. Chem. Phys. **74**, 759 (1981).

Paper IV

INSTITUTE OF PHYSICS PUBLISHING JOURNAL OF PHYSICS B: ATOMIC, MOLECULAR AND OPTICAL PHYSICS

J. Phys. B: At. Mol. Opt. Phys. **35** (2002) 1929–1940 PII: S0953-4075(02)32356-3

A study of atomic and molecular energy transfer channels in Kr–Xe gas mixtures excited with radio frequency discharges

A Morozov[1], B Krylov[2], G Gerasimov[2], A Arnesen[1] and R Hallin[1]

[1] Uppsala University, Department of Physics, Box 530, SE-752 21 Uppsala, Sweden
[2] Vavilov State Optical Institute, Birzhevaja Line 12, St Petersburg, 199034, Russia

E-mail: AndreiMorozov@hotmail.com

Received 3 January 2002, in final form 19 March 2002
Published 10 April 2002
Online at stacks.iop.org/JPhysB/35/1929

Abstract

Simultaneous observations of the vacuum ultraviolet (VUV) and visible–near-IR emission from radio frequency discharges in gaseous Kr with small (<0.1%) Xe admixture concentrations were conducted in the pressure range 80–400 hPa. The spectra were used for investigation of energy transfer from the lowest excited states of both atomic krypton and krypton molecules to the ground state xenon atoms. The VUV emission spectra allowed us to obtain a value of $3.9 \times 10^7 \times P_{Xe}$ hPa^{-1} s^{-1} for the energy transfer rate from the 1_u state of Kr_2^* molecules and a rate of $1.7 \times 10^6 \times P_{Xe}$ hPa^{-1} s^{-1} for the energy transfer rate from the system of the four lowest Kr excited states to Xe ground state atoms. A value of $1.6 \times 10^6 \times P_{Xe}$ hPa^{-1} s^{-1} was independently obtained for this atom-to-atom energy transfer channel based on our observations of IR emission.

1. Introduction

The vacuum ultraviolet (VUV) emission from mixtures of rare gases has been studied in a number of works (see e.g. [1–5]) arising from scientific and technological demands for VUV radiation sources. It has been shown that the emission from binary rare gas mixtures, when the heavier gas constitutes only a small admixture, concentrates under certain conditions in a narrow band close to the resonance lines of the admixture [1, 5]. This suggests the existence of very efficient energy transfer processes from the main lighter gas to the heavy gas. However, only a few experimental studies exist which give rates for energy transfer reactions (see e.g. [1–4, 6, 7]) and these rates vary considerably from each other (see review in [5]).

Knowledge of the VUV emission and absorption from rare gases acquired in recent years [5, 8] permits us to present here a more complete treatment of experimental results concerning the energy transfer in Kr–Xe mixtures, which takes into account more features

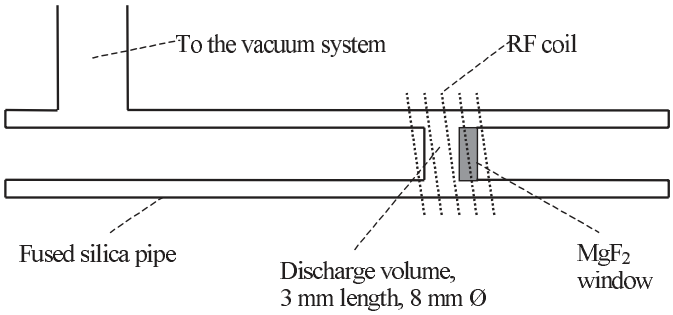

Figure 1. Scheme of the gas discharge tube used for the experiments with RF excitation.

than before, such as the origin of the narrow band emission and radiation trapping properties. To minimize self-absorption, a new radiation source excited with a radio frequency (RF) discharge was constructed. Analysis of the recorded VUV spectra made it possible to define more reliable and consistent rates of energy transfer, especially the relative contributions from atomic and molecular energy transfer channels, i.e. energy transfer from Kr^* atoms and from Kr_2^* molecules to the ground state Xe atoms.

In [5] the observation of emission was limited to the VUV range, while in this work the observation of atomic cascades in Kr I and Xe I (visible and near-IR ranges) was added. This allowed us to verify the scheme of energy transfer from Kr to Xe discussed in [5] and to estimate the rate of atomic energy transfer independently of the VUV observation. Our observation of Kr I radiative cascades in pure Kr and in Kr–Xe mixtures allowed us to also establish the experimental conditions when the direct electron excitation of xenon is negligible in comparison with energy transfer from krypton.

2. Experimental details

We recorded VUV, visible and near-IR emission from pure Kr and from mixtures of Kr with 0.1–0.006% of Xe in the total pressure range 80–400 hPa. The gases were excited by RF discharges. RF excitation took place in a very short cylindrical volume that was 3 mm along the observation axis and 8 mm in diameter (see figure 1). This geometry allowed us to greatly reduce the influence of self-absorption on the narrow band emitted from Kr–Xe mixtures close to the Xe resonance line at 147 nm. RF excitation at 13.56 MHz was performed via a 15-turn 10 mm diameter helical coil of 1 mm copper wire, which surrounded the gas volume. The power inserted into plasmas was estimated to be about 25 W for all gas conditions. Upon ignition, the entire discharge volume was homogeneously filled with plasma.

The VUV radiation was observed through a magnesium fluoride window. The discharge tube was connected to the rest of the vacuum system for pumping and gas filling through a long fused silica pipe, which ensured that the VUV radiation did not hit any metallic parts of the system. This kept the impurity level very low, especially after baking the system. The presence of impurities was monitored by recording C I lines and CO bands. It was essential to reach an extremely low level of CO in order to have a reproducible and intense Kr continuum.

To record the VUV spectra (110–200 nm) we used a 1 m normal-incidence vacuum spectrometer with 0.83 nm mm^{-1} dispersion. A PM tube, operating in the photon counting mode, was used as the detector. The highest spectral resolution attained was 0.015 nm. The registration of the visible and near-IR spectra was performed with a model 1235 spectrometer of

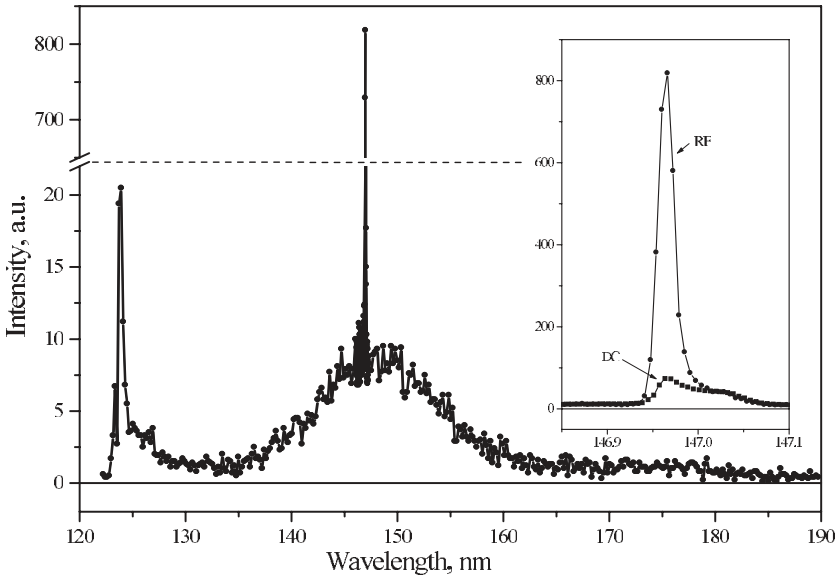

Figure 2. VUV emission spectrum from a RF gas discharge in 200 hPa Kr with 0.01% Xe. The inset shows the area near the Xe resonance line at 146.97 nm from RF and DC discharges, demonstrating very low self-absorption in the first case. The spectrum from the DC setup was scaled to have the same intensity in the long-wavelength part of the shoulder, where absorption is minimal. The spectral resolution is 0.015 nm.

EG & G Princeton Applied Research with a spectral range 400–1000 nm equipped with a CCD detector model 1452A from the same manufacturer. The spectral resolution was approximately 0.2 nm.

Direct current (DC) discharge excitation was used to record visible and near-IR emission to compare the absolute intensity of Kr radiative cascades in pure Kr with those from mixtures of Kr with Xe. We took advantage of the fact that the intensity distribution of Kr radiative cascade lines was identical for RF and DC discharges, while DC discharges gave much better (about 2% in contrast to 10%) absolute intensity reproducibility. The DC discharge was arranged in a fused silica capillary 200 mm long with a 1.4 mm inner diameter (details of the experimental setup could be found in [5]). The discharge current was 10–20 mA. Observations were performed perpendicular to the capillary axis to avoid self-absorption.

2.1. Experimental VUV spectra

An addition of a small admixture of xenon to a krypton RF or DC discharge plasma results in an intensity decrease of the Kr_2^* continuum and the appearance of an intense peak of narrow-band radiation in the immediate vicinity of 147 nm. An example of a VUV emission spectrum from a RF discharge in 200 hPa of Kr with 0.01% Xe is shown in figure 2. The narrow-band radiation at 147 nm was earlier ascribed to the atomic resonance emission of Xe (146.96 nm) [1]. However, this identification is not correct, the origin of the narrow band is in part due to Xe^*Kr molecular emission [5, 8] from the weakly bound state $1(^3P_1)$ to the ground state.

Since the method of energy transfer rate calculations used in this work requires the evaluation of the integrated intensities in the continuum and the narrow band, it was extremely important to minimize the influence of self-absorption on the band near 147 nm. That was the

reason why RF excitation and the design of the discharge tube, described above, were chosen. The insert in figure 2 shows a comparison of the narrow band emitted from a RF discharge with that from the same mixture in a DC discharge (details on DC observations can be found in [5]). The spectrum from the DC setup was scaled to have the same intensity in the long-wavelength part of the shoulder, where absorption is minimal. If one compares the band from the both types of discharge, it is evident that self-absorption is greatly reduced when RF excitation is used. The presence of self-absorption is also considerably reduced in the short-wavelength part of the Kr_2 continuum emission close to the Kr resonance line where self-absorption is very strong.

Note that the effect of self-absorption in the band was not discussed in [1], where the similar method of calculation of energy transfer rates based on VUV spectral intensities was used. It is therefore especially important to take into account the length of the source used in [1] (>140 mm, which is close to our DC discharge source length) when considering a possible effect of self-absorption. Our DC discharge study [5] also indicates that it is extremely important to eliminate the 'cold' absorption region between the end of the discharge and the window, which greatly reduces the intensity of the band at 147 nm.

3. Kinetic scheme

The analysis of the emission spectra from Kr–Xe gas mixture discharges and the calculations of the energy transfer rates are based on the following kinetic scheme.

Excited Kr atoms in their lowest metastable and resonant states ($^3P_0$, $^3P_1$, $^3P_2$ and $^1P_1$) are created by radiative cascades from highly excited states (and ionic states after recombination) and by direct electron excitation (see figure 3). The $^3P_1$ and $^1P_1$ resonant states can be considered in our case as metastable because of the strong radiative trapping which results in their effective lifetimes being of the order of tens of microseconds (see the review in [5]). Since the radiative losses are quite weak, the metastable Kr atoms could either form Kr_2^* molecules (1_u, 0_u^+ states) in three-body collisions (see figure 3) or transfer their energy to ground state Xe atoms, exciting them to the 5d, 6p and possibly 7s states (figures 3 and 4). The exited Xe atoms relax radiatively to the lowest resonant and metastable states of Xe. Kr_2^* molecules, for their part, could either emit VUV radiation (the so-called first and second continua) or transfer their excitation energy to ground state Xe atoms, exciting them to their lowest excited states (see figure 4).

If the total gas pressure and Xe concentration are low enough, the Xe-related VUV emission from Kr–Xe gas mixture discharges is concentrated near 147 nm [1,5] (see figure 2), and one has to conclude that the main final product resulting from energy transfer is Xe in one of the lowest pair of excited (i.e. resonant $^3P_1$ and metastable $^3P_2$) states. These two states are mixed by electrons (see below) and emission from the resonant state is strongly self-absorbed. Therefore, at the moderate Kr pressures (<400 hPa) and small Xe concentrations (<0.1%), used in this work, the dominant emission should be from Xe^*Kr molecules in the weakly bound state $1(^3P_1)$ [5,8], which are created in three-body collisions with two ground state Kr atoms. There will also be some emission from unbound Xe^*–Kr pairs resulting in a broadened Xe resonance line. For details on the Kr–Xe mixture emission see [5].

To determine the energy transfer rate coefficients we have used a technique similar to one described in [1]. It involves a steady state balance for the following reactions:

(1) $Kr^* + Xe \rightarrow Xe^{**} + Kr$ (atomic energy transfer channel), with rate $\boldsymbol{k_A}$.
(2) $Kr^* + 2Kr \rightarrow Kr_2^* + Kr$, with rate $\boldsymbol{k}$.
(3) $Kr_2^* + Xe \rightarrow Xe^* + 2Kr$ (molecular energy transfer channel), with rate $\boldsymbol{k_M}$.
(4) $Kr_2^* \rightarrow 2Kr + h\nu$, with lifetime $\boldsymbol{\tau}$.

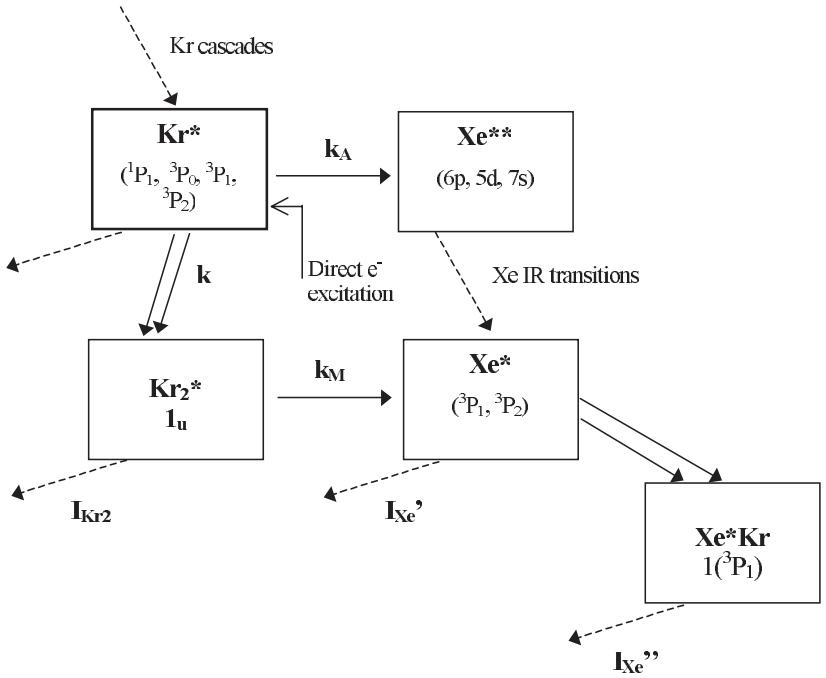

Figure 3. Simplified diagram of energy transfer processes in Kr–Xe gas mixture discharges. The four lowest excited Kr states are populated by radiative cascades from higher Kr states and by direct electron excitation. I_{Kr_2} represents the broad continuum emission (125–190 nm) from Kr dimers. Xe resonance emission (I'_{Xe}) and emission from Xe*Kr $1(^3P_1)$ molecules (I''_{Xe}) overlap and form a strong narrow band at 147 nm.

Where Kr* and Xe* represent the four lowest excited states of krypton and xenon; Kr_2^*—krypton molecules in the lowest 1_u state; Xe**—xenon in 5d, 6p or 7s states; Kr and Xe—ground state krypton and xenon atoms. It is also supposed that all energy acquired by Xe atoms is emitted only in the narrow band around 147 nm.

It has been shown [1] that taking the ratio of the integrated intensity I_{Xe} in the narrow band at 147 nm (which in that work was considered to be exclusively of atomic origin) to the integrated intensity I_{Kr_2} of the continuous emission of Kr_2^* allows one to cancel the unknown population of the Kr metastable state (common energy source) and to obtain the energy transfer rates (atomic and molecular channels) if the behaviour of the ratio as a function of Kr gas pressure is known for a constant Xe admixture:

$$\frac{I_{Xe}}{I_{Kr_2}} = k_M \tau P_{Xe} + \left[\frac{k_A P_{Xe}(k_M \tau P_{Xe} + 1)}{k}\right]\frac{1}{P_{Kr}^2}, \tag{1}$$

where P_{Kr} and P_{Xe} are pressures of Kr and Xe. The first term in the sum is independent of the Kr pressure. This allows one to calculate the molecular channel rate k_M and then to use this rate in the second term, which is linear with $(P_{Kr})^{-2}$, to calculate the atomic channel rate k_A.

Note that in our scheme (figure 3) Xe atoms in the $^3P_1$ state, apart from emitting the strongly reabsorbed resonance line with intensity I'_{Xe}, also form Xe*Kr molecules in the $1(^3P_1)$ state which emit radiation with intensity I''_{Xe} in the band at 147 nm. However, since all energy acquired by Xe $^3P_1$ state atoms is emitted in the narrow band near the Xe resonance line (see figure 2), equation (1) is still valid if I_{Xe} is the integrated intensity in this band (including the resonance line and the molecular emission). Note that this concentration of the emission close

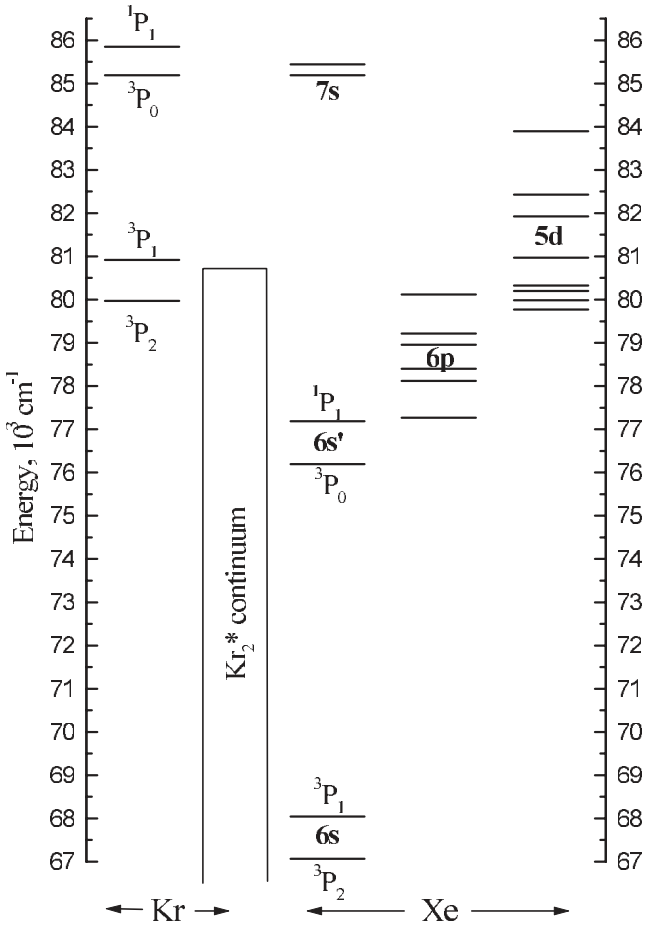

Figure 4. Energy-level diagram for the lowest excited states of atomic Kr and Xe. The photon energies from the Kr_2^* continuum is also indicated.

to the Xe resonance line is observed only for very low Xe concentrations and low Kr pressures such as those which were used in this work. At higher Xe concentrations the emission from Xe*Kr molecules in the lowest strongly bound states becomes noticeable in the range of 147–160 nm [5]. The other reason to use low Xe concentrations is to avoid conditions when direct electron excitation of Xe atoms plays a non-negligible role in comparison with Kr → Xe energy transfer (see section 6).

It is necessary to make the following remarks concerning the kinetic scheme:

(1) Frequent electron–atom collisions mix states $^3P_2$ with $^3P_1$ (lower pair) and $^3P_0$ with $^1P_1$ (upper pair), since the energy gaps between these states in both pairs are only about 1000 cm^{-1} (see figure 4). Despite the considerable gap of about 5000 cm^{-1} between the upper and lower pairs, electron–atom collisions also mix them at low pressures, mainly in favour of the lowest pair. This statement is based on the following estimations: the mixing rate between the upper and lower pairs was reported to be of the order of 10^{-6}–10^{-7} cm^{-3} s^{-1} by Lorents [9] and values of 3×10^{-7} cm^3 s^{-1} for mixing from the lower pair and 8×10^{-7} cm^3 s^{-1} for mixing to the lower pair were deduced by Eckstrom *et al* [10].

We believe the electron concentration to be of the order of 10^{12}–10^{13} cm^{-3}. This value was obtained by extrapolating the results of an experimental work of Schwabedissen *et al* [11], where a value of 3×10^{11} cm^{-3} was calculated based on Langmuir probe measurements in inductively coupled Kr plasmas with the same inserted power as in our experiments but at considerably lower pressures (about 3 Pa). Since the reported results show near linear growth of electron concentration with pressure in the range 0.6–2.66 Pa (from 8×10^{10} to 2.8×10^{11} cm^{-3}), we believe that at considerably higher pressures, as used in our work, the electron density at least reaches a value of 10^{12}–10^{13} cm^{-3}. Using these values we obtain exchange rates of the order of 10^6 s^{-1}, which is about one order of magnitude higher than the effective radiative decay rates of the resonant states and considerably higher than the expected energy transfer rates to Xe (see review in [5]). At low Kr pressures this rate is also considerably higher than the conversion rate to Kr_2 molecules, and only at pressures near 300 hPa and higher, the conversion rate, which is proportional to the square of the gas pressure, becomes comparable with the electron mixing rate.

(2) This method of determination of the energy transfer rate from Kr atoms to Xe does not allow one to distinguish the contributions from each of the four lowest excited Kr states. However, one should keep in mind that electron mixing favours the lower pair and the strong difference in population rates of these four states is also in favour of the lowest states. The latter point will be discussed in section 5.

4. Calculations

The spectral range from 122 to 185 nm was used for the calculations of the integrated continuum intensity (see figure 2). The following factors were taken into account in the analysis of the detection efficiency as a function of wavelength: the MgF_2 windows transmission, the grating efficiency and the detector sensitivity. The window transmission increases rapidly from 0 to about 60% in the range 110–130 nm [12] and then slowly to about 90% at 180 nm with ∼75% transmission at 147 nm (note that two MgF_2 windows should be taken into account—one on the discharge tube and one on the PM tube). The grating (Al covered with MgF_2) has about constant reflectance in the range 120–180 nm, but due to a blazing angle corresponding to a wavelength of 200 nm the efficiency of the grating increases nearly linearly with wavelength in the integration range. The PM tube with Cs–Te photocathode has about constant sensitivity in the range 120–150 nm and then it grows with wavelength, reaching double efficiency at about 160 nm and triple at 180 nm.

Our calculations show that the total efficiency of the system gives practically negligible corrections for the band-to-continuum ratio. A simple explanation of this could be given. The central part of the Kr_2 continuum (135–160 nm) which gives the major contribution to the integrated continuum intensity, is practically symmetric around the resonance line (figure 2) for all gas pressures that were used. The consequence is that in this range the reduction of intensity of the short wavelengths due to reduced sensitivity with respect to the band intensity is compensated by the corresponding intensity increase of the long wavelengths. The reduced integrated intensity of the short-wavelength part of the Kr_2 continuum (122–135 nm) is again partially compensated by the high efficiency for the long-wavelength part of the continuum at 160–185 nm and besides, the intensity contribution from these parts is relatively minor.

In figure 5 the band-to-continuum ratio is shown for Kr–Xe mixtures in the Kr pressure range from 100 to 400 hPa for five different Xe admixtures with partial pressures of 0.005, 0.01, 0.015, 0.025 and 0.05 hPa. Linear least square fits $\boldsymbol{I}_{\mathrm{Xe}}/\boldsymbol{I}_{\mathrm{Kr}_2} = \boldsymbol{A} + \boldsymbol{B} \times (\boldsymbol{P}_{\mathrm{Kr}})^{-2}$ for these series give the $\boldsymbol{A}$ and $\boldsymbol{B}$ values presented in figure 6. The $\boldsymbol{B}$ value for the highest Xe partial pressure of 0.05 hPa does not fit into the pattern of the other series (it was disregarded

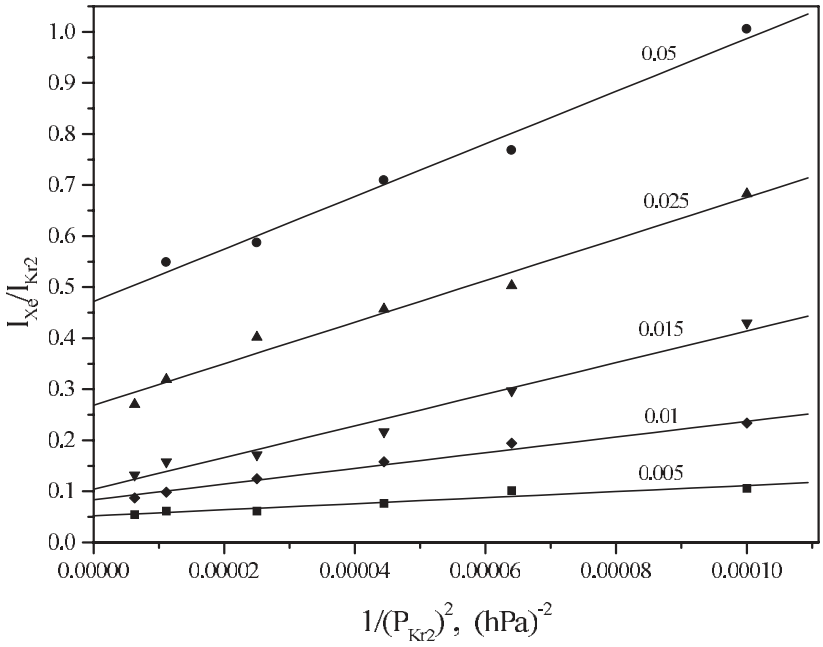

Figure 5. The ratio of integrated intensity in the narrow band around the Xe resonant line at 146.97 nm to the integrated intensity of the Kr_2^* continuum is shown for Kr–Xe mixtures in the Kr pressure range from 100 to 400 hPa for five different Xe admixtures with partial pressures from 0.005 to 0.05 hPa.

from the fitting) since for high Xe concentrations of approximately 0.1% and higher, direct electron excitation of Xe starts to play a non-negligible role. This question will be discussed later in section 5 concerning the IR studies. From the fit we obtain $\boldsymbol{A}/\boldsymbol{P}_{\mathrm{Xe}} = 9.7 \pm 0.6\ \mathrm{hPa}^{-1}$ and $\boldsymbol{B}/\boldsymbol{P}_{\mathrm{Xe}} = (1.7 \pm 0.2) \times 10^5$ hPa.

From the dependence of $\boldsymbol{A}$ on Xe pressure, one can find the molecular energy transfer rate if the Kr_2^* lifetime is known (equation (1)). The situation is complicated by the fact that the resonant 0_u^+ and metastable 1_u Kr_2 states have distinctly different lifetimes: a few nanoseconds for the first state and approximately 250 ns for the second state (a comparison of lifetime values obtained with different experimental techniques can be found in [13]). However, if one compares conversion rates from Kr atoms in the lowest excited states to Kr_2 molecules, obtained in [14], it seems that nearly 90% of the energy accumulated in the Kr^* states should be transferred to the 1_u state of Kr_2. One should also take into account that the vibrational relaxation of the 0_u^+ state can hardly compete with the very fast radiative decay (see discussion in [5]), so the contribution to the second continuum, which is observed to be the main spectral structure, should be mostly from the 1_u state. Consequently, the lifetime value of 250 ns can be used in our calculations as the effective lifetime of Kr_2 molecules. Substituting it in the first term of equation (1) we obtain $\boldsymbol{k}_M = 3.9 \times 10^7 \times \boldsymbol{P}_{\mathrm{Xe}}\ \mathrm{hPa}^{-1}\ \mathrm{s}^{-1}$. For gas temperatures of the order of 1000 K, this rate corresponds to a cross section of $3 \times 10^{-14}\ \mathrm{cm}^2$.

Nevertheless, the 0_u^+ Kr_2 state might obtain energy through collisions of Kr_2 molecules in the 1_u state with Kr atoms and electrons, thus reducing the effective lifetime of the 1_u state. According to [15], the molecular–atom collision contribution is negligible. However the molecular–electron collision rates, given in literature, vary from $1.8 \times 10^{-8}\ \mathrm{cm}^3\ \mathrm{s}^{-1}$ [10] to $1.9 \times 10^{-6}\ \mathrm{cm}^3\ \mathrm{s}^{-1}$ [15]. Using again an electron concentration of the order of 10^{12}–$10^{13}\ \mathrm{cm}^{-3}$,

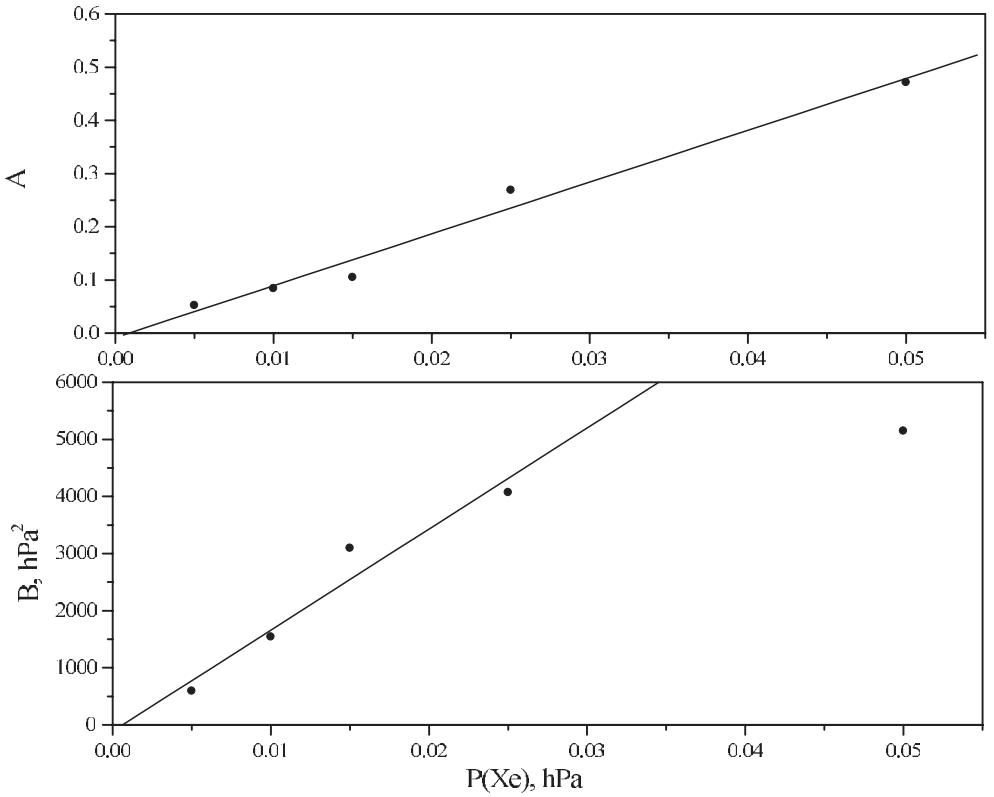

Figure 6. The values of A and B as a function of the Xe admixture pressure are shown, obtained by the linear least square fits $I_{Xe}/I_{Kr_2} = A + B \times (P_{Kr})^{-2}$ for the series, presented in figure 5. The values of A and B show linear dependence on Xe pressure for small admixture concentrations (see text).

the first rate does not change the effective lifetime of the 1_u state, while the second one could shorten it by a factor of 2–3. Besides, experimental results [13] show that high vibrational levels of the 1_u state could have lifetimes several times shorter. Therefore the value of 250 ns can be considered as an upper limit of the Kr_2^* lifetime and, consequently, the value of $3.9 \times 10^7 \times P_{Xe}$ hPa^{-1} s^{-1} as a lower limit of the molecular channel energy transfer rate.

Despite the fact that a lifetime four times shorter than in [1] has been used, we obtain approximately the same value for the molecular channel energy transfer cross section as was presented in that work. This is most probably a consequence of the decreased self-absorption in our experiments compared to previous studies, contributing to considerably higher band-to-continuum ratios.

From equation (1), using the linear part of the dependence of B on Xe pressure (since $k_M \tau P_{Xe} < 0.25$) and taking $k = 11 \times P_{Kr}^2$ hPa^{-2} s^{-1} [14], we find the atomic energy transfer rate k_A to be $1.7 \times 10^6 \times P_{Xe}$ hPa^{-1} s^{-1} which corresponds ($T_{gas} = 1000$ K) to a cross section of 1.4×10^{-15} cm^2. This value is two orders of magnitude smaller than the value calculated by a similar method and presented by Gedanken *et al* [1]. The atomic energy transfer rate measured here is quite close to the value of $4.7 \times 10^6 \times P_{Xe}$ hPa^{-1} s^{-1}, which was obtained by Velazco *et al* [6] for transfer from the $^3P_2$ state of Kr. In comparison with known transfer rates from the Kr $^3P_1$ state, our rate is larger than the value of $7.1 \times 10^5 \times P_{Xe}$ hPa^{-1} s^{-1} obtained

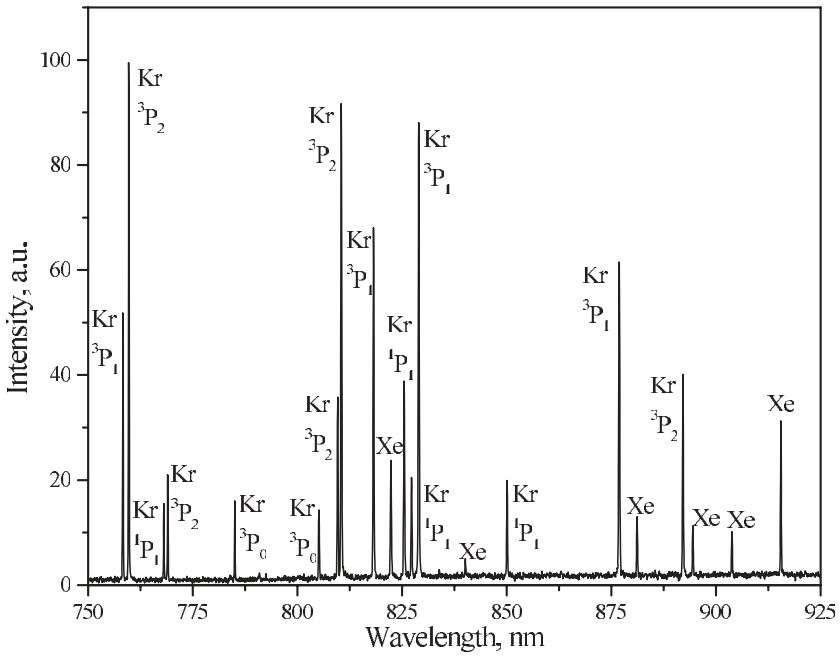

Figure 7. IR emission spectrum from a RF gas discharge in 160 hPa Kr with 0.1% Xe. Krypton and xenon lines are marked with Kr and Xe. For all Kr lines the lower transition state, which belongs to the 5s or 5s′ electron configuration, is indicated.

by Cook and Leichner [7] and three times smaller than the value of $5.3 \times 10^6 \times P_{\mathrm{Xe}}$ hPa^{-1} s^{-1} reported by Salomero *et al* [3]. For more details on these rates see the review in [5]. Note that our transfer rate is the total transfer rate from the entire system comprising the four lowest excited Kr states.

5. IR results

In this work, as stated earlier, we also made observations of the visible and near-IR emission from Kr–Xe mixtures (see an example of spectra in figure 7). This allowed us to check the maximum concentration of the Xe admixture, which could be used in order for direct Xe excitation to be negligible by comparison with energy transfer from the Kr system. Our observations of Kr I radiative cascades in pure Kr and in mixtures with Xe have shown that direct Xe excitation starts to play a noticeable role (i.e. the difference in Kr radiative cascade intensities in pure Kr and in the Kr–Xe mixture are greater than a few per cent) only at Xe concentrations of about 0.1% at Kr pressures of 80–400 hPa.

It was also established that, at low admixture concentrations and for both RF and DC discharges, the visible and near-IR spectra in the range 400–1000 nm show no other spectral features besides Kr and Xe radiative cascades. The latter, together with the fact that at low Xe concentrations the lines of Kr radiative cascades have the same intensities as in pure Kr, suggests that there are no other strong energy transfer mechanisms which pump energy to Xe from ionic Kr or from excited Kr states other than from four lowest excited states.

The dependence of the Xe 6p–6s transition line intensities on Xe concentrations at constant Kr pressure allowed us to make an independent estimate of the atomic energy transfer rate.

Using the same kinetic scheme as described above (figure 2), one can estimate the fraction of the excitation energy that is transferred to the excited Xe states and afterwards emitted as Xe 6p–6s transitions (I_X) from the ratio:

$$I_X \propto \frac{k_A P_{\mathrm{Xe}}}{k_A P_{\mathrm{Xe}} + k P_{\mathrm{Kr}}^2 + \chi}, \tag{2}$$

where P_{Xe} and P_{Kr} are the Xe and Kr pressures and χ is the radiative decay rate for the system of the four lowest Kr states. This ratio is based on the fact that the intensity of the Xe 6p–6s transitions is proportional to the energy transferred to Xe per second in the Kr*–Xe collisions, and this energy is a fraction of the total Kr* energy loss, which is the sum of the energy transfer, conversion and radiative decay.

Taking into account that at a constant Kr pressure the energy that is acquired by these Kr states per second does not change with Xe concentration if it stays lower than a critical value (approximately 0.05%), from equation (2) one can calculate how the Xe 6p–6s transition intensities change if the Xe pressure is halved:

$$\frac{I_X}{I_{X/2}} = \frac{k_A P_{\mathrm{Xe}} + 2(k P_{\mathrm{Kr}}^2 + \chi)}{k_A P_{\mathrm{Xe}} + (k P_{\mathrm{Kr}}^2 + \chi)}, \tag{3}$$

where $I_{X/2}$ is the emission form the mixture with two times smaller Xe concentration ($\frac{1}{2}P_{\mathrm{Xe}}$). From equation (3) one can see that if the energy transfer to Xe is much stronger than the sum of the conversion rate and radiative decay, then the ratio is unity and the Xe transition intensities do not change at all. In the opposite case the ratio is 2 and for equality one obtains a ratio of 1.5.

In our experiments all Xe 6p–6s lines showed a similar dependence on Xe pressure. The line at 823.16 nm, which was the most convenient for measurements, gave the following results for Kr pressure of 80 hPa and Xe admixtures of 0.025, 0.0125 and 0.006 25%: the ratios between the intensities of the line (averaged over five experimental points) for the adjacent pairs of admixtures are 1.81, 1.86 and approximately 2. For the latter, at low Xe concentrations, the experimental uncertainty becomes too large because of the low intensity of the Xe lines. Unfortunately, the conditions when the method has the maximum precision (ratios close to 1.5) are not accessible: the concentration of Xe would be too high and then the direct Xe excitation becomes considerable.

A similar series of experiments at 160 hPa of Kr and 0.025, 0.0125 and 0.006 25% Xe gave for the first pair the ratio of 1.95 and a tentative value close to 2 for the second pair. All spectra were recorded with some fluctuations of the total light intensity. To take this into account, the spectra were rescaled in order to have the same Kr radiative cascade line intensities. Thus the following estimates should be taken only as approximate.

From equation (3) and the intensity ratios we can estimate the atomic energy transfer rate. Taking the total conversion rate $k = 11 \times P_{\mathrm{Kr}}^2$ hPa^{-2}s^{-1} [14] and $\chi = 1.7 \times 10^5$ s^{-1} (the decay constant for the Kr ^{3}P$_1$ state [7]) we find that all listed ratios above are in a fairly good agreement and give an atomic channel energy transfer rate of $1.6 \times 10^6 \times P_{\mathrm{Xe}}$ hPa^{-1}s^{-1} (cross section of 1.3×10^{-15} cm^2 for 1000 K). This value is practically the same as was obtained in our VUV studies.

Finally, the IR observation of radiative cascades in Kr showed that the integrated intensity of the lines having the states ^{3}P$_2$ and ^{3}P$_1$ as the lower state is about four times higher than the integrated intensity of the transitions to the ^{3}P$_0$ and ^{1}P$_1$ states (see figure 7). This suggests that the main part of the electron excitation energy, originating from the krypton ionic states and transferring to the lowest excited states of Kr in radiative cascades is directed towards the lower pair of the Kr states. Direct electron excitation should also be stronger for the lower pair, since

they are situated approximately 0.6 eV lower in the energy scale and have greater statistical weight. Taking into account the electron mixing of the states in favour of the lowest pair as was discussed before, one can conclude that the Kr to Xe atomic channel energy transfer rate, which was found in this work, most probably refers to the transfer rate from the $^3P_2$ and $^3P_1$ pair of states.

6. Conclusion

Our simultaneous observations of the VUV and visible–IR emission from RF discharges in gaseous Kr with small (<0.1%) Xe admixture concentrations support the energy transfer scheme described in our previous work [5]. In this scheme it is assumed that energy accumulated by the Kr system is transferred to the Xe system only by atom to atom (Kr ($^3P_0$, $^3P_1$, $^3P_2$, $^1P_1$) $\rightarrow$ Xe) and molecule to atom (Kr_2^* (1_u) $\rightarrow$ Xe) energy transfer channels.

The VUV spectra allowed us to obtain a value of $3.9 \times 10^7 \times P_{Xe}$ hPa^{-1} s^{-1} for the energy transfer rate from the 1_u state of Kr_2^* molecules to ground state Xe atoms. This value is the lower limit of the molecular channel energy transfer rate, and the actual value could be 2–3 times higher because of the possible shortening of the effective lifetime of the 1_u state (250 ns was used) by the collisions with electrons.

A value of $1.7 \times 10^6 \times P_{Xe}$ hPa^{-1} s^{-1} was obtained for the energy transfer rate from the four lowest Kr excited states to the Xe ground state atoms (atomic channel). Most probably this rate refers to the transfer rate from the $^3P_2$ and $^3P_1$ pair of states, which are mixed by collisions with electrons.

An atomic channel energy transfer rate of $1.6 \times 10^6 \times P_{Xe}$ hPa^{-1} s^{-1} was obtained independently on the basis of our observations of IR emission.

Acknowledgments

We gratefully acknowledge the support of this work received from the Göran Gustafsson Foundation, The Carl Trygger Foundation for Scientific Research and the Royal Swedish Academy of Sciences. The Swedish Institute, through the Visby Programme, is acknowledged for two scolarships (G Gerasimov and B Krylov). We thank Professor G O'Sullivan and Dr P Dunne from University College Dublin for very useful advice and discussions.

References

[1] Gedanken A, Jortner J, Raz B and Szoke A 1972 *J. Chem. Phys.* **57** 3456
[2] Cheshnovsky O, Raz B and Jortner J 1973 *J. Chem. Phys.* **59** 3301
[3] Salomero Y, Briot A, Brunet H, Dijols H, Galy J, Millet P and Montagne J P 1981 *J. Chem. Phys.* **74** 288
[4] Cook J D and Leichner P K 1991 *Phys. Rev.* A **43** 1614
[5] Krylov B, Gerasimov G, Morozov A, Arnesen A, Hallin R and Heijkenskjold F 2000 *Eur. Phys. J.* D **8** 227
[6] Velazco J E, Kolts J H and Setser D W 1978 *J. Chem. Phys.* **69** 4357
[7] Cook J D and Leichner P K 1985 *Phys. Rev.* A **31** 90
[8] Morozov A, Krylov B, Gerasimov G, Hallin R and Arnesen A 2000 *Eur. Phys. J.* D **11** 379
[9] Lorents D C 1976 *Physica* C **82** 19
[10] Eckstrom D J, Nakano H H, Lorents D C, Rothem T, Betts J A, Lainhart M E, Dakin D A and Maenchen J E 1988 *J. Appl. Phys.* **64** 1679
[11] Schwabedissen A, Benck E C and Roberts J R 1997 *Phys. Rev.* E **55** 3450
[12] Elliott D J 1995 *Ultraviolet Laser Technology and Applications* (San Diego, CA: Academic)
[13] Madej A A and Stoicheff B P 1988 *Phys. Rev.* A **38** 3456
[14] Salomero Y, Briot A, Brunet H, Galy J, Millet P and Montagne J P 1979 *J. Phys. B: At. Mol. Phys.* **12** 419
[15] Keto J W, Gleason R E Jr, Bonifield T D, Walters G K and Soley F K 1976 *Chem. Phys. Lett.* **42** 125

Paper V

INSTITUTE OF PHYSICS PUBLISHING JOURNAL OF PHYSICS B: ATOMIC, MOLECULAR AND OPTICAL PHYSICS

J. Phys. B: At. Mol. Opt. Phys. **35** (2002) 4257–4270 PII: S0953-4075(02)37520-5

Channels of energy transfer to atomic nitrogen in excited argon–nitrogen mixtures

B Krylov[1], A Morozov[2], G Gerasimov[1], A Arnesen[2], R Hallin[2] and F Heijkenskjöld[2]

[1] Vavilov State Optical Institute, Birzhevaja Line 12, St Petersburg, 199034, Russia
[2] Department of Physics, Uppsala University, Box 530, SE-751 21 Uppsala, Sweden

E-mail: reinhold.hallin@fysik.uu.se

Received 28 May 2002, in final form 21 August 2002
Published 8 October 2002
Online at stacks.iop.org/JPhysB/35/4257

Abstract

The vacuum ultraviolet (VUV) and ultraviolet (UV) emissions of gaseous mixtures of argon with a small amount of nitrogen were investigated in the afterglow of a pulsed transverse discharge. The time dependences of the intensity of the VUV argon continuum at 126.0 nm, the UV nitrogen molecular band at 337.0 nm, and the VUV nitrogen atomic lines at 149.47 and 174.52 nm were analysed in the total pressure range 150–600 hPa and the range 0.125–1.5 hPa of the admixture concentrations. The results show that all these emissions have a common source of excitation energy, namely the atomic metastable $^3P_2$ state of argon. However, atomic nitrogen also receives energy from the atomic $^3P_1$ state of argon and from the excited Ar_2^* (1_u) molecules.

1. Introduction

If a gaseous mixture of argon and a small amount of nitrogen ($\leqslant 1\%$) is excited in a discharge, the excitation occurs mainly in argon, but nitrogen emissions also appear in the spectrum as a result of energy transfer from excited argon species to nitrogen molecules and atoms, and under suitable pressure conditions the nitrogen emissions are remarkably intense. Strong nitrogen atomic lines in the VUV (vacuum ultraviolet) region have previously been observed in mixtures of argon with a small amount of nitrogen [1].

The excitation of the molecular nitrogen UV bands and VUV atomic lines is associated in the literature with energy transfer from metastable argon atoms in the $^3P_2$ state to ground-state nitrogen molecules [2–8] and atoms [1, 9]. Note that argon molecules, emitting the well known argon VUV continuum [10], also get their energy from the $^3P_2$ argon atoms (which are converted into Ar_2^* molecules in three-body collisions). Hence, there are reasons to suppose that the $^3P_2$ metastables provide the 'common' source of energy for all these species emitting in the UV and VUV.

The role of the resonance $^3P_1$ argon state (the apparent lifetime of which is lengthened in real sources by radiation trapping) in the energy transfer processes and excitation of the nitrogen species has not been investigated before to our knowledge. However, an analysis of the energy level diagrams points out that energy transfer from the $^3P_1$ state could be effective, especially to nitrogen atoms.

In this study we try to clarify the participation of the $^3P_1$ state in the energy transfer processes in the VUV line sources. For that reason we have investigated the afterglow of a pulsed discharge in Ar–N_2 mixtures. If all the listed emitting species acquire energy from the $^3P_2$ metastable state, the emissions should show similarities in the afterglow, and a subsequent analysis of the similarities and distinctions would therefore be fruitful for finding out the role of the $^3P_1$ state in the energy transfer to the nitrogen atoms.

The time dependences of the Ar_2 continuum, N I lines and N_2 band intensities have been recorded in the VUV and UV region, respectively, for different argon pressures and nitrogen concentrations. The results of the analysis of these data are presented below.

2. Experiment

Ar–N_2 mixtures were excited in a pulsed transverse discharge with spark pre-ionization in a commercial excimer UV laser, model MSX-250 of MPB Technologies Inc. However, necessary modifications were made and equipment added to adjust the instrument for investigations in the VUV region. In particular, the pumping efficiency was significantly improved to reduce the impurity level. The volume of the discharge chamber was pumped out by a turbomolecular pump to a pressure of 10^{-6} hPa and then filled with an Ar–N_2 mixture prepared in a special outer volume.

The distance between the electrodes was 15 mm and their length 250 mm. A discharge capacitor of 16.2 nF was charged up to 12 kV with a repetition rate of 5 Hz. The length of the current pulse was not more than 100 ns. The discharge appeared visually as uniform. We estimate that the electron concentration just after the current pulse was about 10^{14} cm^{-3}. The gas temperature in the discharge volume should not differ significantly from the room temperature because a gas flow was maintained between the electrodes.

The discharge and afterglow emission were observed on both sides of the discharge chamber along the optical axis of the discharge volume. Two spectral instruments were used. The VUV spectrum was recorded through a magnesium fluoride window with a 1 m normal-incidence vacuum monochromator with 0.83 nm mm^{-1} dispersion. The spectral resolution was better than 0.02 nm. A pm-tube with a magnesium fluoride window and a caesium–tellurium photocathode (Hamamatsu R1220) was used as detector. A Jarrell–Ash monochromator and a pm-tube with a GaAs photocathode (Hamamatsu R943-02) recorded the UV spectrum through a sapphire window. The spectral resolution was better than 0.3 nm. Both detectors worked in the photon counting mode and a single photon counter (7882 FAST ComTec Gmbh) was used with both spectrometers. This counter has a dwell time of 125 ns and a maximum count rate of 150 MHz.

In order to fulfil the analysis of the excitation transfer from argon metastables, it was important to work with a slow depopulation of the metastables in order to prevent masking of the excitation transfer by other processes. This was ensured by choosing a total pressure range of 150–600 hPa and a N_2 partial pressure range of 0.05–1.50 hPa. Under these conditions, a microsecond rate of the depopulation was estimated. The time resolution, 125 ns, corresponded to this rate.

The following emissions were recorded in the discharge afterglow: the VUV argon continuum at 126.0 nm, the UV nitrogen molecular band at 337.0 nm, and the VUV nitrogen

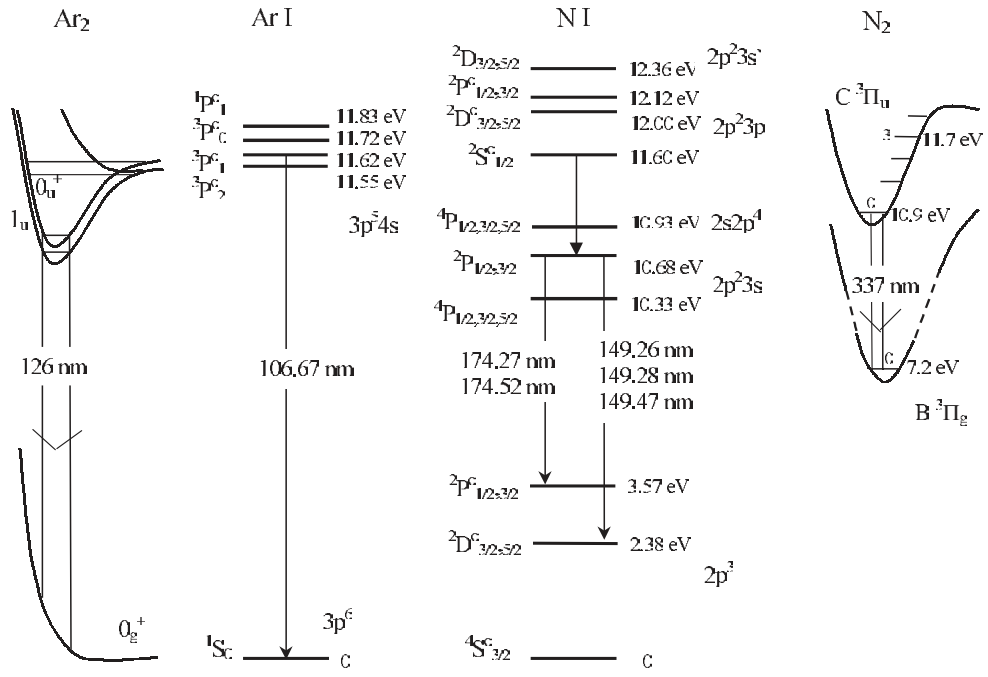

Figure 1. A simplified diagram of atomic and molecular levels for Ar_2, Ar I, N I and N_2. The arrows show transitions investigated or discussed in the work.

atomic lines at 149.47 and 174.52 nm (figure 1). The measurements were aimed at recording only the time dependences so we did not measure the relative intensities of the different emissions. The voltage across the pm-tubes and the width of the exit slit of each monochromator were kept constant, while the width of the entrance slit was changed in order to prevent overloading of the recording system. To get smooth time dependence curves, measurements of 9000 successive pulses were added for each wavelength setting. If the light flow was shut off in any part of the spectrometer, the result of the acquisition was equal to zero in all 125 ns channels.

Figure 2 shows an example of experimental curves in linear and natural logarithmic scales of the intensity for a total pressure of 150 hPa and a nitrogen partial pressure of 0.125 hPa. In the following, the logarithmic scale is used as more convenient for decay presentation. The discharge took place at approximately 150 ns after the beginning of the acquisition. The point at 250 ns is therefore the first acquisition value. Figure 2 gives also an example of the reproducibility of the results: the two curves shown in figure 2 were recorded with gas mixtures prepared on different days.

3. Results and discussion

When a pulsed discharge of a short duration excites argon containing a small quantity of nitrogen, the excited species present immediately after the pulse are mainly atomic argon ions (Ar^+), electrons (e^-) and excited argon atoms in radiative (highly excited Ar** and low excited Ar*) or metastable (Ar^m) states. The later evolution of the system is not simple (as has been shown by post-excitation studies of argon (e.g [11, 12]) and depends on specific

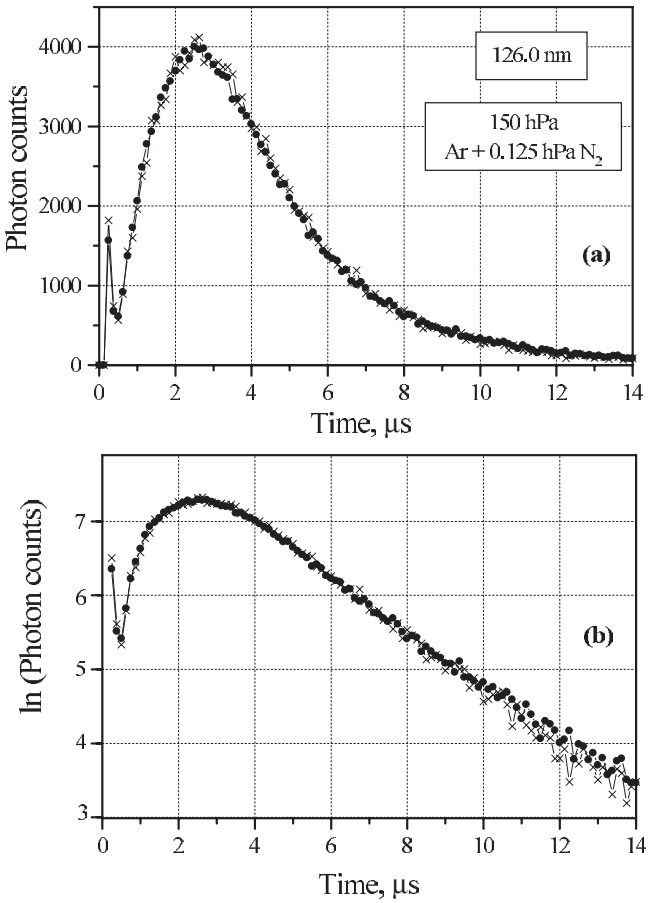

Figure 2. An example of experimental curves and reproducibility of the results in (a) linear and (b) logarithmic intensity scales. The total pressure is 150 hPa and the nitrogen partial pressure is 0.125 hPa.

experimental conditions. It is reasonable, therefore, to begin the analysis of our results with the time dependences for pure argon (without an admixture of N_2).

3.1. Pure argon

Figure 3 shows the time dependences of the Ar_2^* emission at 126.0 nm, which is approximately at the maximum of the argon continuum intensity, for the pressures of 150, 300 and 600 hPa. It is beyond question that the curve for 150 hPa includes an intensity peak at short times. Then the curve reveals a relatively rapid growth and, after the maximum intensity, a relatively slow decay with a decay rate decreasing slowly in time. The curves for 300 and 600 hPa resemble the curve for 150 hPa contracted in time with the only difference that the peak at short time is not seen, most probably because of our limited time resolution.

The interpretation of the curves in figure 3 is the following. The peak of the beginning of the curve for 150 hPa corresponds to the appearance of argon molecules Ar_2^* during and just after the current pulse. They can be produced by direct electron excitation from the weakly bound ground state [12] or in the reactions of conversion of metastable atoms Ar^m that appear

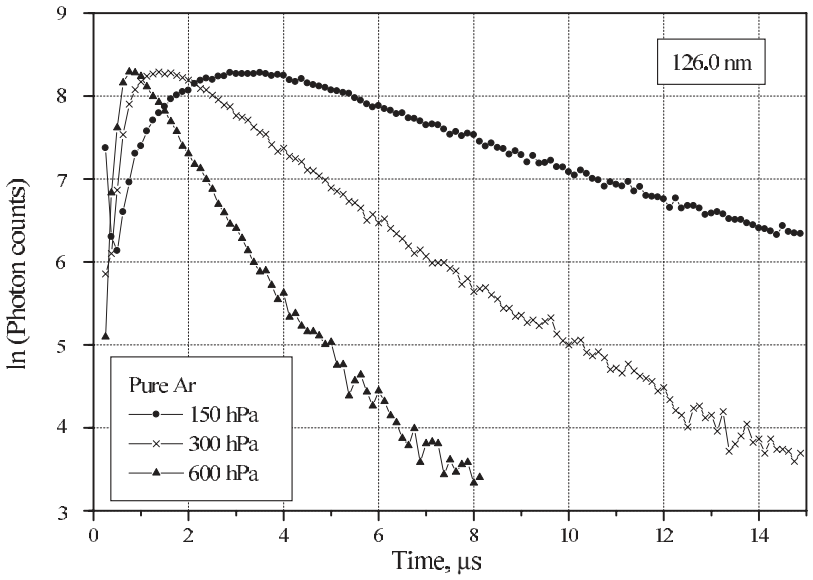

Figure 3. Time dependences of the Ar_2^* continuum emission (at 126.0 nm) in pure argon. The pressure is 150, 300 and 600 hPa. The curves were normalized to have the same peak intensity.

as a result of direct excitation. However, most of the Ar_2^* molecules appear, as the curve for 150 hPa demonstrates, in the afterglow. There is no other way to produce Ar_2^* molecules in the afterglow after electron thermalization except through conversion of metastable argon atoms:

$$Ar^m + 2Ar \rightarrow Ar_2^* + Ar. \tag{1}$$

A model of the production of metastable argon atoms in the afterglow is given by the following set of processes:

$$Ar^+ + 2Ar \rightarrow Ar_2^+ + Ar, \tag{2}$$

$$Ar_2^+ + e^- \rightarrow Ar^{**} + Ar, \tag{3}$$

$$Ar^{**} \xrightarrow{h\nu} \cdots \xrightarrow{h\nu} Ar^m, \tag{4}$$

where Ar^+ and Ar_2^+ are atomic and molecular ions, e^-—electrons, Ar—atoms in the ground state, Ar**—all highly excited atoms produced in the dissociative recombination (3), and Ar^m—metastable atoms, which are a result of cascades (4). Reactions (2)–(4) represent, of course, a simplified model which does not take into account certain processes that could influence the temporal behaviour of the concentration of the metastables. However, in any case, the listed set of processes is the basis for any refined model. The rate coefficients of reactions (1)–(3) were given in [5, 12], [12, 15] and [16, 17], respectively. The values differ significantly. We consider the values of 10^{-32}, 2×10^{-31} cm^6 s^{-1} and 7×10^{-7} cm^3 s^{-1} for reactions (1)–(3) respectively to be the most realistic at room temperature. Note that the rate coefficient of reaction (2) is $\geqslant$10 times higher than that of reaction (1). Note also that the rate of reaction (3) is very high at high electron densities (10^{13}–10^{14} cm^{-3}) but that the reaction contributes with a very slowly decaying component at low electron densities (10^{12} cm^{-3}).

The curves in figure 3 show the change of the concentration of the Ar_2^* molecules produced from the metastables A^m in reaction (1). As will be shown below, the lifetime of the Ar_2^* molecules is shorter than the time constant of reaction (1), hence we can say that the curves in figure 3 also reflect the concentration of the metastables A^m. Consequently, they reflect

the competition between the processes populating and depopulating the metastable states; that is, in our simplified description, the competition between reactions (2)–(4) and (1). The ion and electron concentrations and, therefore, the populating flow of the reactions (2)–(4) fall in time, whereas the depopulating flow of the reaction (1) grows with increasing metastable atom concentration. The maximum of the curve corresponds to the equilibrium of the flows populating and depopulating the metastables. When the argon pressure increases, the rates of the reactions (2) and (1) become higher, and as a result we observe the contraction of the afterglow in time (figure 3).

Two remarks should be made. Firstly, at our pressures the four lowest excited atomic states have long radiative lifetimes and should be considered as metastables, namely the $^3P_2$ (11.55 eV) and $^3P_0$ (11.72 eV) metastable states but also the $^3P_1$ (11.62 eV) and $^1P_1$ (11.83 eV) resonant states (figure 1) because their effective lifetime, lengthened by radiation trapping, is of the order of 10^{-5} s [18, 19]. Not all the metastables, only $^3P_1$ and $^3P_2$, are converted in reaction (1) into molecules emitting the continuum at 126.0 nm (the corresponding molecular states are 0_u^+ ($^3P_1$) and 1_u ($^3P_2$)). However, it is precisely the two lower levels $^3P_1$ and $^3P_2$ that are mainly populated through the cascades (4) [20–23]. Collisions with electrons tend to mix the metastables toward an equilibrium determined by the electron temperature and the statistical weights (the rate constant of the mixing processes is of the order of 10^{-6}–10^{-7} cm^3 s^{-1} [12]). The mixing is also in favour of the lower $^3P_1$ and $^3P_2$ states with the ratio of the $^3P_1$ to $^3P_2$ state populations of about 1:2. The mixing efficiency depends on the electron concentration; therefore the mixing is more effective at short times. On the other hand, the $^1P_1$,$^3P_0$, and $^3P_1$ metastable states relax to the lowest $^3P_2$ level through reaction (1) followed by predissociation due to molecular curve crossing [12, 24]. In summary, the lower $^3P_1$ and $^3P_2$ states, and especially the $^3P_2$ state, can be considered as the most populated with our experimental conditions.

Secondly, the emission around 126.0 nm is largely caused by transitions from the lowest vibrational levels of the $Ar_2^*(0_u^+)$ and/or $Ar_2^*(1_u)$ states. These levels are populated through vibrational relaxation from the higher levels populated in reaction (1). The radiative lifetimes of the 0_u^+ vibrational levels are very short, 4.2 ns [25], and at our pressures the frequency of atomic collisions is not high enough for vibrational relaxation to the lowest 0_u^+ levels [24]. Hence only the lowest 1_u levels are populated through vibrational relaxation. The radiative lifetime of the lowest vibrational level of the 1_u state is $\sim$3 μs [12, 26]. Then, the question of how the curves for 300 and 600 hPa (figure 3) can show a decay with a time constant shorter than 3 μs, namely about 1 μs for 600 hPa, arises. The answer is that the electron concentration in the afterglow is high enough to induce effective excitation transfer from the 1_u levels to the short-lived levels of the 0_u^+ state. The rate coefficient for this process, 10^{-6}–10^{-7} cm^3 s^{-1}, was estimated in [12] and measured for xenon, 1.9×10^{-6} cm^3 s^{-1}, in [27]. This process should be even more effective at times preceding the decay part of the curves because of the higher electron concentration.

3.2. Ar–N_2 mixtures

When nitrogen is added to argon, the time dependence of the argon continuum at 126.0 nm changes as shown in figure 4. The decay rate increases with increasing nitrogen partial pressure and, as a result, the peak intensity is shifted toward shorter times.

In our mixtures, nitrogen cannot have an appreciable influence on the processes populating the metastable states of argon (the precursors of the $Ar_2^*(1_u)$ state), but it can efficiently depopulate these states in the reaction

$$Ar^m + N_2 \rightarrow N_2^* + Ar, \tag{5}$$

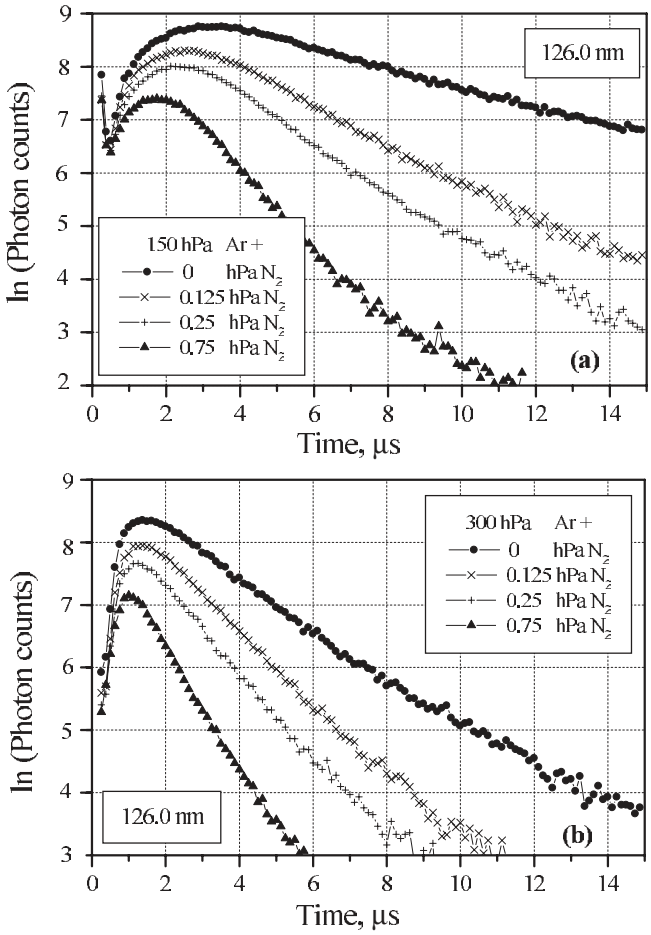

Figure 4. Time dependences of the Ar_2^* emission (at 126.0 nm) in Ar–N_2 mixtures. The total pressure is (a) 150 hPa and (b) 300 hPa. The nitrogen partial pressure is 0.125, 0.25 and 0.75 hPa. The experimental curves were scaled in intensity to show the peak of the emission in the best way.

where N_2^* represents all possible molecular excited states, in particular the $N_2^*(C\,^3\Pi_u)$ state (figure 1) emitting the band at 337 nm. The total rate coefficient of reaction (5) is $\sim 3 \times 10^{-11}$ cm^3 s^{-1} [4–6] and about one-half of this value corresponds to excitation of the $N_2^*(C\,^3\Pi_u)$ state [28].

The changes of the Ar_2^* time dependence in figure 4 may also suggest a growth of depopulation of the $Ar_2^*(1_u)$ state itself with increasing N_2 pressure. However, it seems unlikely that energy could be transferred from the lowest $Ar_2^*(1_u)$ levels to the $N_2^*(C\,^3\Pi_u)$ state, owing to energetic considerations. Namely, the 1_u state can transfer energy corresponding to the energy of radiative transitions and for the lowest $Ar_2^*(1_u)$ levels this energy is approximately 10 eV whereas the energy of the lowest vibrational level of the $C\,^3\Pi_u$ state is 11 eV (figure 1). It also seems unlikely that energy is effectively transferred from the upper 1_u levels because the radiative lifetime shortens as the vibrational quantum number of the level increases (about 20 times for higher levels which could transfer energy to the $C\,^3\Pi_u$ state, owing to energetic considerations [26]). At the highest N_2 concentration, 1.5 hPa, the time constant of reaction (5) is about 1.5 μs, which is significantly longer than the radiative lifetimes of the upper vibrational

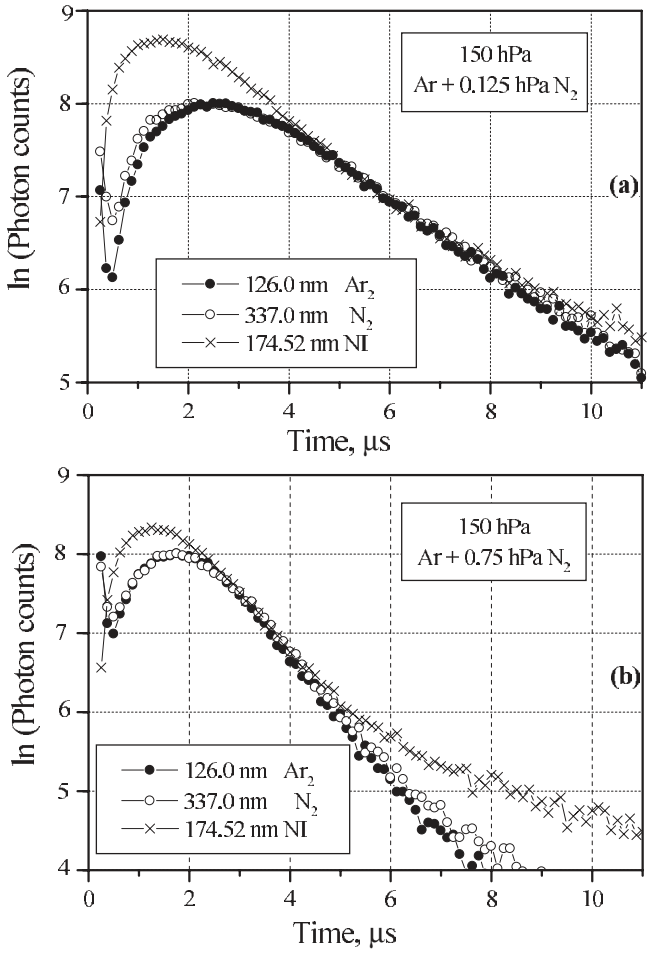

Figure 5. Time dependences of the Ar_2^* (126.0 nm), N_2^* (337.0 nm) and N* (174.52 nm) emissions in Ar–N_2 mixtures. The total pressure is 150 hPa. The nitrogen partial pressure is (a) 0.125 hPa and (b) 0.75 hPa. The experimental curves were scaled in intensity to show the similarity of the curves for the Ar_2^* and N_2^* emissions and to show the coincidence of the decay rates of all the emissions in a certain time range.

levels of the $Ar_2^*(1_u)$ state. Therefore, we believe that the C $^3\Pi_u$ state emission is a result of energy transfer only from the metastable states and that this emission should be a good indicator of the population of the Ar^m states, since the C $^3\Pi_u$ state has a short radiative lifetime of 30–40 ns [29–31]. On the other hand, the $Ar_2^*(1_u)$ state emission would be a good indicator of the Ar^m ($^3P_2$) state population if the effective lifetime of the lowest $Ar_2^*(1_u)$ levels was short enough.

Figures 5 and 6 show time dependences for the Ar_2^* (126.0 nm), N_2^* (337.0 nm) and N* (174.52 nm) emissions, recorded at the total pressures 150 and 300 hPa with the admixture pressures 0.125 and 0.75 hPa. The experimental curves were shifted along the intensity scale to show the coincidence of the decay rates of the listed emissions in a significant time range. The common decay rate can be interpreted as evidence of the energy acquisition from a common source. This means that at a definite time in the afterglow, when both the flow populating the A^m states and the mixing of the A^m states by electrons become weak, the population of the

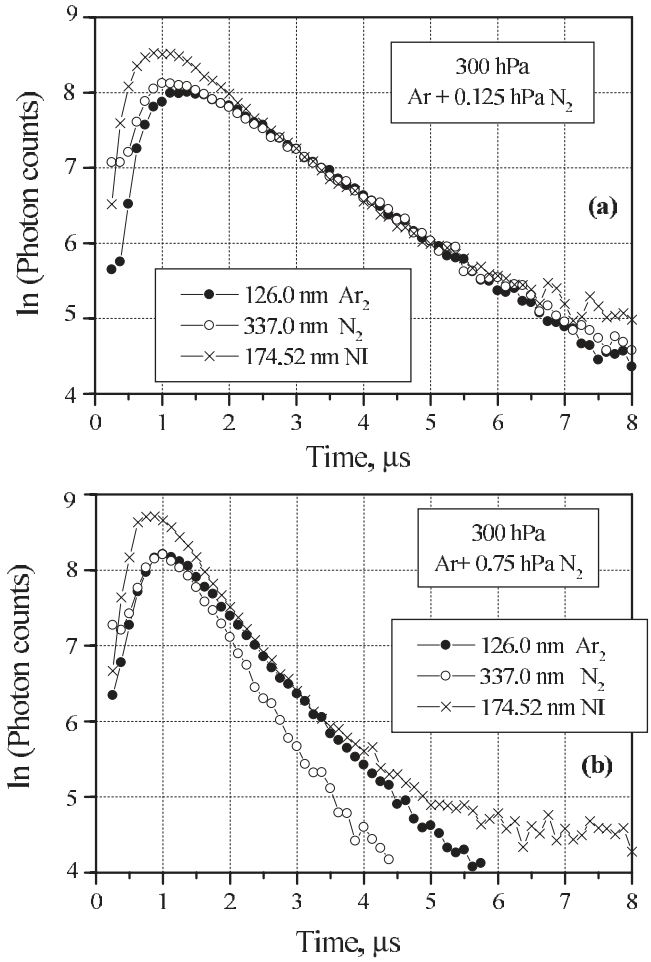

Figure 6. Time dependences of the Ar_2^* (126.0 nm), N_2^* (337.0 nm) and N* (174.52 nm) emissions in Ar–N_2 mixtures. The total pressure is 300 hPa. The nitrogen partial pressure is (a) 0.125 hPa and (b) 0.75 hPa. (a) The experimental curves were scaled in intensity as in figure 5. (b) The curves for Ar_2^* and N_2^* were scaled in intensity to show the similarity of these curves at short times.

A^m states will be concentrated in the $^3P_2$ state through relaxation processes. This state then becomes the main source of energy for the recorded emissions until the population stored in the $^3P_2$ state is high in comparison with the weak cascade flow.

The Ar_2^* and N_2^* emissions have very similar growth and decay (figures 5 and 6(a)) until the decay time constant for the N_2^* emission becomes appreciably less than 1 μs (figure 6(b)). The similarity of the curves for the Ar_2^* and N_2^* emissions confirms that the $Ar_2^*(1_u)$ state transfers its energy to the short-lived 0_u^+ state through mixing by electrons, and that the lifetime of the 1_u state at the experimental conditions of figures 5 and 6(a) is short enough for adequate reproducibility of the A^m ($^3P_2$) state concentration. The discrepancy in the Ar_2^* and N_2^* curve behaviour in figure 6(b) shows that in this case the lifetime of the 1_u state is not short enough to show adequately the depopulation of the $^3P_2$ metastables.

The similarity of the curves for Ar_2^* and N_2^* means that the C $^3\Pi_u$ state gets energy mainly from the A^m ($^3P_2$) state. However, there is the noticeable difference in the curves for Ar_2^* and N_2^* before maximum intensity in figures 5(a) and 6(a). This difference has nothing to do with

the accuracy of the experimental results but is reproducible, and we ascribe this difference to energy transfer to N_2 molecules from other metastable states than the $^3P_2$ state (mainly from the $^3P_1$ state).

The most interesting thing, taking into account the purposes of this work, is the behaviour of the nitrogen line. Firstly, its time dependence is quite different for short times (this is better seen in figure 5(a)). Secondly, the line emits maximum intensity before the Ar_2^* and N_2^* molecules (figures 5 and 6). The position of the maximum intensity is not sensitive to the N_2 partial pressure, but depends on the total pressure. Thirdly, the line emission follows the decay of the molecular emissions in a significant time interval; however, it does not follow the decay of the molecular emissions as long as they follow each other (this is better seen in figure 5(b)). Furthermore, in figure 6(b) the decay of the line does not follow the N_2^* but the Ar_2^* emission decay in spite of the short radiative lifetime of the state emitting the line, $\leqslant$10 ns [32].

To understand the difference in the time behaviour of the atomic and molecular emissions it is appropriate to begin with the question of production of the atomic nitrogen during the discharge and in the afterglow. In the investigations concerning nitrogen-atom plasma sources (e.g. [33]), the production of atomic nitrogen is connected with the dissociation of N_2 molecules by electron impact and with vibrational excitation of the N_2 ground state. We want to call attention to another channel of atomic nitrogen production, namely the charge transfer process

$$Ar^+ + N_2 \rightarrow N_2^+ + Ar \tag{6}$$

followed by the dissociative recombination

$$N_2^+ + e \rightarrow N^m + N, \tag{7}$$

where the Ar^+ ions are in their ground or first excited states, the N_2, N_2^+, Ar, and N are in their ground states, and N^m are metastable states. The rate coefficient for process (6) is 1×10^{-11} cm^3 s^{-1} at 300 K [34, 35]. The rate coefficient for reaction (7) is 2.6×10^{-7} cm^3 s^{-1} [36]. The atomic nitrogen that is created in the processes (6), (7) is mainly in the ground ^{4}S and in the first excited (metastable) ^{2}D state [37] (figure 1). At room temperature the process (6) populates the two lowest vibrational levels of N_2^+ with vibrational quantum numbers $\upsilon = 0$ and 1 and with the $\upsilon = 1$ level more populated. The reverse of reaction (6) depopulates the $\upsilon = 1$ level with a higher rate than reaction (7) but the $\upsilon = 0$ level is depopulated in reaction (7) [34–36].

There is also another process of charge transfer where molecular Ar_2^+ ions participate:

$$Ar_2^+ + N_2 \rightarrow (ArN_2)^+ + Ar. \tag{8}$$

In [38] the very high rate coefficient of this reaction, 2.2×10^{-9} cm^3 s^{-1}, is given. However, the products of the $(ArN_2)^+$ ion recombination were not investigated.

In any case the nitrogen atoms should be produced mainly during and just after the current pulse. Figures 5 and 6 support this conclusion: a sharp growth of the atomic emission is seen at short afterglow times. Note that the influence of three-body conversion on the atomic nitrogen concentration is negligible during the afterglow observation. Here we refer to the three-body conversion of atomic nitrogen into nitrogen molecules where the third body is an argon atom. The rate coefficient of this reaction is $\sim 1.4 \times 10^{-33}$ cm^6 s^{-1} at room temperature [39]. Note also that in our experiments the atomic nitrogen is not saved from one pulse to another because of the gas flow through the discharge volume.

The processes of atomic nitrogen production cannot explain why the N I line shows maximum intensity before the Ar_2^* and N_2^* molecules (figures 5, 6). Therefore, our explanation is the following: the atomic nitrogen gets energy effectively not only from the Ar* ($^3P_2$) state (like the Ar_2 and N_2 molecules do) but also from the Ar* ($^3P_1$) state. This seems very probable if we analyse the scheme of levels (figure 1). Energy transfer from the Ar* ($^3P_2$)

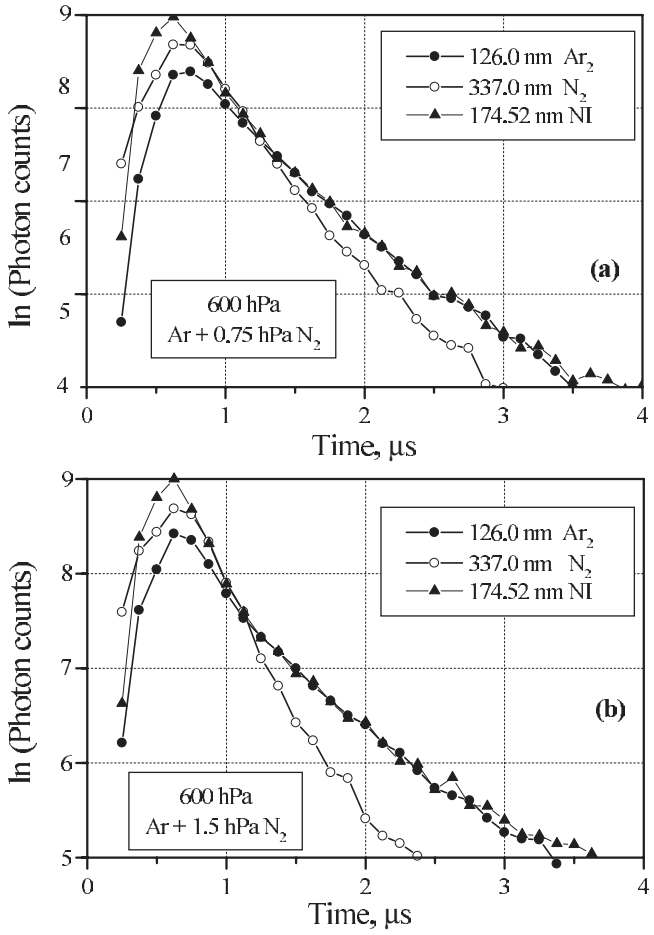

Figure 7. Time dependences of the Ar_2^* (126.0 nm), N_2^* (337.0 nm) and N* (174.52 nm) emissions in Ar–N_2 mixtures. The total pressure is 600 hPa. The nitrogen partial pressure is (a) 0.75 hPa and (b) 1.5 hPa.

state (11.55 eV) to the N (^{4}S) state with the excitation of the $2p^2 3s\ ^2P$ states (10.68 eV) has the high rate coefficient, 9×10^{-11} cm^3 s^{-1} [9], despite the large energy gap between the donor and acceptor states. In contrast to the Ar* ($^3P_2$) state, the Ar* ($^3P_1$) state (11.62 eV) has an excellent partner for energy transfer in the sense of a small energy gap, namely the $2p^2 3p\ ^2S$ state of N I (11.60 eV) (figure 1). The subsequent strong infrared transitions populate the upper state of the investigated transition. Therefore, the line emission peak position may be correlated to a significant population of the Ar* ($^3P_1$) state at the same time.

Later, behind the maximum, the atomic line shows the same decay as the Ar_2^* and N_2^* molecules, i.e. energy is accepted mainly from the Ar^m ($^3P_2$) state (figures 5 and 6(a)). Further on, when the energy stored in the $^3P_2$ state is spent and the only source of energy is the weak cascade flow, the atomic line shows a slower decay because energy is again accepted from both the $^3P_2$ and $^3P_1$ states.

The situation shown in figure 6(b), where the decay of the N I line does not mainly follow the decay of the nitrogen molecular emission but rather the decay of the argon continuum, is also reproduced distinctly in figure 7 where the time dependences at the higher total pressure

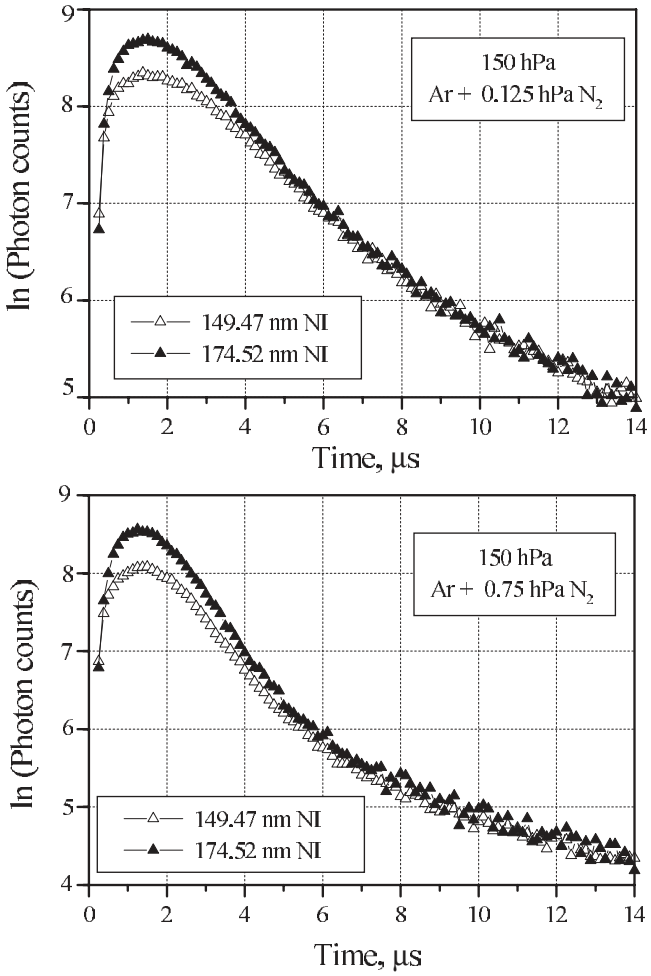

Figure 8. Time dependences of the atomic nitrogen lines at 149.47 and 174.52 nm. Both transitions have the same upper level.

600 hPa are shown. On the basis of these data we conclude that there is one more channel of energy transfer to the atomic nitrogen, namely from the molecular $Ar_2^*(1_u)$ state. The possible acceptors in this case are nitrogen atoms in the first metastable $2p^3\ ^2D$ state (figure 1):

$$Ar_2^*(1_u) + N^m(^2D) \rightarrow N^* + 2Ar^*(^1S_0), \tag{9}$$

and the result of the energy transfer could be the excitation of the $2p^2 3p\ ^2D,^2P$ and $2p^2 3s'\ ^2D$ states. The energy difference between the latter states and the metastable $2p^3\ ^2D$ state corresponds to the energy of photons emitted at the maximum of the Ar_2^* continuum and, consequently, corresponds to the energy which can be transferred from the lowest $Ar_2^*(1_u)$ levels. The result shown in figure 8 confirms a significant population of the metastable ^2D state. There is a perceptible difference between the curves for the 149.47 and 174.52 nm lines having a common upper level and this difference should be ascribed to self-absorption by the ^2D state (see the products of reaction (7)).

Note that in figure 7 just after the peak of the intensity the nitrogen line shows the same decay rate as the nitrogen molecules and that this decay rate is higher than the argon continuum

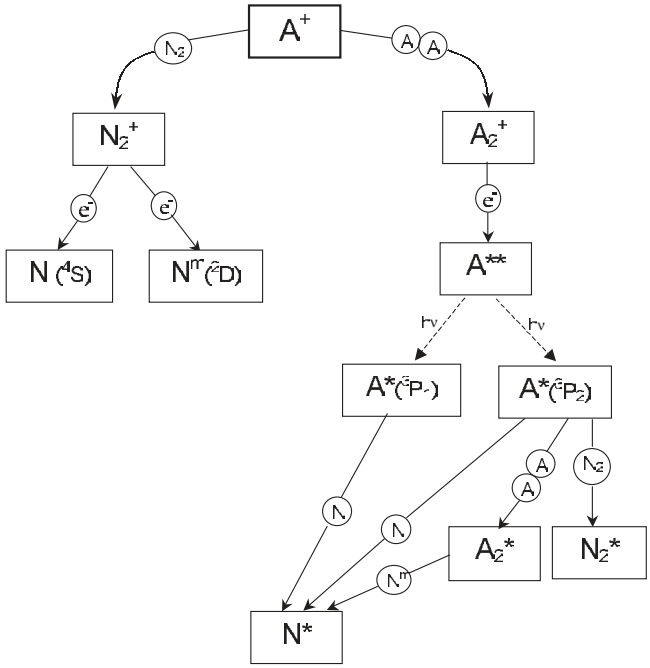

Figure 9. A scheme of energy transfer processes in excited mixtures of argon with a small admixture of nitrogen.

decay rate at the same time. This means that both nitrogen species receive energy at this time mainly from the atomic metastables Ar^m and that the switching of the atomic nitrogen into an acceptor of energy from the molecular metastables $Ar_2^*(1_u)$ occurs later when the $Ar_2^*(1_u)$ molecules become the main source of energy for the atomic nitrogen.

4. Conclusion

The scheme of energy transfer in excited mixtures of argon with a small admixture of nitrogen, as outlined in the text above, is shown in figure 9. Our experimental results demonstrate the existence of a common source of energy (the atomic argon metastable $^3P_2$ state) for a few acceptors (argon and nitrogen molecules and also atomic nitrogen) and, consequently, a competition between these acceptors, which is governed by the conditions in the plasma volume. Further, the presented results indicate that atomic nitrogen can effectively acquire energy from the argon $^3P_1$ state and therefore atomic nitrogen emits its peak intensity before the molecules. Moreover, the atomic nitrogen also acquires energy from the excited $Ar_2^*(1_u)$ molecules. According to our experimental curves, the molecular nitrogen competes weakly with the atomic nitrogen in the energy acquisition from the argon $^3P_1$ state and, as was indicated above, cannot compete in the acquisition of energy from the $Ar_2^*(1_u)$ molecules. The latter channel of energy transfer should become especially efficient at higher total pressures than in our experiment.

We have used a simplified model of processes, taking into account only the dominant processes. It is of interest to compare our conclusions with the results of calculations based on a more refined model, i.e. the solution of a system of coupled differential equations describing the time variation of the concentrations of the atomic, molecular and ionic states (as in [40]).

This could be the purpose of an additional investigation. The scheme of processes indicated in figure 9 might be useful for research and development of VUV line sources.

Acknowledgments

We gratefully acknowledge the support of this work received from the Carl Trygger Foundation for Scientific Research and the Göran Gustafsson Foundation. The Swedish Institute through the Visby Program is acknowledged for two scholarships (B Krylov and G Gerasimov).

References

[1] Rawlins W T and Piper L G 1981 *SPIE* **279** 58
[2] Stedman D H and Setser D W 1970 *J. Chem. Phys.* **52** 3957
[3] Setser D W, Stedman D H and Coxon J A 1970 *J. Chem. Phys.* **53** 1004
[4] Calo J M and Axtmann R C 1971 *J. Chem. Phys.* **54** 4961
Calo J M and Axtmann R C 1972 *J. Chem. Phys.* **55** 682
[5] Piper L G, Richardson W C, Taylor G W and Setser D W 1972 *Discuss. Faraday Soc.* **53** 100
[6] Le Calve J and Bourene M 1973 *J. Chem. Phys.* **58** 1446
[7] Bochkova O P, Chernysheva N V and Tolmachev Ju A 1974 *Opt. Spektrosk.* **36** 36
[8] Winicur D H and Fraites J L 1974 *J. Chem. Phys.* **61** 1548
[9] Piper L G, Clyne M A A and Monkhouse P B 1980 *Chem. Phys.* **51** 107
[10] Samson J A R 1967 *Techniques of Vacuum Ultraviolet Spectroscopy* (New York: Wiley)
[11] Bennet W R 1962 *Ann. Phys., NY* **18** 367
[12] Lorents D C 1976 *Physica* C **82** 19
[13] Liu W F and Convey D C 1975 *J. Chem. Phys.* **62** 3070
[14] Gaur J P and Chanin L M 1969 *Phys. Rev.* **182** 167
[15] Bhattacharya A K 1970 *J. Appl. Phys.* **41** 1707
[16] Oskam H J and Mittelstadt V P 1963 *Phys. Rev.* **132** 1445
[17] Mehr F J and Biondi M A 1968 *Phys. Rev.* **176** 322
[18] Krylov B, Gerasimov G, Morozov A, Arnesen A, Hallin R and Heijkenskjold F 2000 *Eur. Phys. J.* D **8** 227
[19] Sewraj N, Gardou J P, Salamero Y and Milet P 2000 *Phys. Rev.* A **62** 052721
[20] Gerasimov G N, Petrov S Ja and Sabirova I L 1976 *Opt. Spektrosk.* **42** 596
[21] Gerasimov G N, Petrov S Ja and Sabirova I L 1977 *Opt. Spektrosk.* **43** 596
[22] Gerasimov G N, Petrov S Ja and Sabirova I L 1978 *Opt. Spektrosk.* **44** 385
[23] Morozov A, Krylov B, Gerasimov G, Arnesen A and Hallin R 2002 *J. Phys. B: At. Mol. Opt. Phys.* **35** 1929
[24] Moutard P, Laporte P, Subtil J-L, Damany N and Damany H 1988 *J. Chem. Phys.* **88** 7485
[25] Keto J W, Gleason R E and Walters G K 1974 *Phys. Rev. Lett.* **33** 1375
[26] Madej A A and Stoichev B P 1988 *Phys. Rev.* A **38** 3456
[27] Keto J W, Gleason R E, Bonifield T D, Walters G K and Soley F K 1976 *Chem. Phys. Lett.* **42** 125
[28] Sadeghi N and Setser D W 1981 *Chem. Phys. Lett.* **82** 44
[29] Jonson A W and Fowler R G 1970 *J. Chem. Phys.* **53** 65
[30] Lofthus A and Krupenie P H 1977 *J. Chem. Phys. Ref. Data* **6** 113
[31] Dotchin L W and Chupp B L 1973 *J. Chem. Phys.* **59** 3960
[32] Wiese W L, Smith M W and Glennon B M 1966 *Atomic Transition Probabilities* vol 1 (Washington, DC: National Bureau of Standards)
[33] Tabbal M, Kazopoulo M, Christidis T and Isber S 2001 *Appl. Phys. Lett.* **78** 2131
[34] Smith D and Adams N G 1981 *Phys. Rev.* A **23** 2327
[35] Lindinger W, Howorka F, Lukac P, Kuhn S, Villinger H, Alge E and Ramler H 1981 *Phys. Rev.* A **23** 2319
[36] Canosa A, Gomet J C, Rowe B R and Queffelec J L 1991 *J. Chem. Phys.* **94** 7159
[37] Kella D, Johnson P J, Pedersen H B, Vejby-Christensen L and Andersen L H 1996 *Phys. Rev. Lett.* **77** 2432
[38] Shul J, Passarella R, Upschulte B L, Keesee R G and Castleman A W 1987 *J. Chem. Phys.* **86** 4446
[39] Sa P A and Loureiro J 1997 *J. Phys. D: Appl. Phys.* **30** 2320
[40] Gerasimov G, Krylov B, Loginov A, Zvereva G, Hallin R, Arnesen A and Heijkenskjold F 1998 *Appl. Phys.* B **66** 81